



**Pacific Northwest**  
NATIONAL LABORATORY

*Proudly Operated by Battelle Since 1965*

# Lidar Buoy Data Analysis

Basic Assessment of Observed  
Conditions and Instrument Performance  
Off Virginia and New Jersey

**September 2018**

WJ Shaw  
RK Newsom

MI Pekour

## DISCLAIMER

This report was prepared as an account of work sponsored by an agency of the United States Government. Neither the United States Government nor any agency thereof, nor Battelle Memorial Institute, nor any of their employees, makes **any warranty, express or implied, or assumes any legal liability or responsibility for the accuracy, completeness, or usefulness of any information, apparatus, product, or process disclosed, or represents that its use would not infringe privately owned rights.** Reference herein to any specific commercial product, process, or service by trade name, trademark, manufacturer, or otherwise does not necessarily constitute or imply its endorsement, recommendation, or favoring by the United States Government or any agency thereof, or Battelle Memorial Institute. The views and opinions of authors expressed herein do not necessarily state or reflect those of the United States Government or any agency thereof.

PACIFIC NORTHWEST NATIONAL LABORATORY  
*operated by*  
BATTELLE  
*for the*  
UNITED STATES DEPARTMENT OF ENERGY  
*under Contract DE-AC05-76RL01830*

Printed in the United States of America

Available to DOE and DOE contractors from the  
Office of Scientific and Technical Information,  
P.O. Box 62, Oak Ridge, TN 37831-0062;  
ph: (865) 576-8401  
fax: (865) 576-5728  
email: [reports@adonis.osti.gov](mailto:reports@adonis.osti.gov)

Available to the public from the National Technical Information Service  
5301 Shawnee Rd., Alexandria, VA 22312  
ph: (800) 553-NTIS (6847)  
email: [orders@ntis.gov](mailto:orders@ntis.gov) <<http://www.ntis.gov/about/form.aspx>>  
Online ordering: <http://www.ntis.gov>



This document was printed on recycled paper.

(8/2010)

# **Lidar Buoy Data Analysis**

Basic Assessment of Observed Conditions and Instrument  
Performance Off Virginia and New Jersey

WJ Shaw  
RK Newson

MI Pekour

September 2018

Prepared for  
the U.S. Department of Energy  
under Contract DE-AC05-76RL01830

Pacific Northwest National Laboratory  
Richland, Washington 99352

## Summary

One of the challenges for developing offshore wind energy in the United States has been a lack of long-term observations to characterize the wind resource and design load conditions and to provide validation for the numerical weather prediction models. To address this challenge, the U.S. Department of Energy supported the procurement in 2014 and subsequent deployment of two buoys equipped with motion-compensated lidars and a comprehensive set of supporting meteorological and oceanographic (“metocean”) measurement systems. Each of the systems was deployed off the U.S. East Coast in excess of one year—one each near the coasts of Virginia and New Jersey. One notable observation from both buoys is the dramatic dependence of the wind shear on atmospheric stability as indicated by the air-sea temperature difference. This observation suggests that the commonly used neutral log law will not be a fully suitable representation of wind shear off the U.S. East Coast. This report provides a basic summary of observations at each location from key systems on each of the buoys as well as an assessment of instrument performance. These data are beginning to fill a long-standing observational gap for the wind energy community in the United States.

## **Acknowledgments**

This work was funded by the Wind Energy Technologies Office of the DOE's Office of Energy Efficiency and Renewable Energy. We express our appreciation in particular to Alana Duerr, DOE Team Lead, for her support of this effort. Pacific Northwest National Laboratory is operated by the Battelle Memorial Institute for the U.S. DOE under Contract DE AC05 76RL01830.

## Acronyms and Abbreviations

ADCP	acoustic Doppler current profiler
ADP	acoustic Doppler profiler
BAO	Boulder Atmospheric Observatory
BOEM	Bureau of Ocean Energy Management
CNR	carrier-to-noise ratio
CTD	conductivity temperature depth
DOE	U.S. Department of Energy
DOI	U.S. Department of the Interior
GPS	Global Positioning System
lidar	light detection and ranging
MSL	mean sea level
NWP	numerical weather prediction
PNNL	Pacific Northwest National Laboratory

# Contents

Summary .....	iii
Acknowledgments.....	iv
Acronyms and Abbreviations .....	v
1.0 Introduction .....	1.1
1.1 Motivation.....	1.1
1.2 Deployments .....	1.1
1.3 Instrumentation.....	1.2
1.4 Data Recovery .....	1.3
1.4.1 Virginia Buoy.....	1.3
1.4.2 New Jersey Buoy.....	1.5
2.0 Observations during Deployment.....	2.1
2.1 Virginia Buoy Observations.....	2.1
2.1.1 Lidar Winds.....	2.1
2.1.2 Ocean Currents, Wave Properties, and Surface Winds .....	2.4
2.1.3 Wind Shear and Air-Sea Temperature Difference .....	2.6
2.1.4 Conductivity.....	2.8
2.2 New Jersey Buoy Observations.....	2.9
2.2.1 Lidar Winds.....	2.9
2.2.2 Ocean Currents, Wave Properties, and Surface Winds .....	2.14
2.2.3 Wind Shear and Air-Sea Temperature Difference .....	2.16
2.2.4 Conductivity.....	2.18
3.0 Discussion and Summary .....	3.1
4.0 References .....	4.1
Appendix A – Distributions and Diurnal Composites of Wind, Temperature and Current Data from the Lidar Buoys.....	A.1

# Figures

Figure 1.1.	Location of the Virginia and New Jersey buoys relative to BOEM lease blocks and the mainland.....	1.2
Figure 1.2.	Availability for various variables measured by the lidar from the Virginia buoy for the duration of the deployment .....	1.3
Figure 1.3.	Availability for the surface meteorological and buoy motion measurements from the Virginia buoy .....	1.4
Figure 1.4.	Data availability of oceanographic variables .....	1.4
Figure 1.5.	Wave data availability from the Virginia buoy.....	1.5
Figure 1.6.	As in Figure 1.2, but for the New Jersey buoy.....	1.6
Figure 1.7.	As in Figure 1.3, but for the New Jersey buoy.....	1.6
Figure 1.8.	As in Figure 1.4, but for the New Jersey buoy.....	1.7
Figure 1.9.	As in Figure 1.5, but for the New Jersey buoy.....	1.7
Figure 2.1.	Profiles of a) wind speed, b) wind direction, and c) data availability averaged over the winter season (January through March) during the Virginia deployment.....	2.2
Figure 2.2.	Profiles of a) wind speed, b) wind direction, and c) data availability averaged over the spring season (April through June) during the Virginia deployment.....	2.2
Figure 2.3.	Profiles of a) wind speed, b) wind direction, and c) data availability averaged over the summer season (July through September) during the Virginia deployment.....	2.3
Figure 2.4.	Profiles of a) wind speed, b) wind direction, and c) data availability averaged over the fall season (October through December) during the Virginia deployment.....	2.3
Figure 2.5.	Profiles of a) wind speed, b) wind direction, and c) data availability averaged over the entire annual cycle.....	2.4
Figure 2.6.	Wind roses from the lidar at the 90 m level for a) the entire annual cycle, b) winter (January through March), c) spring (April through June), d) summer (July through September), and e) fall (October through December).....	2.4
Figure 2.7.	Distributions of a) ocean current and direction, b) significant wave height and direction, c) surface wind speed and direction for January through March.....	2.5
Figure 2.8.	Distributions of a) ocean current and direction, b) significant wave height and direction, c) surface wind speed and direction for April through June.....	2.5
Figure 2.9.	Distributions of a) ocean current and direction, b) significant wave height and direction, c) surface wind speed and direction for July through September.....	2.6
Figure 2.10.	Distributions of a) ocean current and direction, b) significant wave height and direction, c) surface wind speed and direction for October through December.....	2.6
Figure 2.11.	Distributions of a) ocean current and direction, b) significant wave height and direction, c) surface wind speed and direction averaged over all seasons.....	2.6
Figure 2.12.	a) Wind speed from the surface (blue) and the Vindicator III at 90 m (red), b) wind direction from the surface (blue) and the Vindicator III at 90 m (red), and c) ocean water temperature (blue) and air temperature (red).....	2.7
Figure 2.13.	Wind speed difference between the lidar at 90 m and the surface as a function of the air-sea temperature difference for the Virginia deployment.....	2.8

Figure 2.14.	Frequency of occurrence of ocean water conductivities covering the entire deployment period (12 Dec 2014 to 31 May 2016) .....	2.9
Figure 2.15.	a) Wind speed from the surface (blue) and the Vindicator III at 90 m (red), b) wind direction from the surface (blue) and the Vindicator III at 90 m (red), c) ocean water temperature (blue) and air temperature (red).....	2.10
Figure 2.16.	Profiles of a) wind speed, b) wind direction, and c) data availability averaged over the winter season (January through March) during the New Jersey deployment.....	2.11
Figure 2.17.	Profiles of a) wind speed, b) wind direction, and c) data availability averaged over the spring season (April through June) during the New Jersey deployment.....	2.11
Figure 2.18.	Profiles of a) wind speed, b) wind direction, and c) data availability averaged over the summer season (July through September) during the New Jersey deployment .....	2.12
Figure 2.19.	Profiles of a) wind speed, b) wind direction, and c) data availability averaged over the fall season (October through December) during the New Jersey deployment .....	2.12
Figure 2.20.	Profiles of a) wind speed, b) wind direction, and c) data availability averaged over the entire annual cycle.....	2.13
Figure 2.21.	Wind roses from the lidar at the 90 m level for a) the entire annual cycle, b) winter (January through March), c) spring (April through June), d) summer (July through September), and e) fall (October through December).....	2.14
Figure 2.22.	Distributions of a) ocean current and direction, b) significant wave height and direction, c) surface wind speed and direction for January through March. ....	2.15
Figure 2.23.	Distributions of a) ocean current and direction, b) significant wave height and direction, c) surface wind speed and direction for April through June. ....	2.15
Figure 2.24.	Distributions of a) ocean current and direction, b) significant wave height and direction, c) surface wind speed and direction for July through September. ....	2.15
Figure 2.25.	Distributions of a) ocean current and direction, b) significant wave height and direction, c) surface wind speed and direction for October through December.....	2.16
Figure 2.26.	Distributions of a) ocean current and direction, b) significant wave height and direction, c) surface wind speed and direction averaged over all seasons. ....	2.16
Figure 2.27.	a) Wind speed from the surface (blue) and the Vindicator III at 90 m (red), b) wind direction from the surface (blue) and the Vindicator III at 90 m (red), c) ocean water temperature (blue) and air temperature (red).....	2.17
Figure 2.28.	Wind speed difference between the lidar at 90 m and the surface as a function of the air-sea temperature difference for the New Jersey deployment. ....	2.18
Figure 2.29.	Frequency of occurrence of ocean water conductivities covering the entire deployment period (11 Nov 2015 to 7 Feb 2017) .....	2.19

## Tables

Table 1.1.	Table of Instruments .....	1.2
------------	----------------------------	-----

# 1.0 Introduction

## 1.1 Motivation

One of the challenges for developing offshore wind energy in the United States has been a lack of long-term observations to characterize the wind resource and design load conditions and to provide validation for the numerical weather prediction (NWP) models. This was recognized as a continuing key challenge in the National Offshore Wind Strategy (U.S. DOE and U.S. DOI 2016) jointly released by the U.S. Department of Energy (DOE) and the U.S. Department of the Interior (DOI). To address this challenge, the DOE supported the procurement in 2014 and subsequent deployment of two buoys equipped with motion-compensated lidars and a comprehensive set of supporting meteorological and oceanographic (“metocean”) measurement systems. Each of the systems was deployed off the U.S. East Coast in excess of one year—one each near the coasts of Virginia and New Jersey. This report provides a basic summary of observations at each location from key systems on each of the buoys as well as an assessment of instrument performance.

Both buoys are WindSentinel® systems manufactured by AXYS Technologies, Inc. and were delivered to Pacific Northwest National Laboratory (PNNL) in September 2014. Following a brief deployment for consistency checks in Washington’s Strait of Juan de Fuca, the buoys were prepared for their initial year-long deployments.

## 1.2 Deployments

Buoy 6NB00120 (hereafter referred to as “the Virginia buoy”) was deployed on 12 December 2014 approximately 42 km east of Virginia Beach, Virginia, at a location just west of wind energy lease blocks designated by the Bureau of Ocean Energy Management (BOEM). The buoy location was determined by the Global Positioning System (GPS) following deployment to be 36° 51’ 59.9” N and 75° 29’ 30.9” W. This location is shown in Figure 1.1. Except for one brief maintenance interruption, the buoy operated continuously until its recovery on 31 May 2016.

Buoy 6NB00130 (hereafter referred to as “the New Jersey buoy”) was deployed on 11 November 2015 approximately 5 km east of Atlantic City, New Jersey. The buoy location was determined by GPS following deployment to be 39° 18’ 51.9” N and 74° 24’ 2.1” W. This location is also shown in Figure 1.1. The buoy operated nearly continuously at this location until its recovery on 7 February 2017.

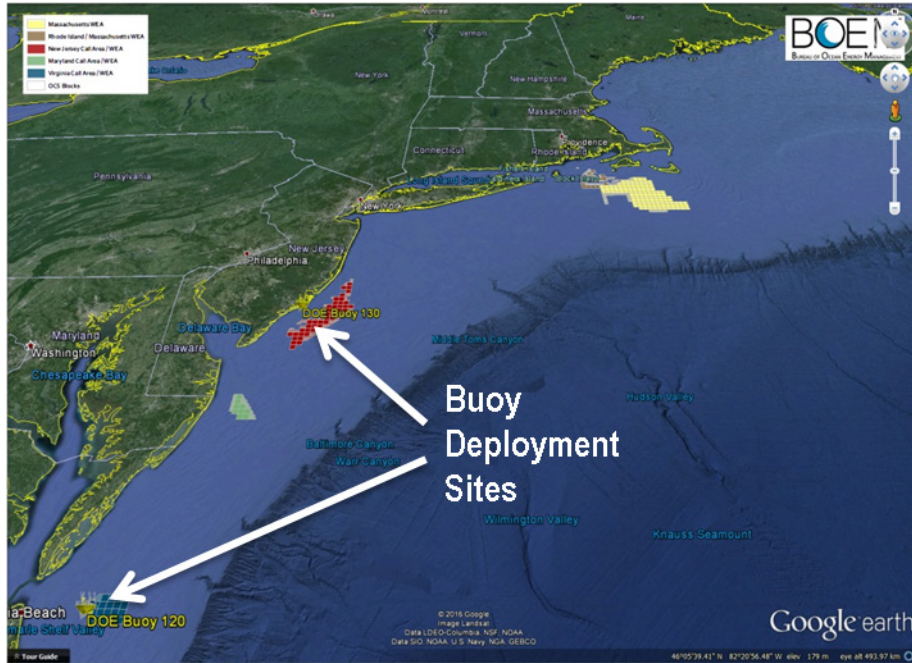


Figure 1.1. Location of the Virginia and New Jersey buoys relative to BOEM lease blocks and the mainland.

### 1.3 Instrumentation

Instrumentation on the two buoys is identical by manufacturer and model, and the complement of instruments is provided in the following table.

Table 1.1. Table of Instruments

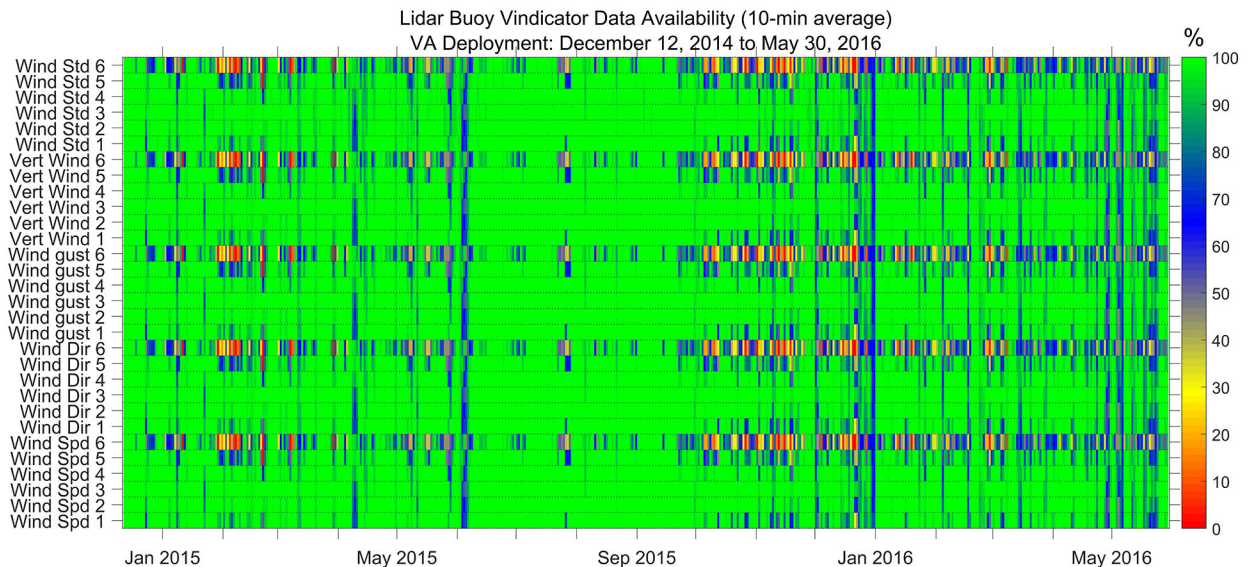
Sensor Type	Manufacturer	Model
Wind Profile (6 range gates to ~200 m above MSL)	OADS	Vindicator III
Wind Speed (2)	Vector Instruments	A100R
Wind Direction	Vector Instruments	WP200
Temperature, Relative Humidity	Rotronic	MP101A
Barometer	RM Young	61302V
Pyranometer	Licor	LI-200
Water Temperature	AXYS	YSI
CTD	Seabird	SBE 37SMP-1j-2-3c
Wave	AXYS	TRIAXYS NW III
Current Profile (ADP)	Nortek	Aquadopp 400 kHz
Tilt/Compass	MicroStrain	3DM GX3 25

ADP = acoustic Doppler profiler  
 CTD = conductivity temperature depth  
 MSL = mean sea level

## 1.4 Data Recovery

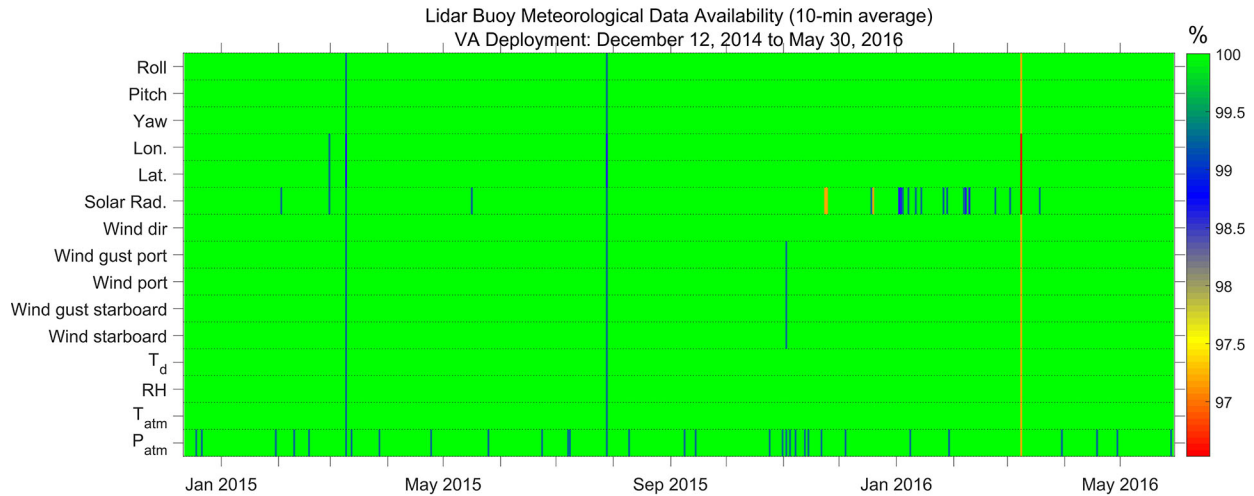
### 1.4.1 Virginia Buoy

Figure 1.2 shows the recovery for various variables measured by the lidar from the Virginia buoy for the duration of the deployment. The derived variables include 10-minute averages of wind speed and direction, the wind gust (maximum 3-second wind in a 10-minute period), the vertical velocity, and the 10-minute standard deviation of the wind speed. The availability is calculated from the number of 10-minute periods in 24 hours that pass required signal thresholds at each range gate. The six range gates (labeled 1–6 in the figure) for the lidar generate values at 55 m, 70 m, 90 m, 110 m, 130 m, and 160 m above the sea surface. In general, the lidar signal is weakest for the most distant range gates, and the figure shows the greatest occurrence of missing data in range gates 5 and 6. The focus of the lidar optics is at 90 m (range gate 3), and the figure shows that this was the attitude with the greatest data recovery for all lidar-derived variables. As is the case with most remote sensing systems, the lidar returns are weather-dependent. Clean air, which has low concentrations of the aerosol particles that scatter the laser light back to the surface, is a common cause of poorer returns at the higher range gates. Fog will attenuate the beams so that returns are lost at all range gates.



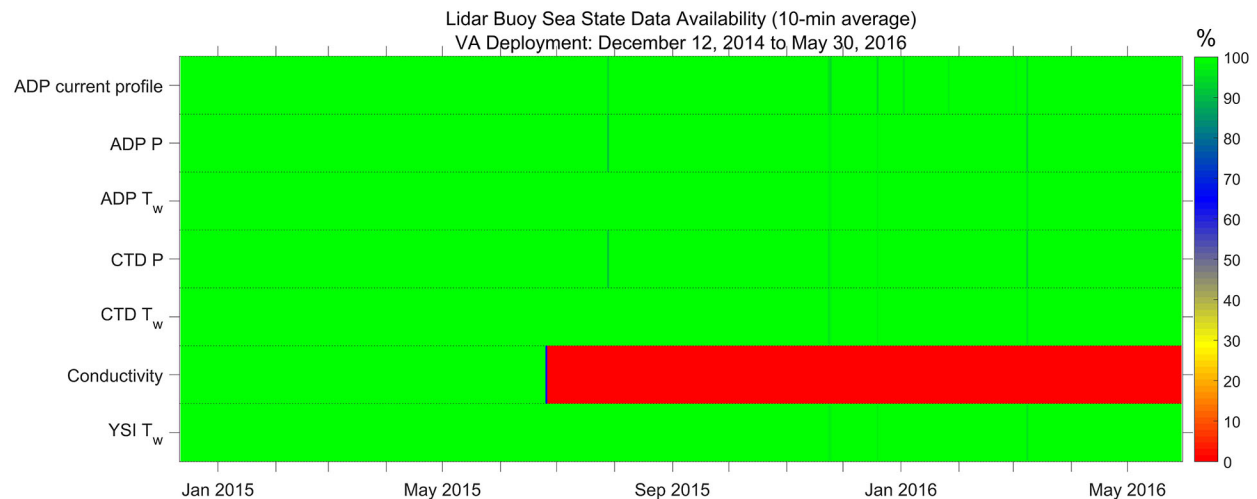
**Figure 1.2. Availability for various variables measured by the lidar from the Virginia buoy for the duration of the deployment. The numerical value is the lidar measurement height number beginning at the lowest height. From bottom to top of the figure, variables are wind speed, wind direction, wind gust, mean vertical wind speed, and standard deviation of the wind speed.**

Figure 1.3 shows the data recovery for the surface meteorological and buoy motion measurements from the Virginia buoy. Note that the recovery color scale is adjusted in this figure to highlight times of some missing data. However, the recovery for all of these measurements was near 100% for almost all of the deployment.



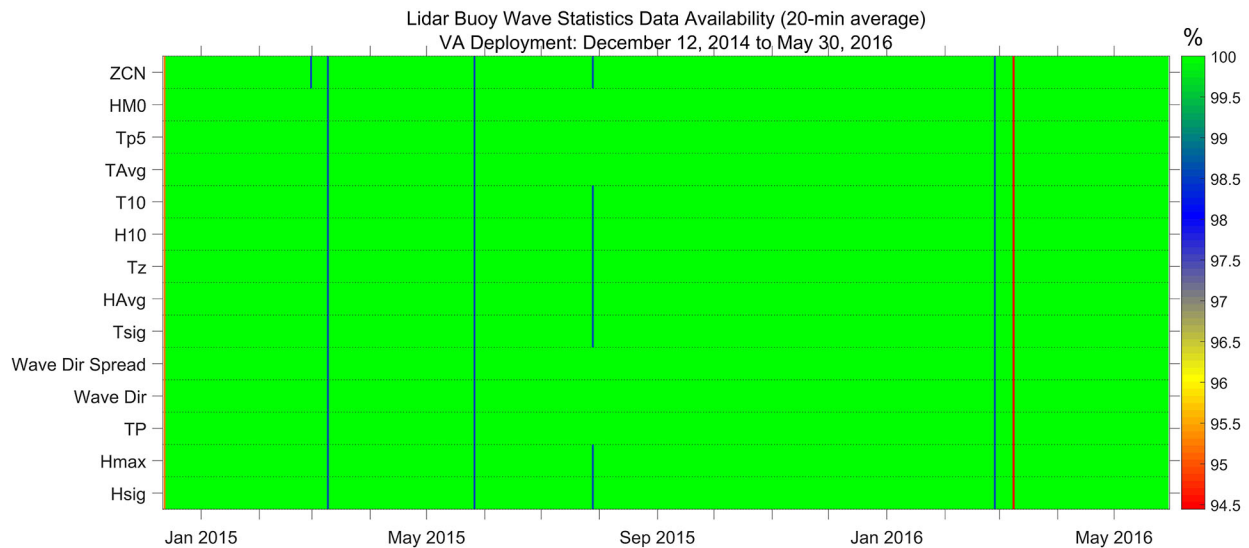
**Figure 1.3. Availability for the surface meteorological and buoy motion measurements from the Virginia buoy. Note the expanded scale owing to the very high availability of this suite of measurements. From bottom to top of the figure, variables are atmospheric pressure, surface air temperature, relative humidity, dew point, wind speed (starboard cup anemometer), wind gust (starboard), wind speed (port), wind gust (port), solar radiation, latitude, longitude, yaw, pitch, and roll.**

With one exception, the oceanographic measurements had near-perfect recovery rates (Figure 1.4). The figure shows data recovery for current profiles, pressure, and water temperature from the acoustic Doppler profiler (ADP); pressure, water temperature, and conductivity from the CTD probe; and an additional water temperature measurement from the AXYS YSI probe. The conductivity measurement from the CTD probe failed near the end of June, approximately six months into the deployment, due to biofouling. Because salinity was not a key observation for this particular deployment, the probe was not repaired until after final buoy recovery.



**Figure 1.4. Data availability of oceanographic variables. From bottom, variables are water temperature, CTD conductivity, CTD water temperature, CTD pressure, ADP water temperature, ADP pressure, and ADP current profile.**

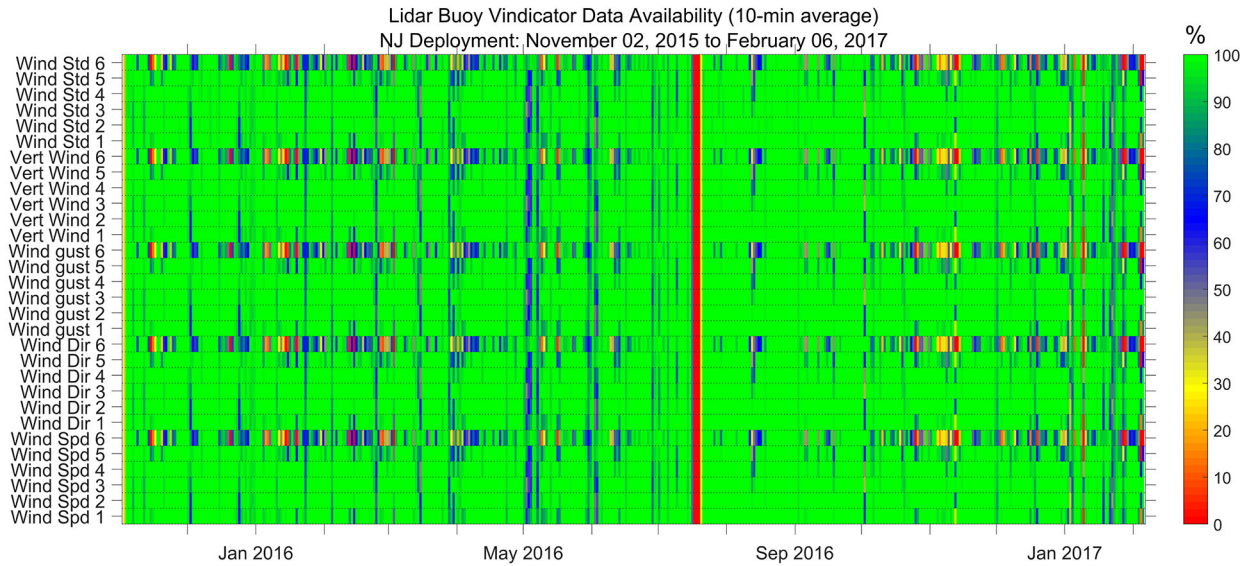
Wave measurement availability rates, shown in Figure 1.5 are displayed as in Figure 1.3 using an expanded scale near 100% to highlight the very small number of occurrences across all of the wave measurements.



**Figure 1.5. Wave data availability from the Virginia buoy. Note the expanded scale owing to the very high availability of data from this measurement suite. From bottom, the variables are significant wave height, maximum wave height, peak period, wave direction, wave direction spread, significant period, average wave height, mean spectral period, mean height of largest 10 percent of waves, mean period of H10 waves, average wave period, peak spectral period from Read Method, spectral value for significant wave height, and number of zero crossings.**

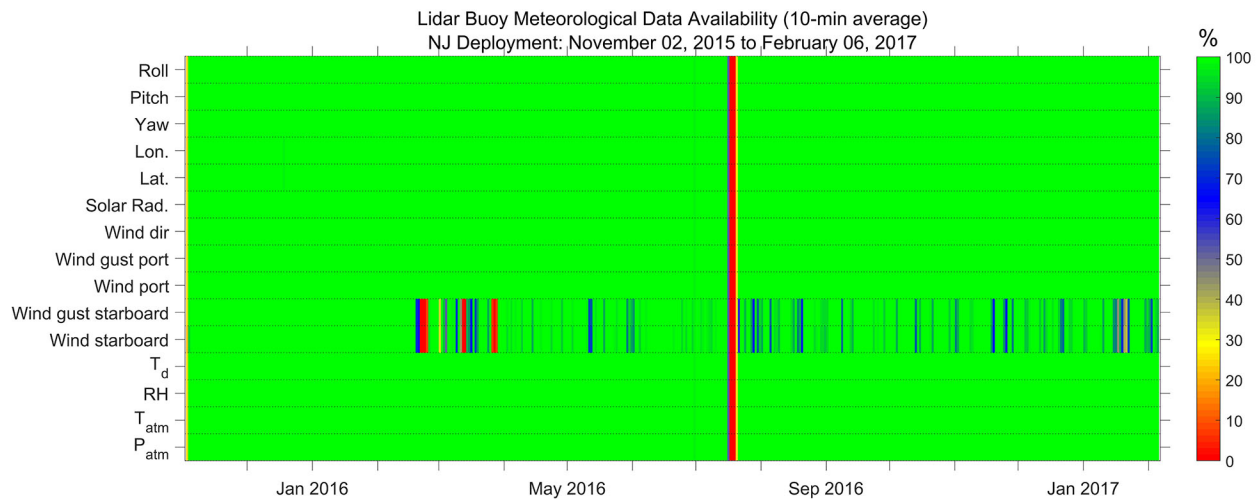
### 1.4.2 New Jersey Buoy

Figure 1.6 shows the data availability for various variables derived from the lidars for the New Jersey buoy. The variables are as in Figure 1.2. In general, the pattern of data availability is the same as for the Virginia buoy, with poorer data recovery at the higher altitudes. A notable period of complete data loss is shown in Figure 1.6 during July. On July 14, 2016, the New Jersey buoy became separated from its mooring. The buoy broadcast that it was outside its watch circle and a recovery team was dispatched. The buoy was recovered within about 12 hours and towed to shore. Data were not collected until the buoy was redeployed on July 21, and this data gap appears in the timelines for all range gates in this figure and for all sensors in the other figures below.



**Figure 1.6.** As in Figure 1.2, but for the New Jersey buoy.

Data recovery rates for the surface and buoy attitude and position data for the New Jersey buoy are shown in Figure 1.7. Apart from the July buoy disengagement, the recovery rates were generally very high. The exception is the data from the starboard cup anemometer. This device had intermittent signal problems beginning February 2016 that continued for the duration of the deployment. The starboard anemometer is redundant with an anemometer on the port side of the buoy, so this did not constitute a significant data issue.



**Figure 1.7.** As in Figure 1.3, but for the New Jersey buoy.

Recovery rates for the oceanographic suite of instruments on the New Jersey buoy are shown in Figure 1.8. In general, the data recovery was nearly 100% for all devices. As was the case for the Virginia buoy, the conductivity sensor for the CTD probe was affected by biofouling and did not report good data beginning in early June 2016. The recovery of the buoy in July afforded an opportunity to clean the probe, and it reported good measurements on its return to the measurement site. However, the biofouling issue recurred, and good data were not obtained for the majority of the buoy's remaining time on station.

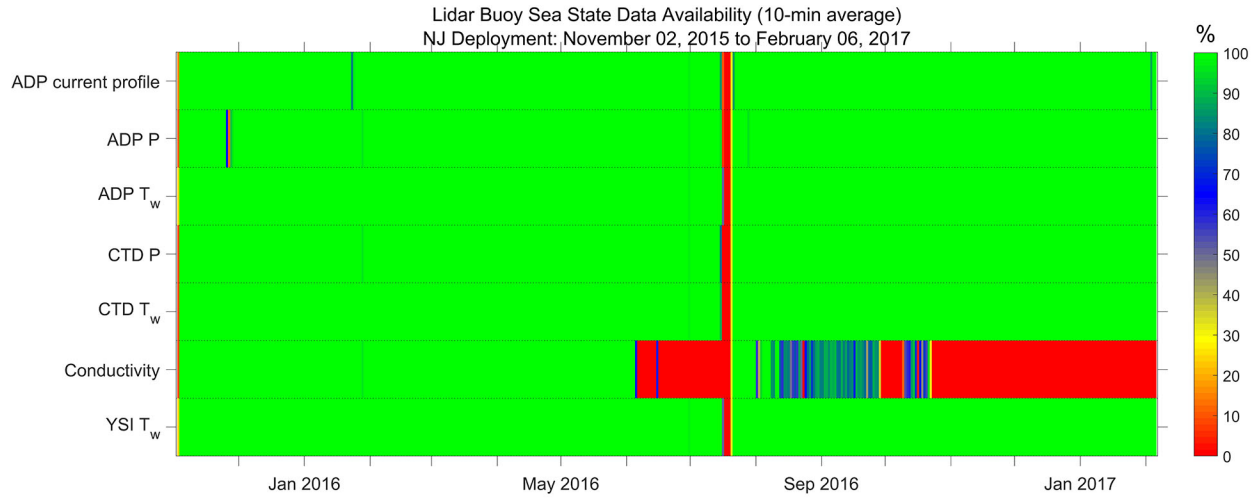


**Figure 1.8.** As in Figure 1.4, but for the New Jersey buoy.

Figure 1.9 shows wave data availability for the New Jersey buoy. Apart from the general buoy incident in July, all wave variables were available essentially 100% of the time during the deployment.

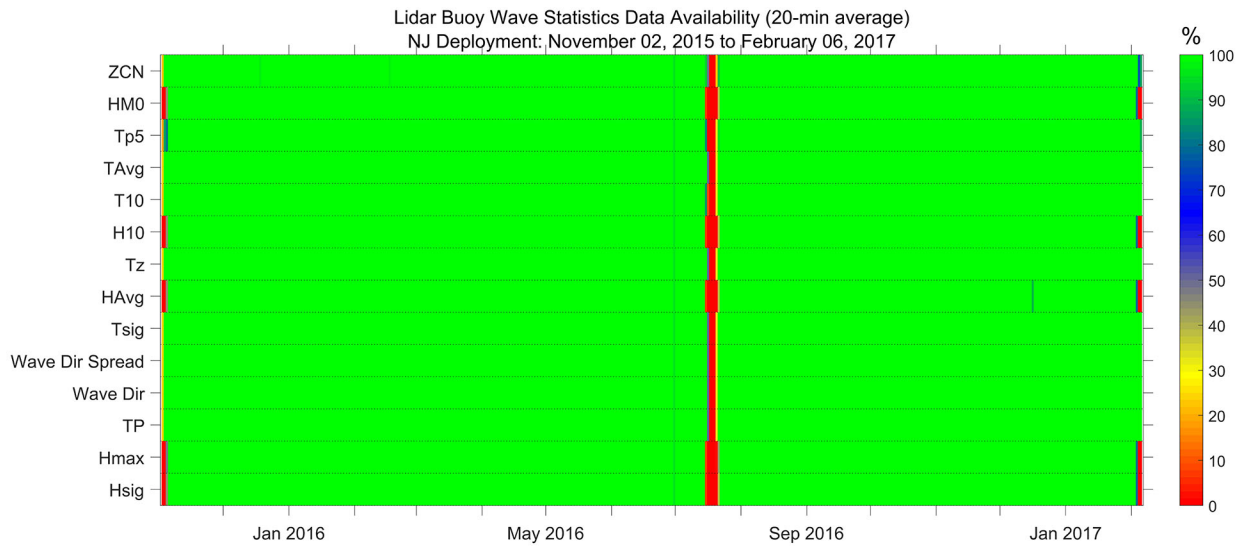


**Figure 1.9.** As in Figure 1.5, but for the New Jersey buoy.

## 2.0 Observations during Deployment

The Virginia buoy and the New Jersey buoy were deployed in consecutive years. Thus, while broad seasonal behaviors can be compared between the two locations, it is not possible to effectively compare details of atmospheric or oceanographic behavior during the deployments, and there is no information about spatial variability of individual significant events. In this section, we describe the behavior of atmospheric and oceanographic variables over the annual cycle. Because of the sequential nature of the deployments, we discuss the observations from the Virginia buoy first and then from the New Jersey buoy. Supplemental plots of data from the buoys are provided in the appendix.

### 2.1 Virginia Buoy Observations

#### 2.1.1 Lidar Winds

Figures 2.1 through 2.4 show seasonally averaged profiles of wind speed and direction from the lidar. Also included in these plots for reference are the winds from the cup anemometers on the buoy. These figures show results for winter (January through March), spring (April through June), summer (July through September), and fall (October through December), respectively. Figure 2.5 shows the wind speed and direction profile averaged over the entire annual cycle.

We note that the wind speed profiles exhibit a slight maximum at the 90 m range gate. A previous validation study using the same model of Vindicator at the Boulder Atmospheric Observatory (BAO) suggests that this instrument tends to underestimate wind speed both above and below the 90 m level. The Vindicator is designed such that the laser is focused at the 90 m level, thus optimizing its performance at this level. The BAO study indicates that the Vindicator performs well at this level, but tends to exhibit a slow bias above and below the 90 m level, particularly above about 100 m where the return signal strength decreases rapidly with altitude.

With this in mind, we focus our initial attention on the results at the 90 m level. Overall we find the mean winds tend to blow from northwest at about  $8 \text{ ms}^{-1}$ , when averaged over the entire annual cycle (Figure 2.5). The weakest winds occur during the summer months ( $\sim 6 \text{ ms}^{-1}$ ), and the strongest winds occur during the winter months ( $\sim 10 \text{ ms}^{-1}$ ). Wind directions tend to be northwesterly during the fall and winter and more southerly during summer.

Also shown in Figures 2.1 through 2.5 are profiles of data availability. The data availability profiles closely mimic the mean return signal strength and provide a rough indicator of data quality. As noted previously, the Vindicator is designed such that the laser beam is focused at the 90 m level, and this is precisely where the data availability profiles exhibit their maximum values. The annually averaged data availability was about 95% at 90 m. The lowest ( $\sim 90\%$ ) data availabilities occurred during the fall, and the highest ( $\sim 100\%$ ) data availabilities occurred during the summer.

Figure 2.6 summarizes the results from the Vindicator lidar at the 90 m level in the form of seasonally averaged wind roses. The annually averaged wind rose shows that the strongest winds tend to blow from two dominant directions—the southwest and the north-northeast. Strong northerly flow tends to occur during the winter months, and strong southwesterly flows dominate in the spring.

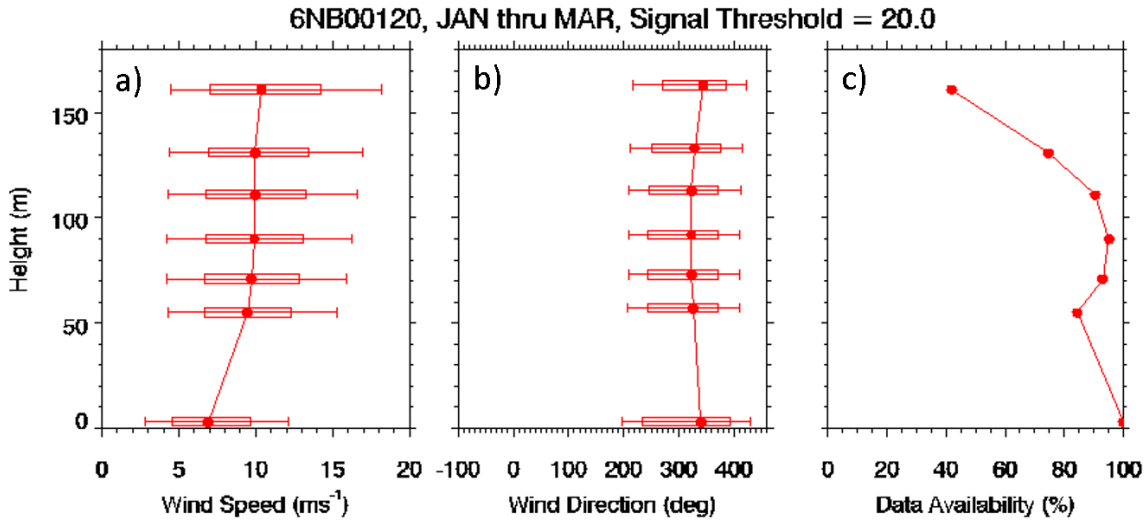


**Figure 2.1. Profiles of a) wind speed, b) wind direction, and c) data availability averaged over the winter season (January through March) during the Virginia deployment.**

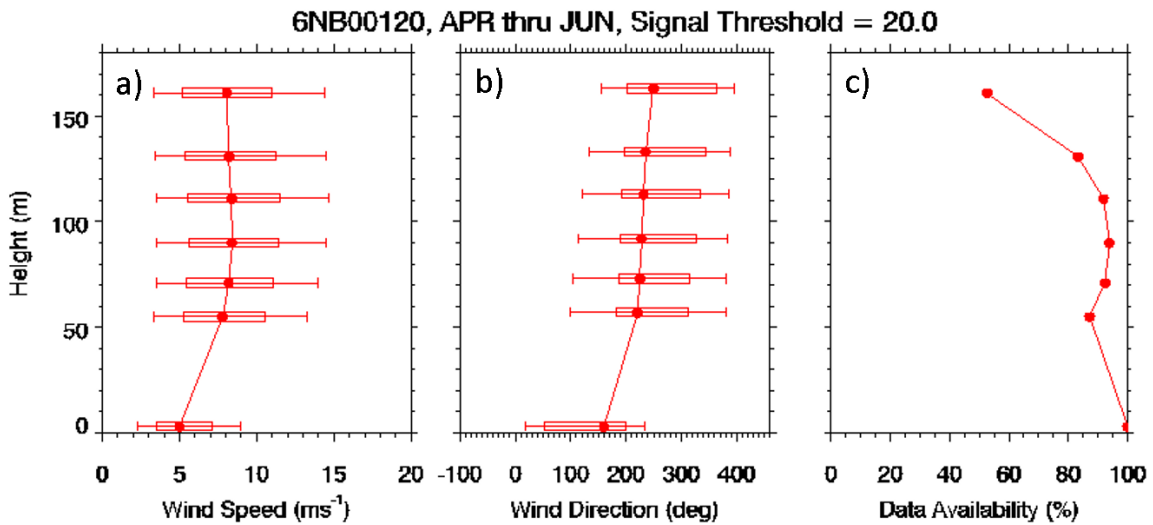


**Figure 2.2. Profiles of a) wind speed, b) wind direction, and c) data availability averaged over the spring season (April through June) during the Virginia deployment.**

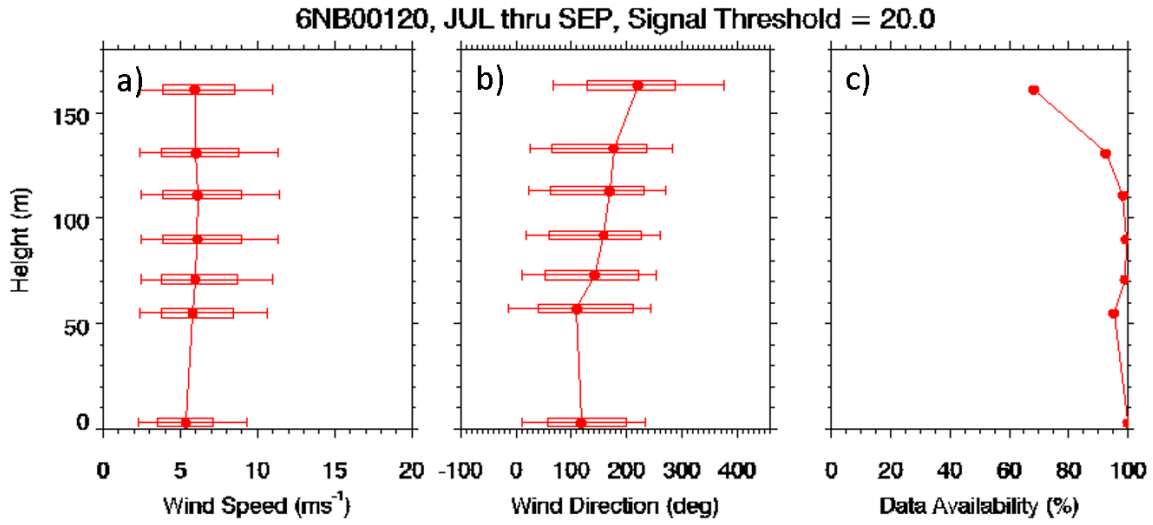


Figure 2.3. Profiles of a) wind speed, b) wind direction, and c) data availability averaged over the summer season (July through September) during the Virginia deployment.

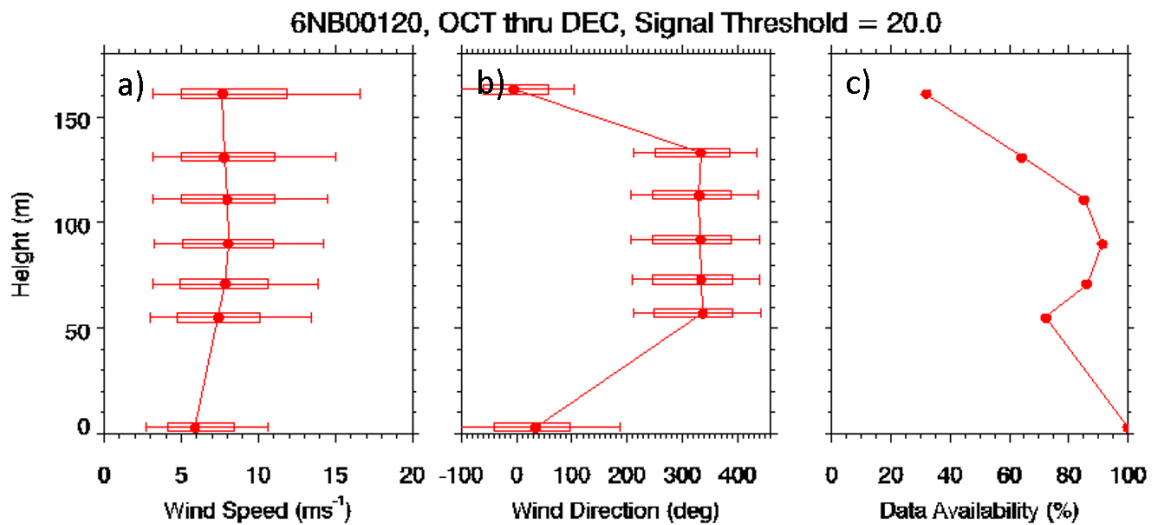


Figure 2.4. Profiles of a) wind speed, b) wind direction, and c) data availability averaged over the fall season (October through December) during the Virginia deployment.

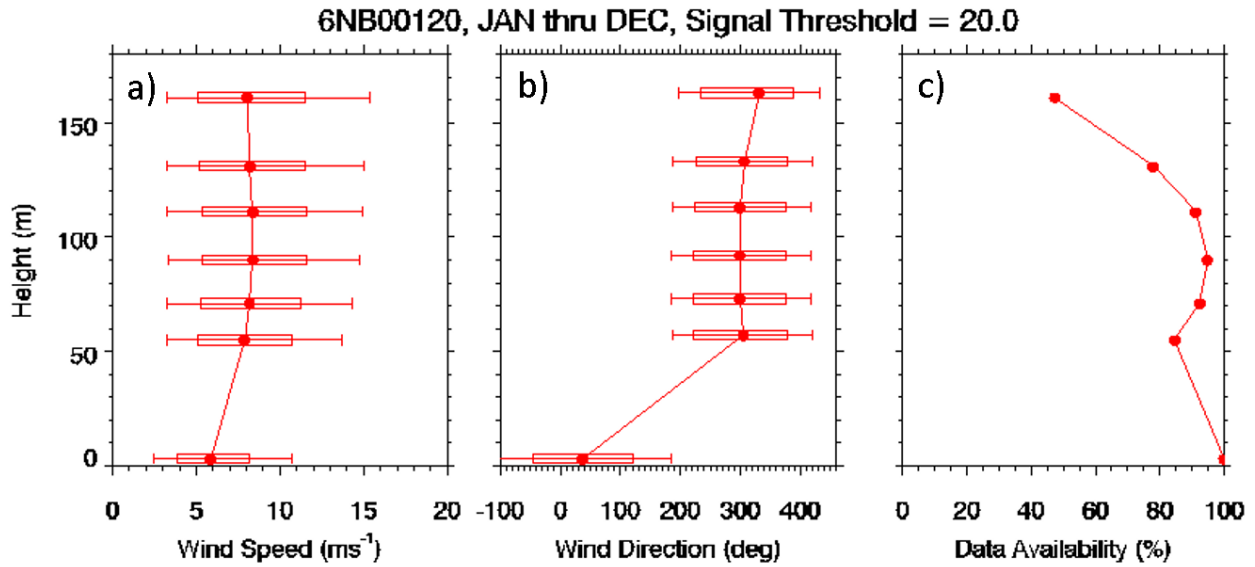


Figure 2.5. Profiles of a) wind speed, b) wind direction, and c) data availability averaged over the entire annual cycle.

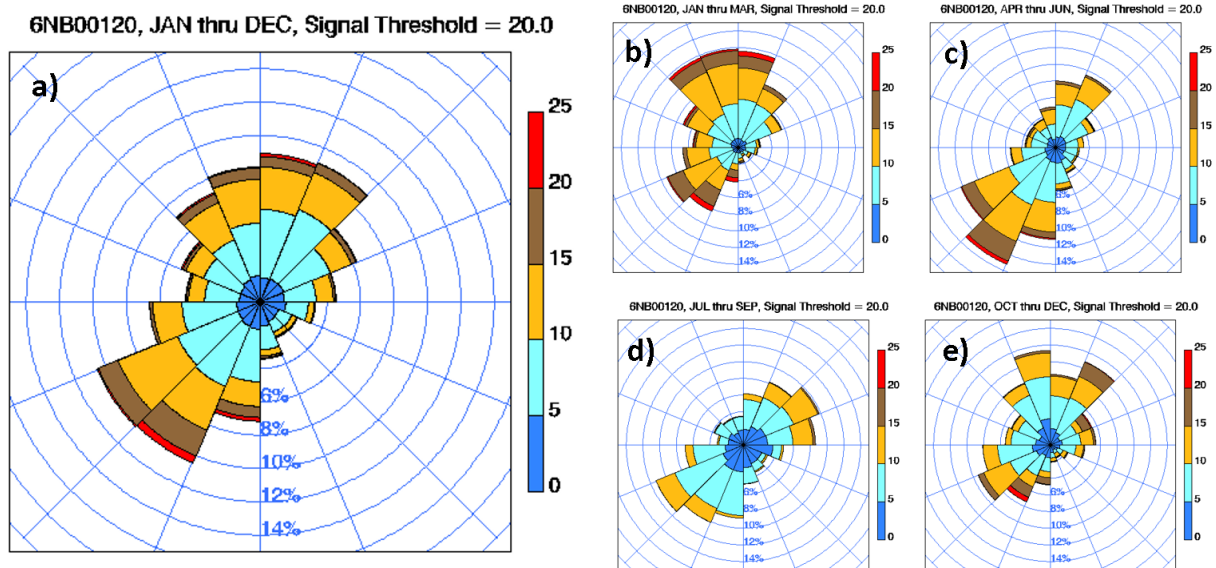


Figure 2.6. Wind roses from the lidar at the 90 m level for a) the entire annual cycle, b) winter (January through March), c) spring (April through June), d) summer (July through September), and e) fall (October through December).

## 2.1.2 Ocean Currents, Wave Properties, and Surface Winds

The WindSentinel buoys are each equipped with an acoustic Doppler current profiler (ADCP) from Nortek (Aquadopp Profiler) that provides measurements of ocean current at three depths (3.7 m, 7.7 m, and 11.7 m). Wave properties such as significant wave height, wave direction, and wave periods are measured with the TRIAXYS Next Wave II sensor. Two cup anemometers (Vector Instruments A100R/K) provide surface wind speed measurements. These sensors are located port and starboard at a height of about 4.1 m above the nominal water line. Surface wind direction is measured with a single

wind vane (Vector Instruments W200P-01/WR). This sensor is located near the port-side cup anemometer at a height of about 3.9 m above the nominal water line.

We note that all directions are measured relative to magnetic north, as opposed to true north. The magnetic declination at the 6NB00120 deployment site was about 11.3° during the deployment period. Thus, one needs to subtract 11.3° from the directions shown in this report in order to reference to true north.

Figures 2.7 through 2.10 show seasonally averaged distributions of ocean current and direction at -7.7 m, significant wave height and direction, and surface wind speed and direction. These figures show results for winter (January through March), spring (April through June), summer (July through September), and fall (October through December) respectively. Figure 2.11 shows distributions averaged over the entire annual cycle.

The surface wind speed shown in Figures 2.7 through 2.11 were obtained by averaging the data from the port and starboard anemometers.

Overall, ocean currents tend to show a slight preference for north to northeasterly flow (vector direction, i.e., the “to” direction). The largest waves tend to propagate from the northeast quadrant, but lower amplitude waves from the southeast quadrant are also quite common. The surface wind roses indicate that there are primarily two preferred directions: north-northeasterly and south-southwesterly. The strongest winds tends to blow to the north-northeast. The ocean current information depicted here is from a single depth. Current vectors from all depths are shown in the appendix.

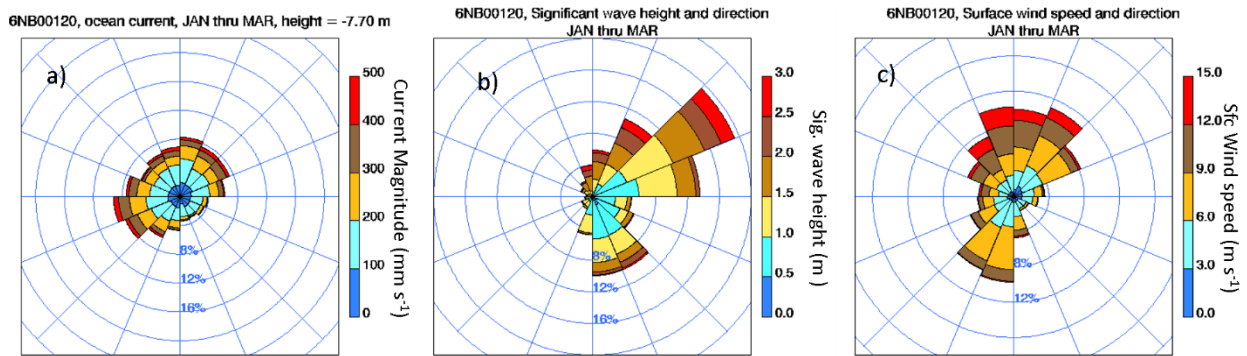


**Figure 2.7. Distributions of a) ocean current and direction, b) significant wave height and direction, c) surface wind speed and direction for January through March.**

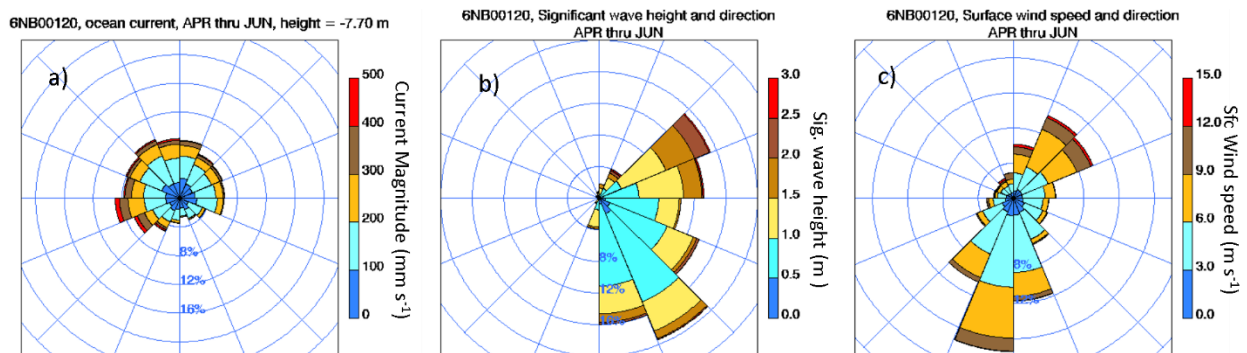


**Figure 2.8. Distributions of a) ocean current and direction, b) significant wave height and direction, c) surface wind speed and direction for April through June.**

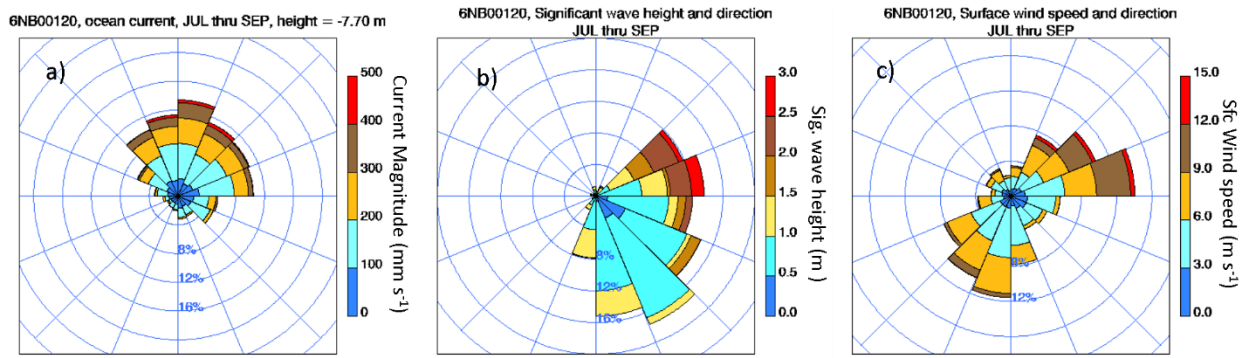


**Figure 2.9. Distributions of a) ocean current and direction, b) significant wave height and direction, c) surface wind speed and direction for July through September.**

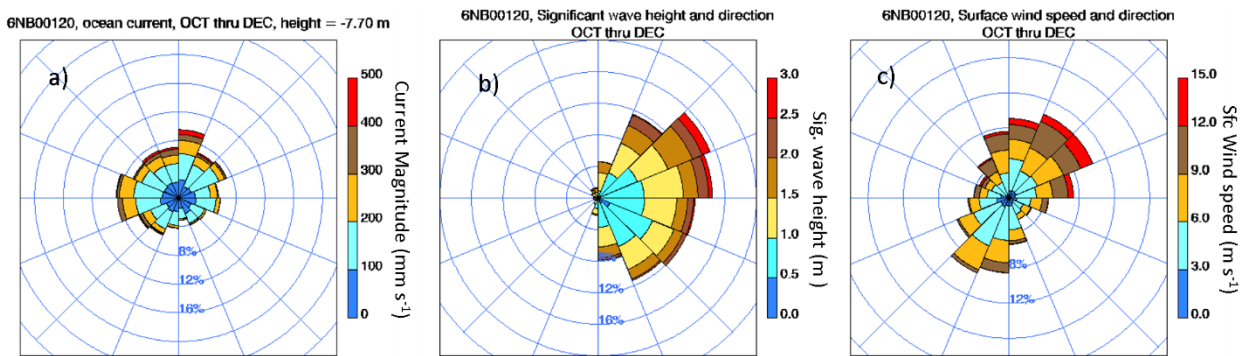


**Figure 2.10. Distributions of a) ocean current and direction, b) significant wave height and direction, c) surface wind speed and direction for October through December.**

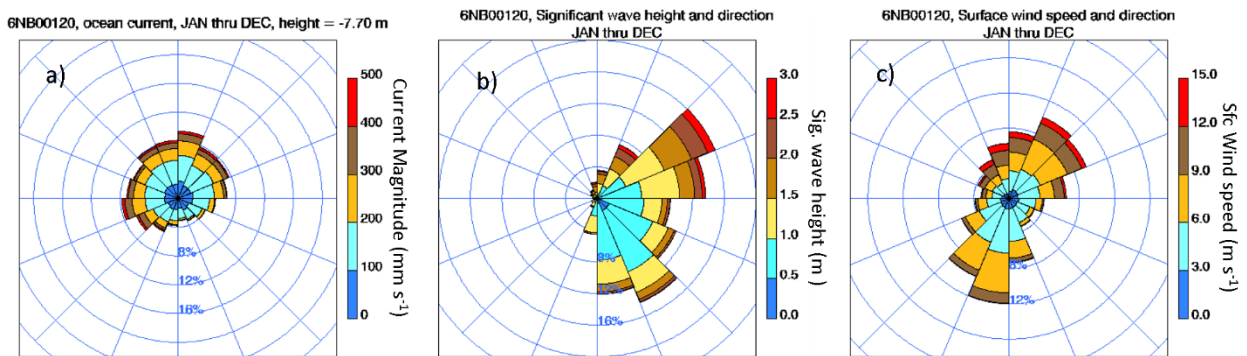


**Figure 2.11. Distributions of a) ocean current and direction, b) significant wave height and direction, c) surface wind speed and direction averaged over all seasons.**

### 2.1.3 Wind Shear and Air-Sea Temperature Difference

As we began our analysis of the Virginia buoy, it became obvious there was a strong relationship between wind speed shear and the air-sea temperature differential. Figure 2.12 displays a time series of the lidar wind speed and direction at 90 m, the surface wind and direction, and the air and sea temperature. This time series covers the entire deployment period from December 2014 through May 2016. We note the large temperature differences tend to correspond to the large wind speed differences.

Figure 2.13 shows the wind speed difference between the lidar at 90 m and the surface anemometer versus the air-sea temperature difference. This figure shows that under unstable conditions (air temperature < sea temperature) the wind shear is small, as expected. Under stable conditions (air temperature > sea temperature) the wind shear increases rapidly as the temperature differential increases.

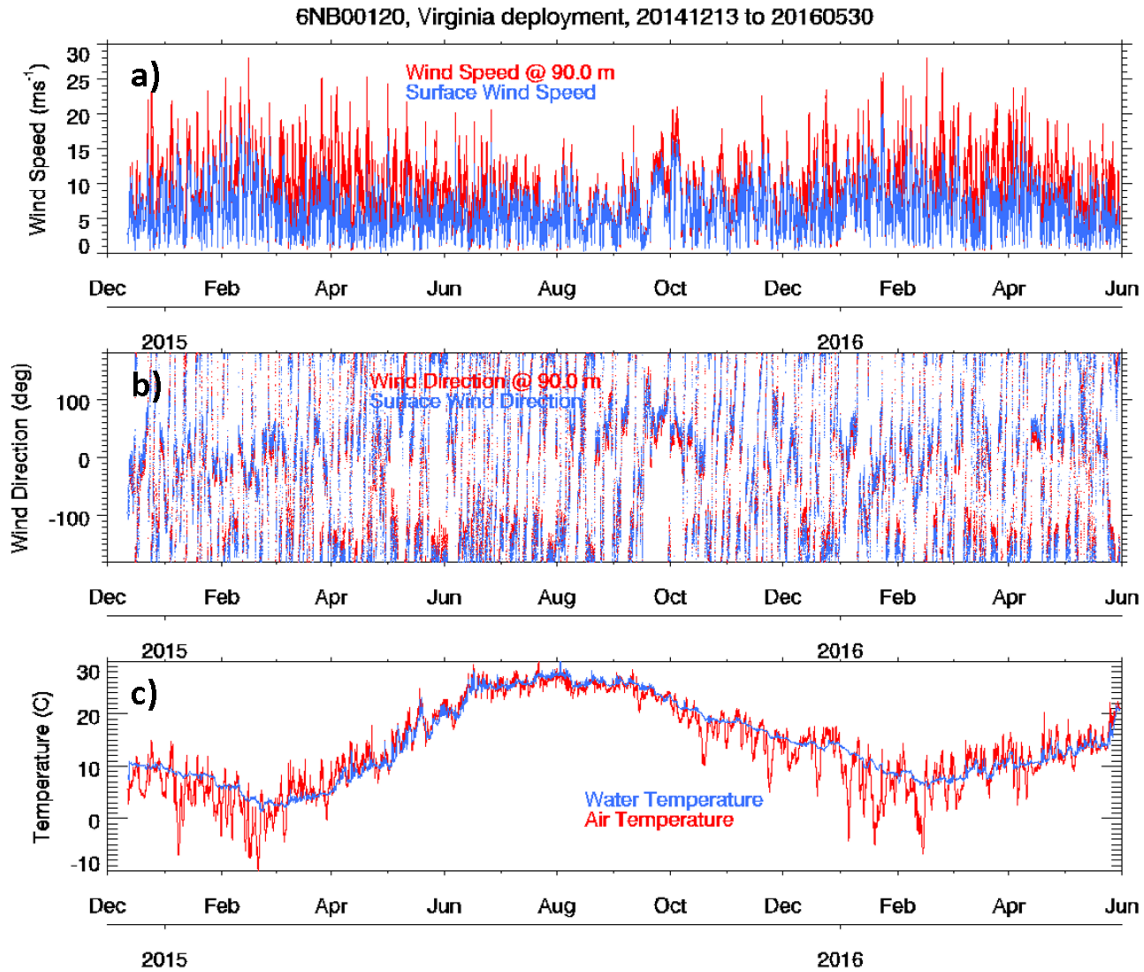


Figure 2.12. a) Wind speed from the surface (blue) and the Vindicator III at 90 m (red), b) wind direction from the surface (blue) and the Vindicator III at 90 m (red), and c) ocean water temperature (blue) and air temperature (red).

## 6NB00120, Virginia deployment, 20141212 to 20160530

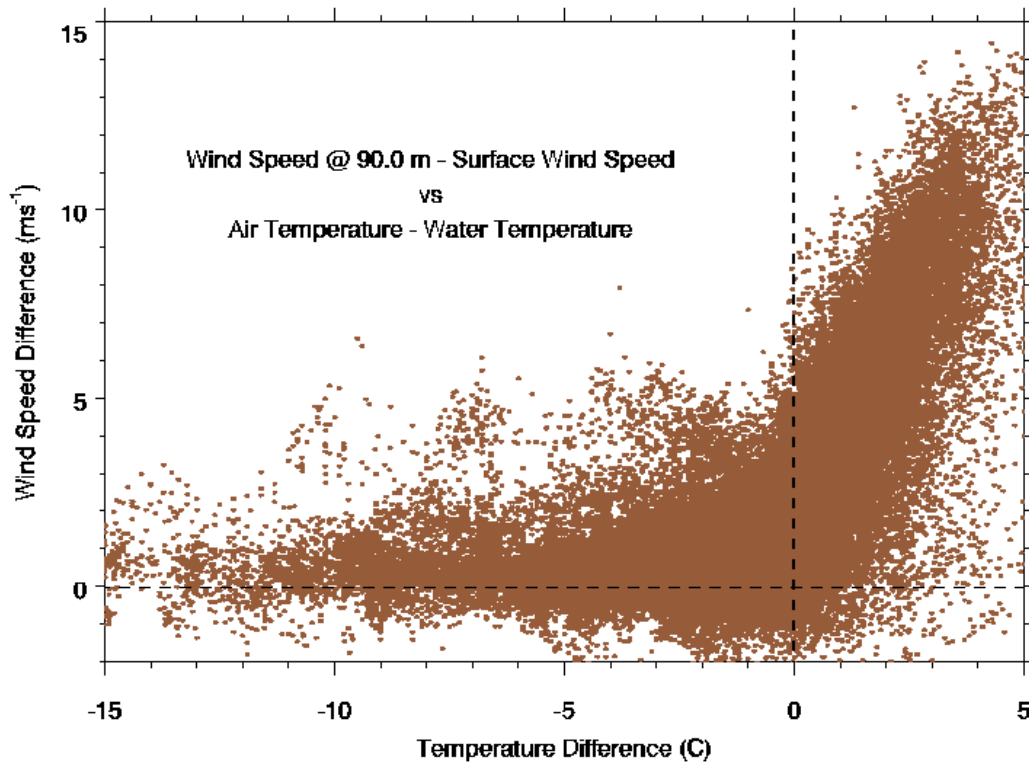
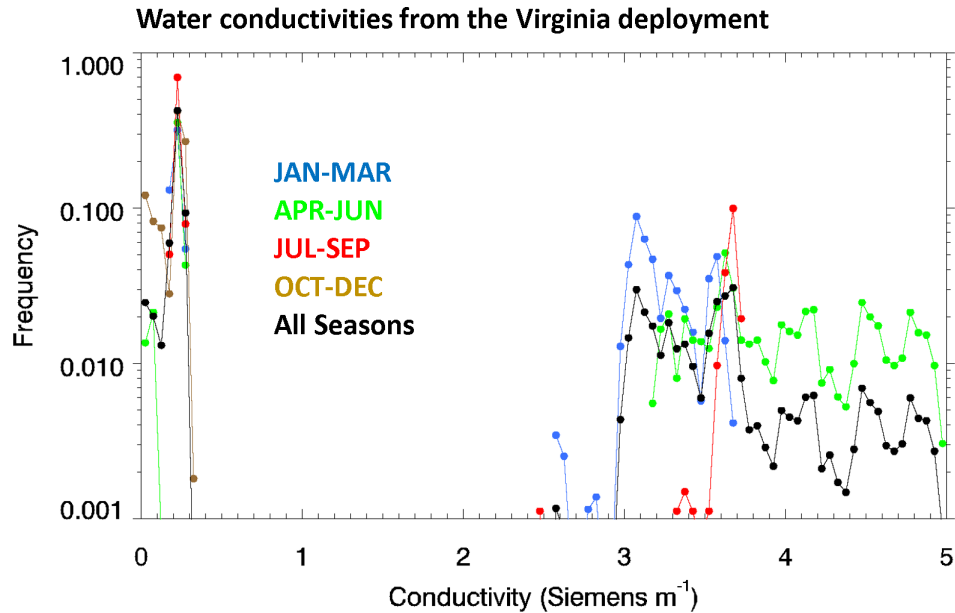


Figure 2.13. Wind speed difference between the lidar at 90 m and the surface as a function of the air-sea temperature difference for the Virginia deployment.

### 2.1.4 Conductivity

Figure 2.14 shows the frequency of occurrence of ocean water conductivities measured by the SeaBird CTD sensor (Model 37SMP-1j-2-3c) on the Virginia buoy. The conductivity histograms tend to show a bimodal distribution for all seasons. There is a prominent peak at low conductivities at about 0.2 Siemens m<sup>-1</sup>. This peak does not change much seasonally. The secondary maxima at higher conductivities do, however, show some variation with season. In the winter (January through March), the secondary max occurs at about 3 Siemens m<sup>-1</sup>, then shifts to ~3.6 Siemens m<sup>-1</sup> in the spring (April through June). And then it shifts to about 3.7 Siemens m<sup>-1</sup> in the summer (July through September).



**Figure 2.14.** Frequency of occurrence of ocean water conductivities covering the entire deployment period (12 Dec 2014 to 31 May 2016). The blue curve is for winter (January through March), the green curve is for spring (April through June), the red curve corresponds to summer (July through September), the brown curve is for fall (October through December), and the black curve covers all seasons.

## 2.2 New Jersey Buoy Observations

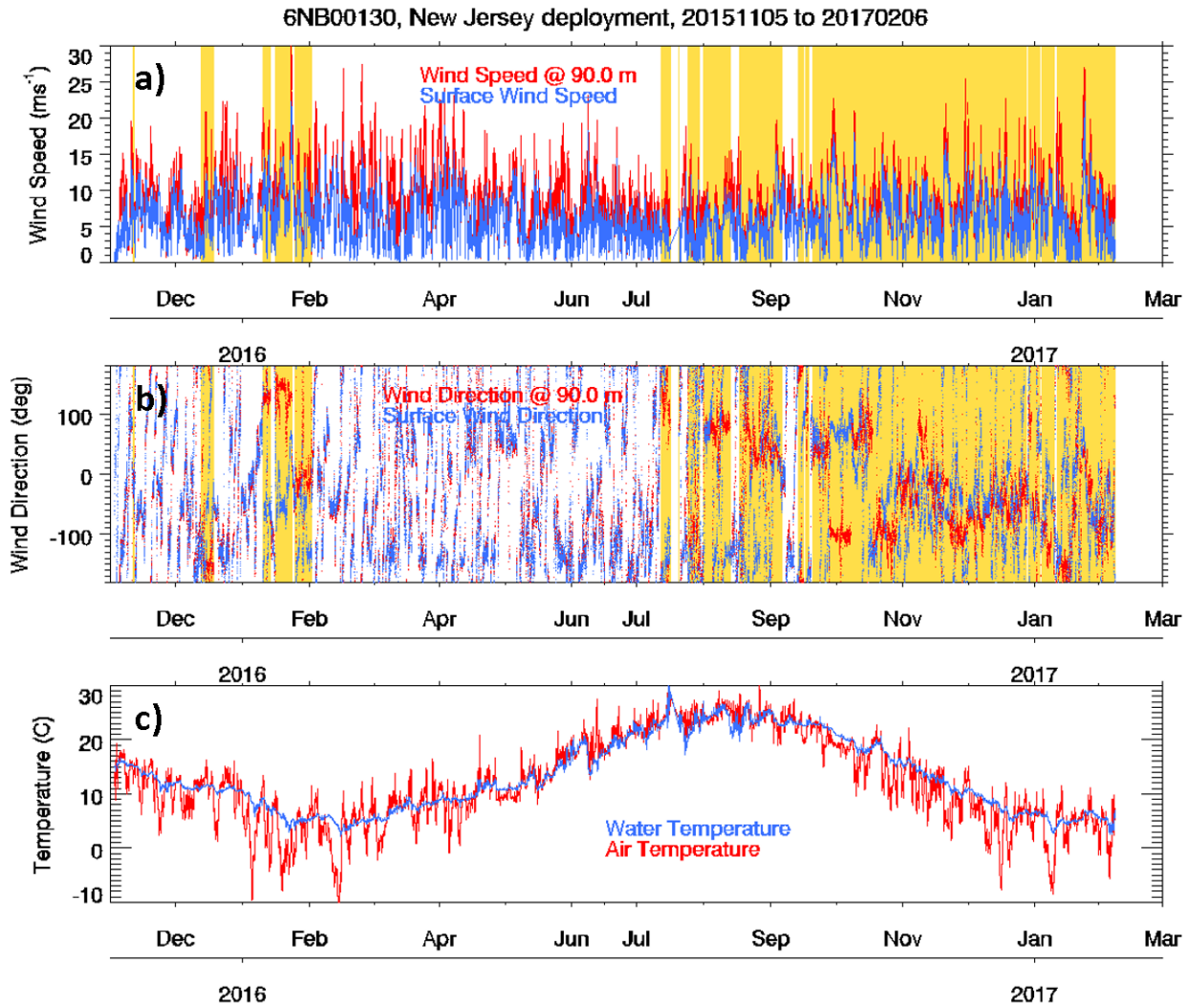
### 2.2.1 Lidar Winds

Figure 2.15 displays a time series of the lidar wind speed and direction at 90 m, the surface wind and direction, and the air and sea temperature. This time series covers the entire deployment period from November 2015 to February 2017. We note the large temperature differences tend to correspond to the large wind speed differences.

The yellow shaded regions in Figure 2.15 a) and b) represent time periods with invalid roll, pitch, and yaw data from the Vindicator internal attitude sensor. These invalid data were discovered in the course of reprocessing the raw radial velocity data, and we suspect may be caused by some sort of data logging error. The Vindicator uses the roll, pitch, and yaw data to perform motion compensation. Since the Vindicator “motion compensation” algorithm is basically a coordinate rotation (i.e., a rotation from the Vindicator’s coordinate to an Earth-fixed frame of reference), this affects the wind direction, but does not affect the wind speed since the vector magnitude is invariant under rotation.

The effect of the invalid attitude data on the wind direction can be seen by comparing the surface wind direction with the lidar wind direction in Figure 2.15b). During periods with good attitude data, the surface and lidar wind directions are well correlated and in close agreement. During the periods with bad attitude the two measurements can disagree substantially.

As indicated in Figure 2.15, the problems with the Vindicator attitude data became more frequent with time over the course of the deployment.



**Figure 2.15.** a) Wind speed from the surface (blue) and the Vindicator III at 90 m (red), b) wind direction from the surface (blue) and the Vindicator III at 90 m (red), c) ocean water temperature (blue) and air temperature (red). The yellow shaded regions in panels a) and b) represent time periods with invalid roll, pitch, and yaw data from the Vindicator internal attitude sensor.

Figures 2.16 through 2.20 show seasonally averaged profiles of wind speed and direction from the lidar. Also included in these plots for reference are the winds from the cup anemometers on the buoy. Figures 2.16 through 2.19 show results for winter (January through March), spring (April through June), summer (July through September), and fall (October through December), respectively. Figure 2.20 shows the wind speed and direction profile averaged over the entire annual cycle.

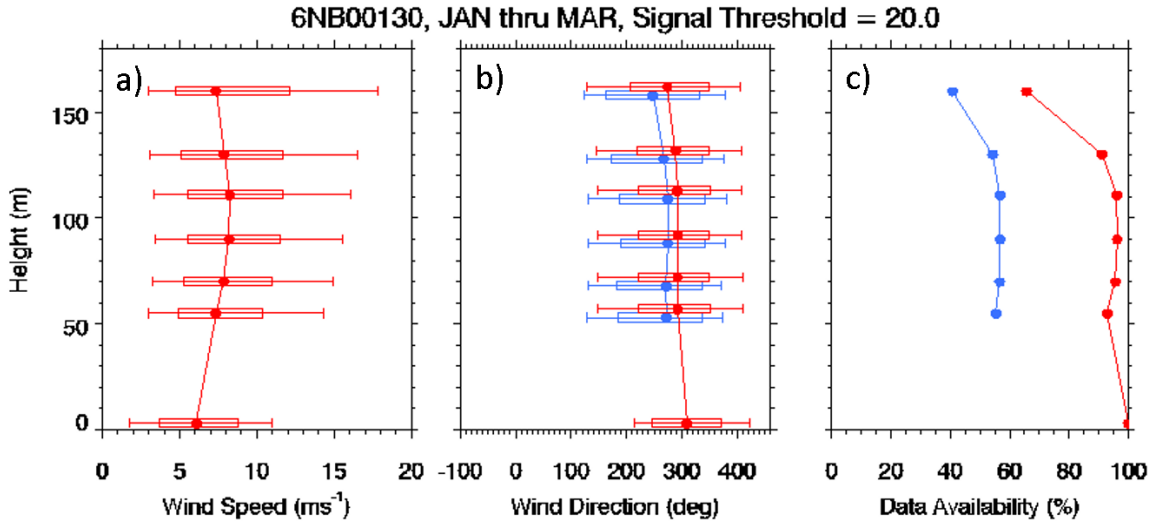


Figure 2.16. Profiles of a) wind speed, b) wind direction, and c) data availability averaged over the winter season (January through March) during the New Jersey deployment. Red curves use all data, and the blue curves use only data when the Vindicator attitude sensor was operating well.

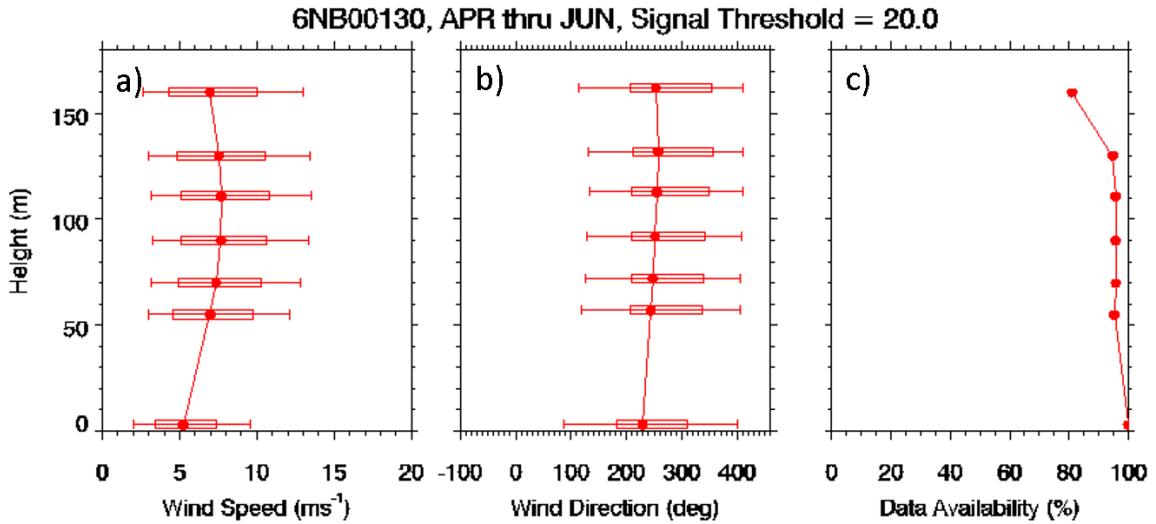
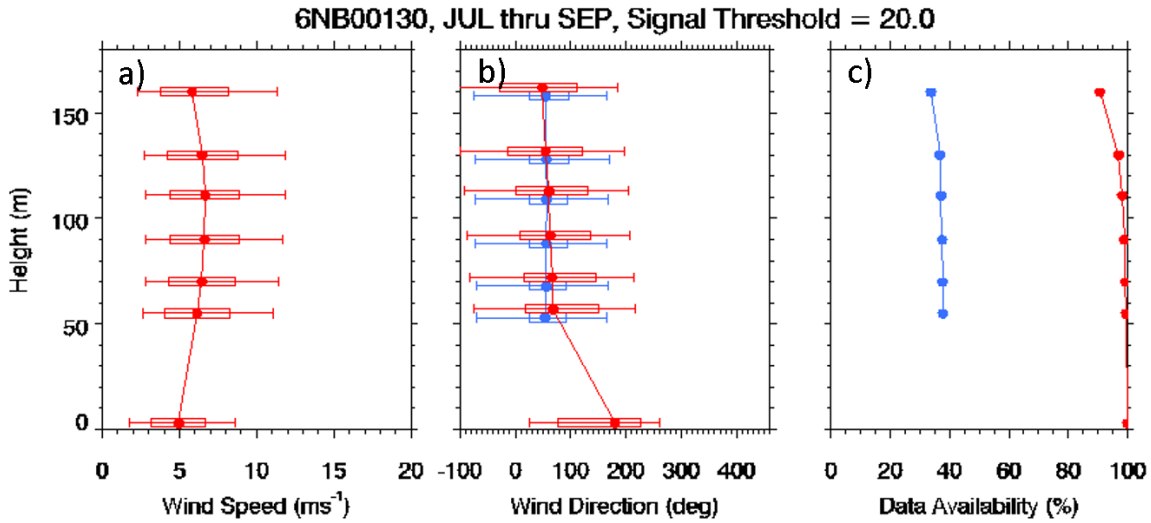
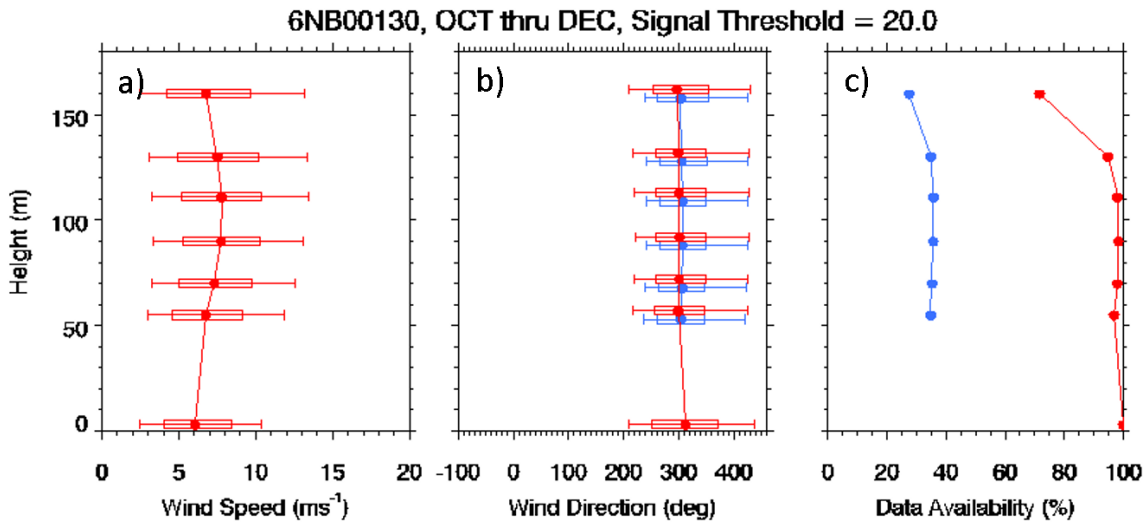


Figure 2.17. Profiles of a) wind speed, b) wind direction, and c) data availability averaged over the spring season (April through June) during the New Jersey deployment.



**Figure 2.18.** Profiles of a) wind speed, b) wind direction, and c) data availability averaged over the summer season (July through September) during the New Jersey deployment. Red curves use all data, and the blue curves use only data when the Vindicator attitude sensor was behaving.



**Figure 2.19.** Profiles of a) wind speed, b) wind direction, and c) data availability averaged over the fall season (October through December) during the New Jersey deployment. Red curves use all data, and the blue curves use only data when the Vindicator attitude sensor was behaving.

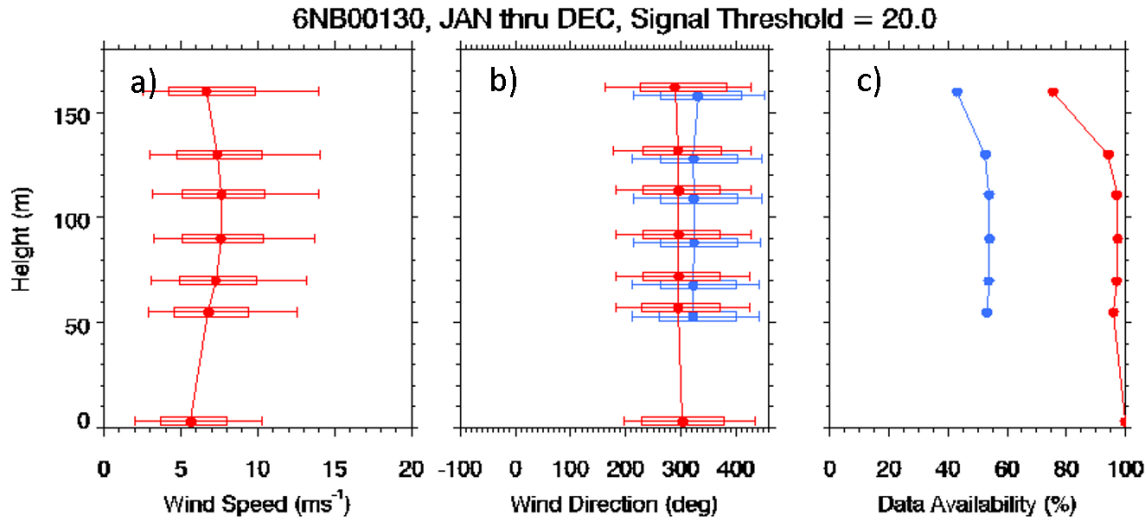


**Figure 2.20. Profiles of a) wind speed, b) wind direction, and c) data availability averaged over the entire annual cycle. Red curves use all data, and the blue curves use only data when the Vindicator attitude sensor was behaving.**

The wind direction profiles shown in Figures 2.16b) through 2.19b) were computed by filtering out the periods with bad attitude data. The blue curves in Figures 2.16 through 2.20 show the results *with* filtering, and the red curves use no such filtering.

We note that the wind speed profiles tend to show a slight maximum at 90 m. A previous validation study using the same model of Vindicator at the BAO suggests that this instrument tends to underestimate wind speed both above and below the 90 m level. The Vindicator is designed such that the laser is focused at the 90 m level, thus optimizing its performance at this level. The BAO study indicates that the Vindicator performs well at this level, but tends to exhibit a slow bias above and below the 90 m level, particularly above about 100 m where the return signal strength decreases rapidly with attitude.

With this in mind we initially focused our attention on the results at the 90 m level. Overall we find the mean winds tend to blow from northwest at about  $8 \text{ ms}^{-1}$ , when averaged of the entire annual cycle (Figure 2.20). The weakest winds occur during the summer months ( $\sim 6 \text{ m s}^{-1}$ ), and the strongest winds occur during the winter months ( $\sim 9 \text{ m s}^{-1}$ ).

Also shown in Figures 2.16 through 2.20 are profiles of data availability. The data availability profiles closely mimic the mean return signal strength and provide a rough indicator of data quality. As noted previously, the Vindicator is designed such that the laser beam is focused at the 90 m level, and this is precisely where the data availability profiles exhibit their maximum values. The annually averaged data availability was about 95% at 90 m. The lowest ( $\sim 90\%$ ) data availabilities occurred during the winter, and the highest ( $\sim 100\%$ ) data availabilities occurred during the summer.

Figure 2.21 summarizes the results from the Vindicator lidar at the 90 m level in the form of seasonally averaged wind roses. The annually averaged wind rose shows that the predominate wind direction is from the southwest. Somewhat weaker flow out of the northwest occurs frequently during the fall and winter months. The results shown in Figure 2.21 were computed by filtering out periods with bad Vindicator attitude data.

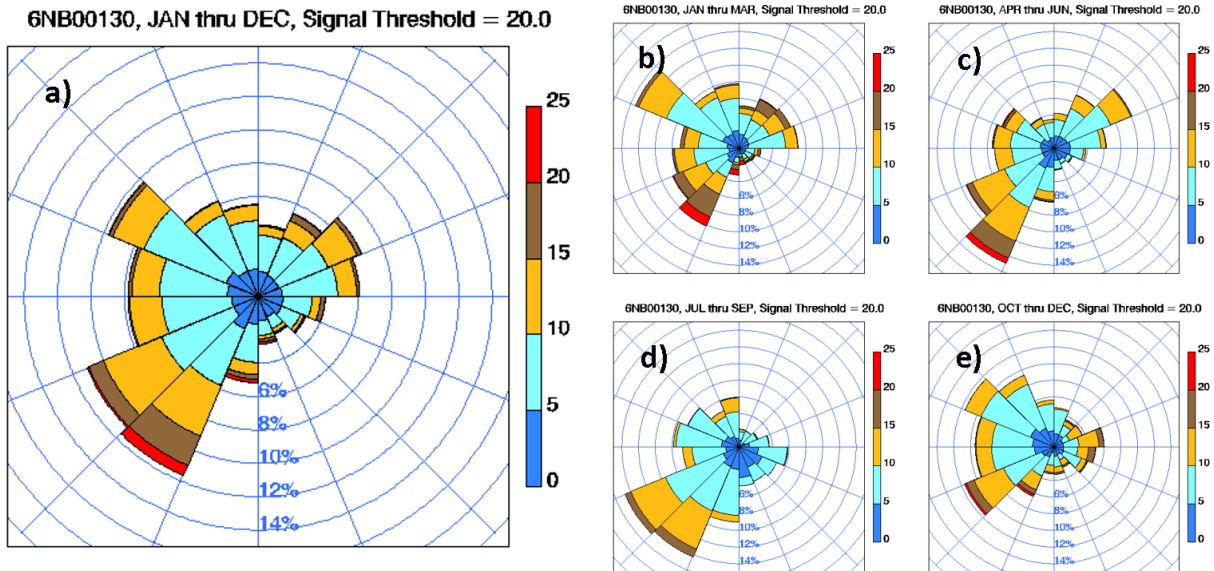


**Figure 2.21. Wind roses from the lidar at the 90 m level for a) the entire annual cycle, b) winter (January through March), c) spring (April through June), d) summer (July through September), and e) fall (October through December). Data have been filtered to remove periods with bad attitude data.**

## 2.2.2 Ocean Currents, Wave Properties, and Surface Winds

We note that all directions are measured relative to magnetic north, as opposed to true north. The magnetic declination at the 6NB00120 deployment site was about  $12.4^\circ$  during the deployment period. Thus, one needs to subtract  $12.4^\circ$  from the directions shown in this report in order to reference to true north.

Figures 2.22 through 2.25 show seasonally averaged distributions of ocean current and direction at  $-7.7$  m, significant wave height and direction, and surface wind speed and direction. These figures show results for winter (January through March), spring (April through June), summer (July through September), and fall (October through December), respectively. Figure 2.26 shows distributions averaged over the entire annual cycle.

The surface wind roses shown in Figures 2.22 through 2.26c) were obtained by averaging the data from the port and starboard anemometers.

Overall, ocean currents tend to show a strong preference for flow towards the east-northeast (northeasterly) flow (vector direction, i.e., the “to” direction) in all seasons. We note that this is consistent with the configuration of the coast and the fact that the direction is measured relative to magnetic north. Wave directions are almost exclusively from the southeast quadrant. This is consistent the configuration of the coast line and with how close this buoy is to the coast (i.e., only 5 km out). The strongest surface winds tend to blow from the northwest during the fall and winter and from either the southwest or northeast during the spring and summer.

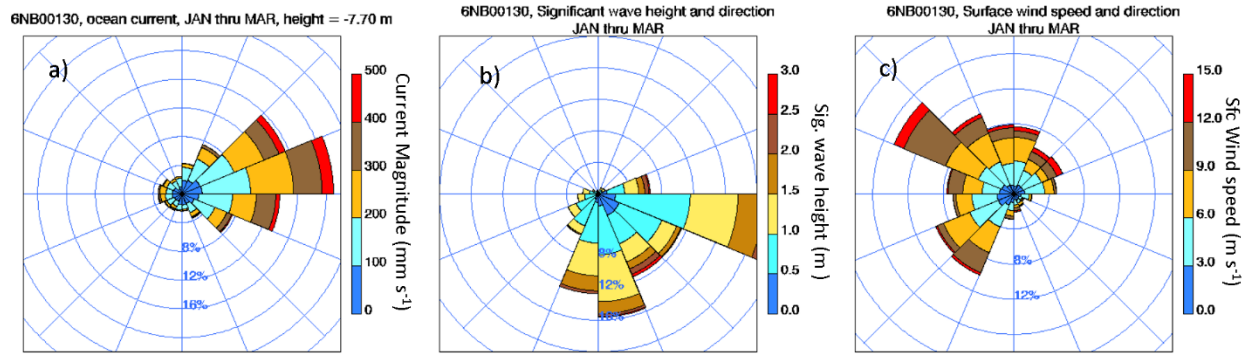


Figure 2.22. Distributions of a) ocean current and direction, b) significant wave height and direction, c) surface wind speed and direction for January through March.

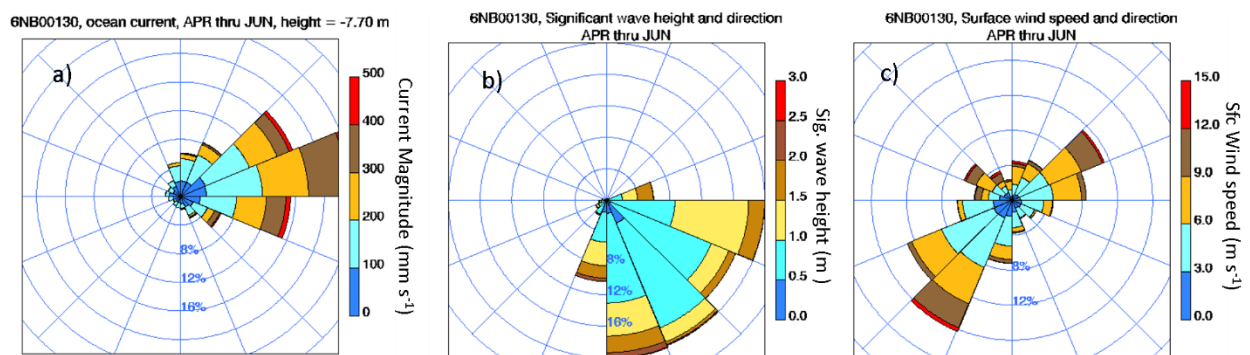


Figure 2.23. Distributions of a) ocean current and direction, b) significant wave height and direction, c) surface wind speed and direction for April through June.

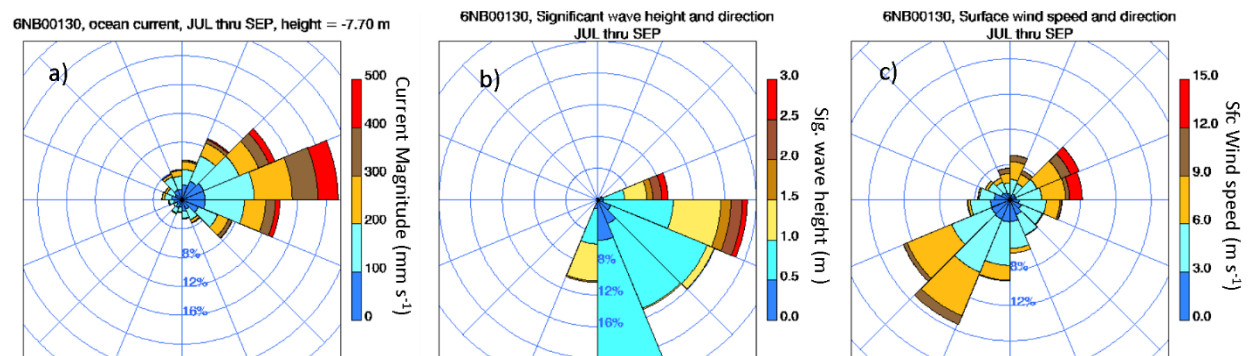
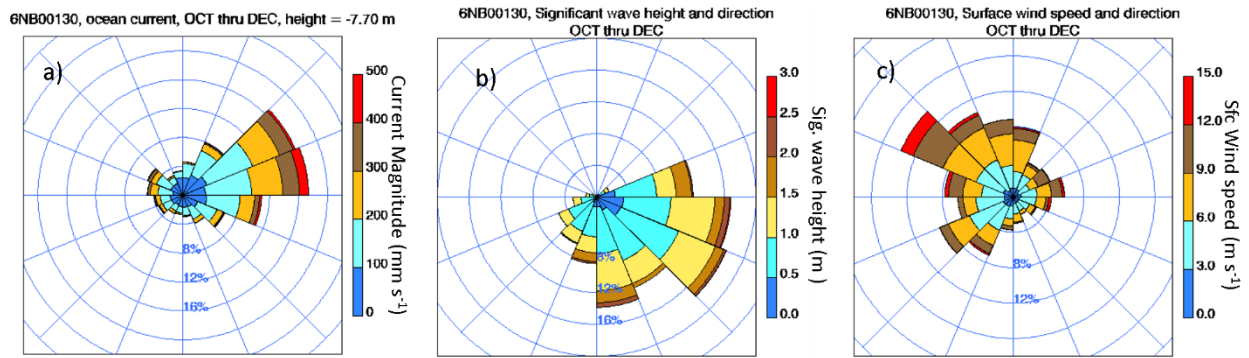
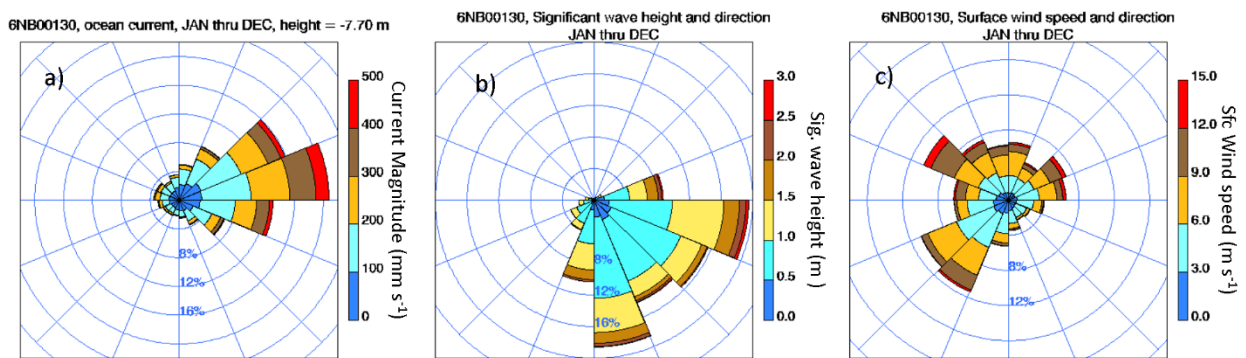


Figure 2.24. Distributions of a) ocean current and direction, b) significant wave height and direction, c) surface wind speed and direction for July through September.



**Figure 2.25. Distributions of a) ocean current and direction, b) significant wave height and direction, c) surface wind speed and direction for October through December.**



**Figure 2.26. Distributions of a) ocean current and direction, b) significant wave height and direction, c) surface wind speed and direction averaged over all seasons.**

### 2.2.3 Wind Shear and Air-Sea Temperature Difference

Consistent with the results for the Virginia buoy, there was a similarly strong relationship between wind speed shear and the air-sea temperature differential. The time-series shown in Figure 2.27 shows that large temperature differences tend to correspond to the large wind speed differences.

Figure 2.28 shows the wind speed difference between the lidar at 90 m and the surface anemometer versus the air-sea temperature difference. This figure shows that under unstable conditions (air temperature < sea temperature), the wind shear is small, as expected. Under stable conditions (air temperature > sea temperature), the wind shear increases rapidly as the temperature differential increases.

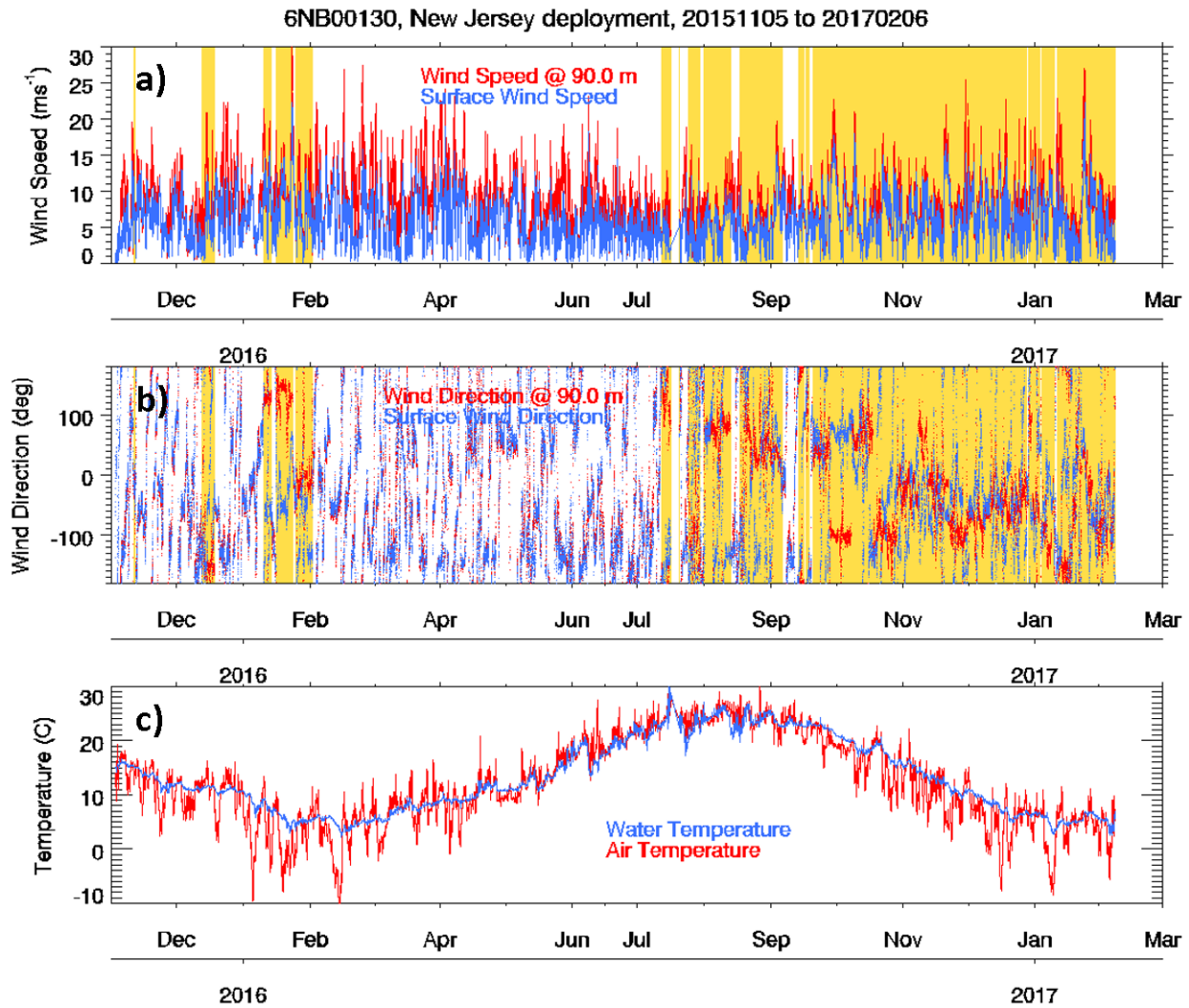


**Figure 2.27.** a) Wind speed from the surface (blue) and the Vindicator III at 90 m (red), b) wind direction from the surface (blue) and the Vindicator III at 90 m (red), c) ocean water temperature (blue) and air temperature (red). The yellow shaded regions in panels a) and b) represent time periods with invalid roll, pitch, and yaw data from the Vindicator internal attitude sensor.

6NB00130, New Jersey deployment, 20151103 to 20170206

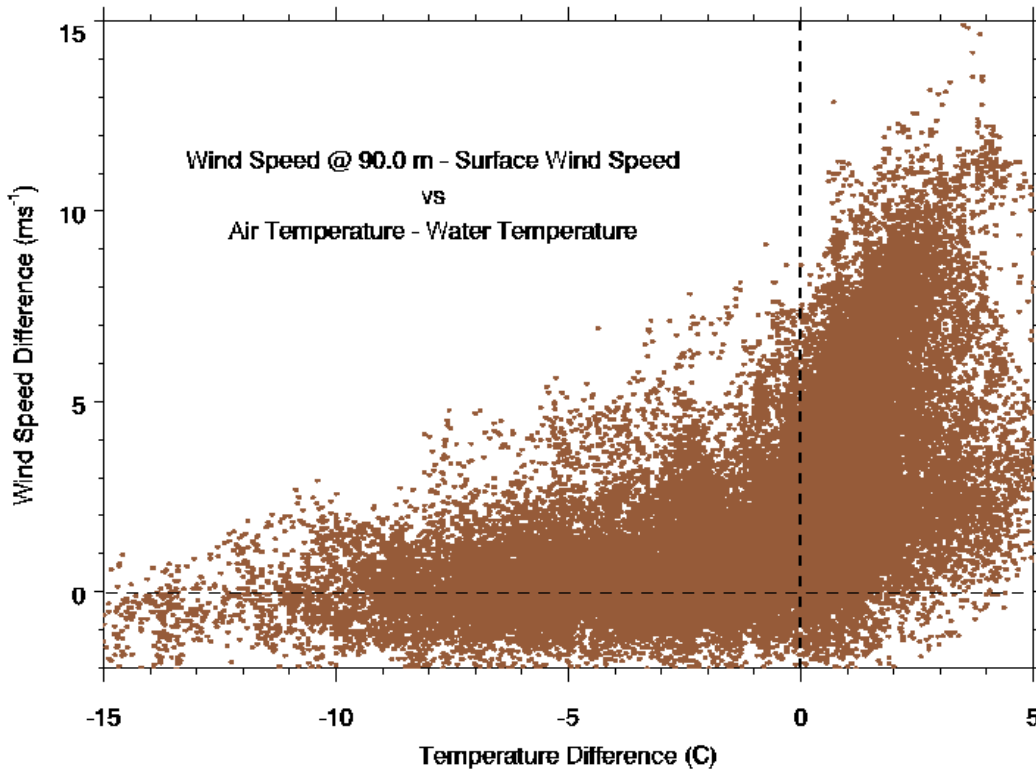
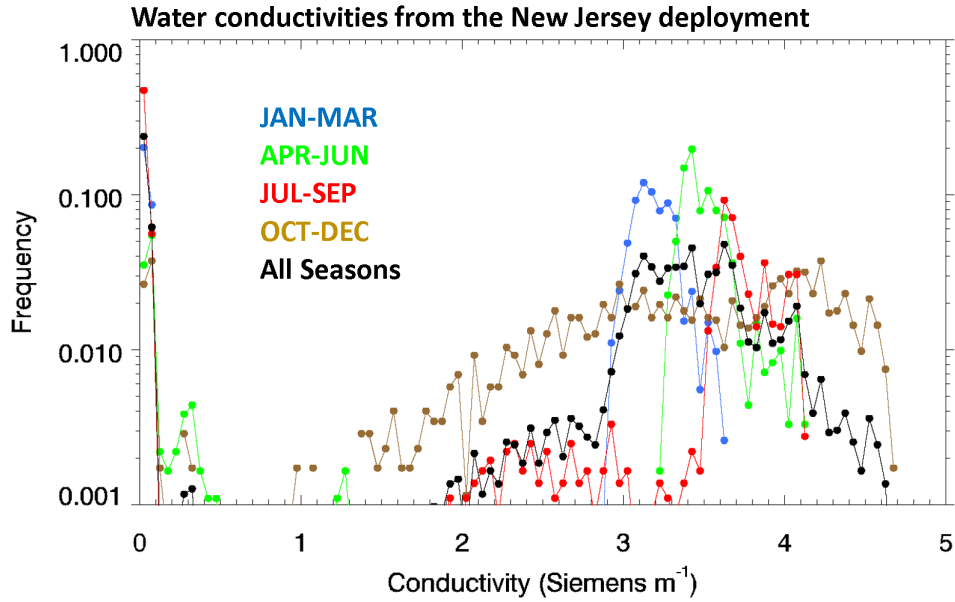


Figure 2.28. Wind speed difference between the lidar at 90 m and the surface as a function of the air-sea temperature difference for the New Jersey deployment.

## 2.2.4 Conductivity

Figure 2.29 shows the frequency of occurrence of ocean water conductivities measured by the SeaBird CTD sensor (Model 37SMP-1j-2-3c) from the New Jersey buoy. The conductivity histograms tend to show a bimodal distribution for all seasons. There is a prominent peak at low conductivities at  $< 0.1$  Siemens  $\text{m}^{-1}$ . This peak does not change much seasonally. The secondary maximum at higher conductivities does, however, show some variation with season. In the winter (January through March) the secondary max occurs at about 3.1 Siemens  $\text{m}^{-1}$ , then shifts to  $\sim 3.4$  Siemens  $\text{m}^{-1}$  in the spring (April through June). And then about 3.6 Siemens  $\text{m}^{-1}$  in the summer (July through September)



**Figure 2.29.** Frequency of occurrence of ocean water conductivities covering the entire deployment period (11 Nov 2015 to 7 Feb 2017). The blue curve is for winter (January through March), the green curve is for spring (April through June), the red curve corresponds to summer (July through September), the brown curve is for fall (October through December), and the black curve covers all seasons.

## 3.0 Discussion and Summary

PNNL has deployed DOE's lidar buoys off the coasts of Virginia and New Jersey in excess of a year in each location. The lidars have provided the first observations of hub-height winds that cover a full annual cycle in open offshore waters in the United States. In general, data recovery from the buoy systems was good as was the correspondence among redundant sensors. There were a few notable exceptions. On both buoys, the CTD probes lost their ability to measure conductivity several months into the deployment due to biofouling. For applications in which this is a critical measurement, additional maintenance will need to be planned. One of the cup anemometers on the New Jersey buoy also deteriorated during the deployments, demonstrating the value of redundant surface wind speed measurements. The most serious issue affected the New Jersey buoy's lidar, which failed to record critical attitude information during a significant fraction of the deployment. This did not affect the wind speed measurement from the lidar, but the absence of attitude information prevented calculation of wind direction as a function of height. (Following recovery, the problem was traced to a faulty circuit board, which was replaced by the manufacturer.)

Beyond the faulty attitude information for the New Jersey lidar, the lidars revealed some limitations. While they functioned as designed, the laser power appeared to be low for the sometimes very clean marine environment. As a result, during periods of low carrier-to-noise ratio (CNR; similar to signal-to-noise ratio), they tended to report wind speeds that were too low. This is a characteristic of Doppler lidars when the signal processing algorithms include samples with CNR values that are too low. The result was a tendency for the range gates above and below the 90 m level (tuned for the best signal) to report wind speeds that were biased low. Post-processing (not described here) with higher CNR thresholds was largely able to eliminate the low-speed bias but at the cost of significantly reduced data availability. For some range gates, this dropped availability below the Carbon Trust (2013) recommendation of at least 85%. We believe the wind data reported here after post-processing to be of good quality. However, PNNL is also in the process of upgrading the buoys to have more powerful lidar systems.

One notable observation from both buoys is the dramatic dependence of the wind shear on atmospheric stability as indicated by the air-sea temperature difference. Additional analysis will be reported elsewhere that places this behavior in the context of atmospheric surface layer theory, but it is clear that the commonly used neutral log law will not be a fully suitable representation of wind shear off the U.S. East Coast.

In summary, the initial deployments of the DOE lidar buoys have each yielded more than a year of atmospheric and oceanographic data by including hub-height winds, and they represent the first such observations in U.S. waters. These data are beginning to fill a long-standing observational gap for the wind energy community in the United States.

## 4.0 References

Carbon Trust Offshore Wind Accelerator Roadmap for the Commercial Acceptance of Floating Lidar Technology, CTC819 Version 1, 21 November 2013,

<http://www.carbontrust.com/news/2013/11/roadmap-for-commercial-acceptance-of-floating-lidartechnologies>

U.S. DOE and U.S. DOI. 2016. *National Offshore Wind Strategy: Facilitating the Development of the Offshore Wind Industry in the United States*. DOE/GO-102016-4866, U.S. Department of Energy and U.S. Department of Energy, Washington, D.C. Available at

<https://www.energy.gov/sites/prod/files/2016/09/f33/National-Offshore-Wind-Strategy-report-09082016.pdf>.

# Appendix A

## Distributions and Diurnal Composites of Wind, Temperature and Current Data from the Lidar Buoys

### A.1 Virginia Buoy

#### A.1.1 Distributions of Surface Wind Information

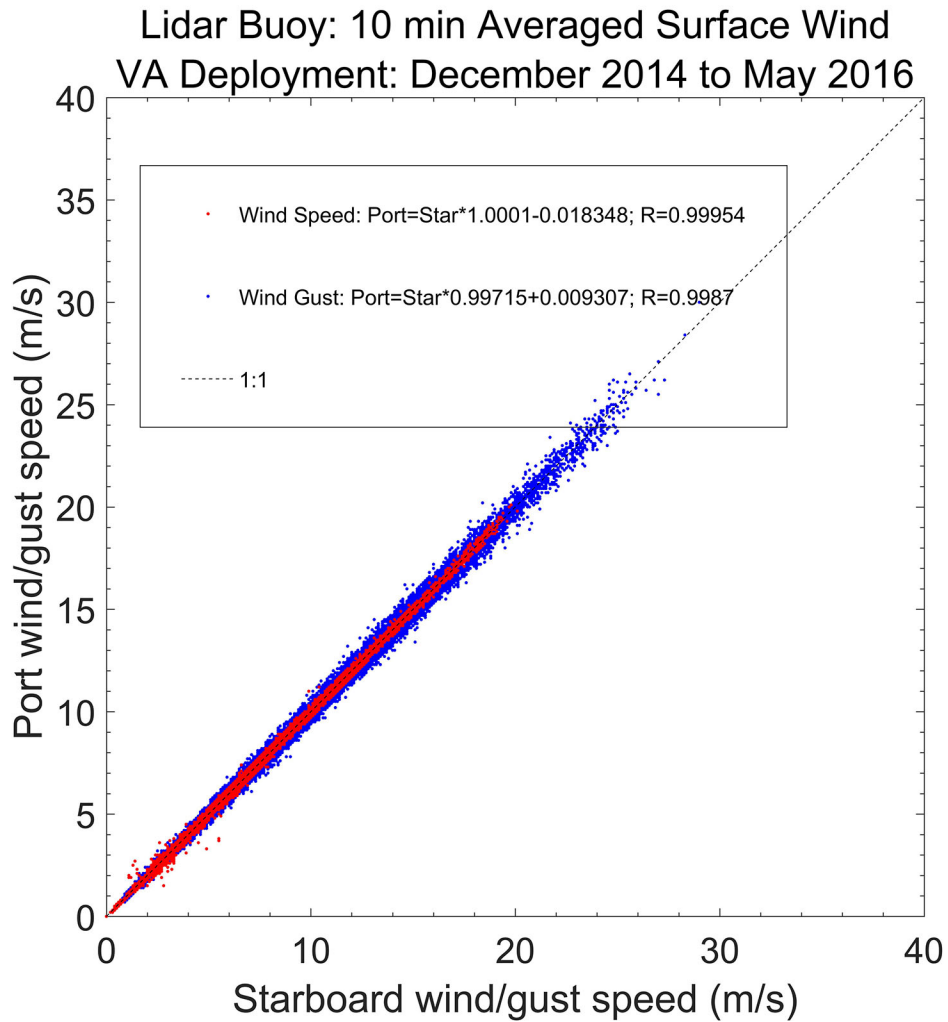


Figure A.1. Correlation of 10 min averaged wind speeds between the port and starboard anemometers on the Virginia buoy.

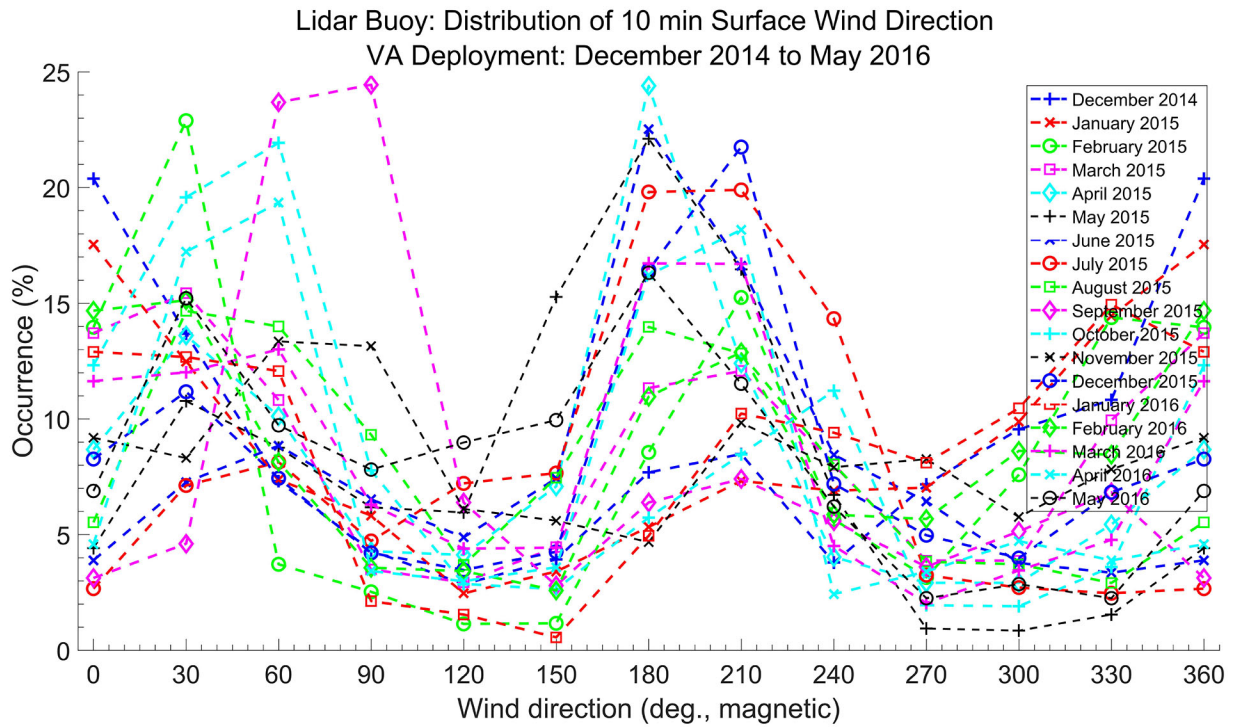


Figure A.2. Distributions by month of wind direction from the wind vane on the Virginia buoy.

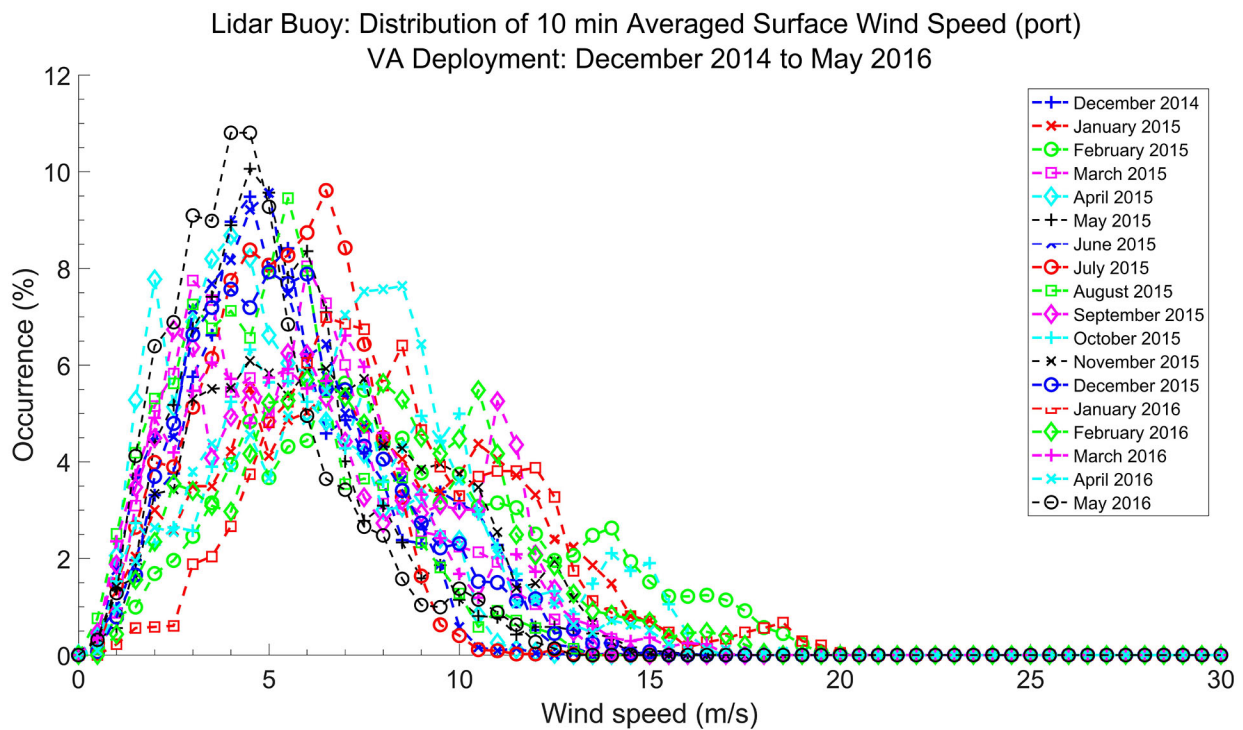
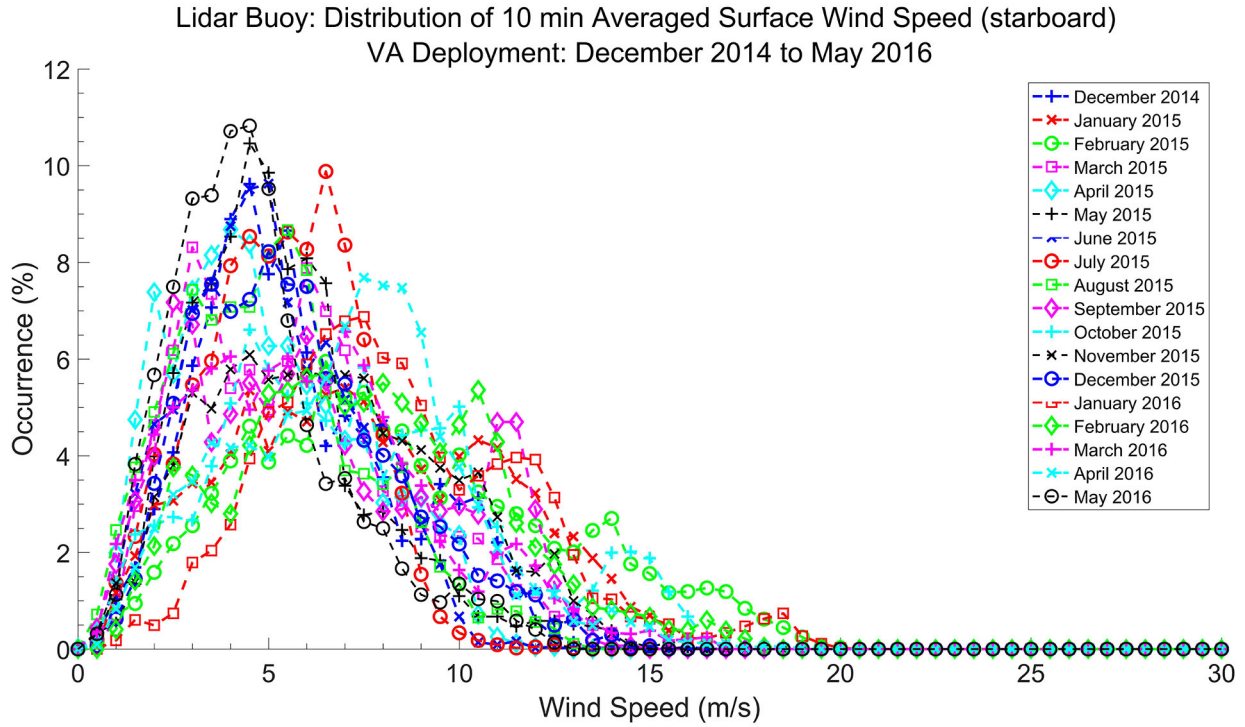
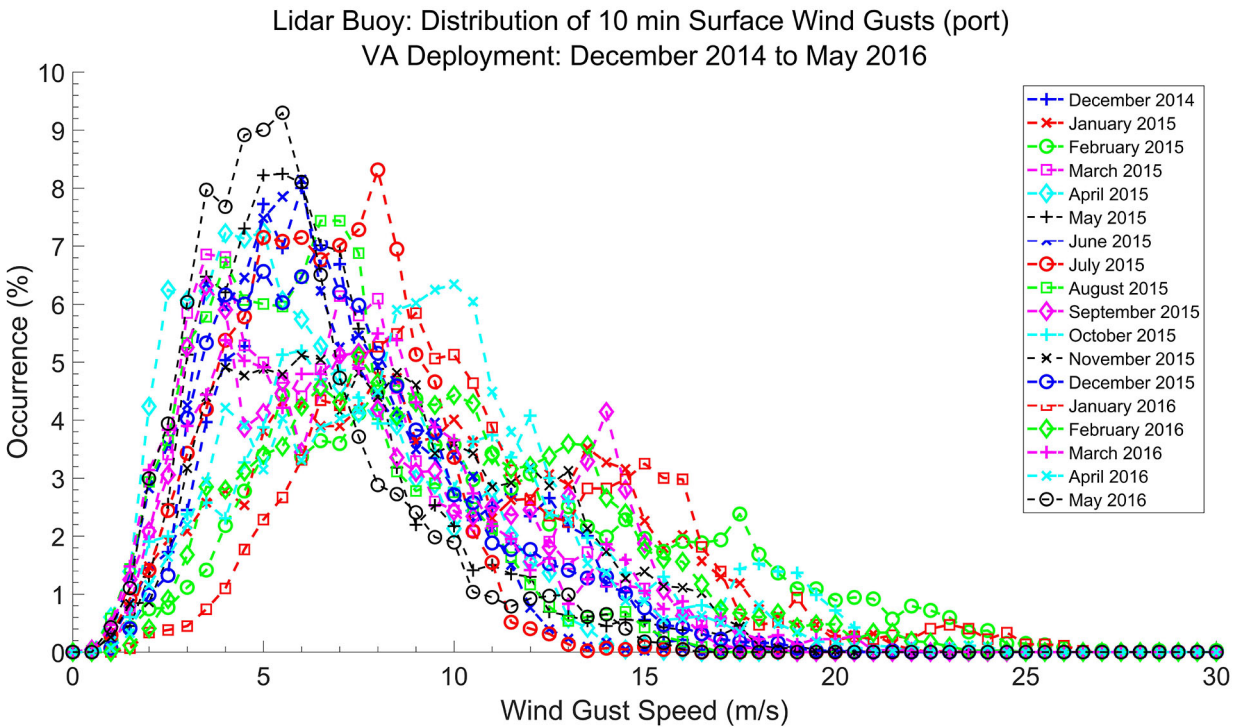


Figure A.3. Distributions by month of surface wind speed from the port cup anemometer.



**Figure A.4. Distributions by month of surface wind speed from the starboard cup anemometer.**



**Figure A.5. Distributions by month of surface wind gusts from the port cup anemometer.**

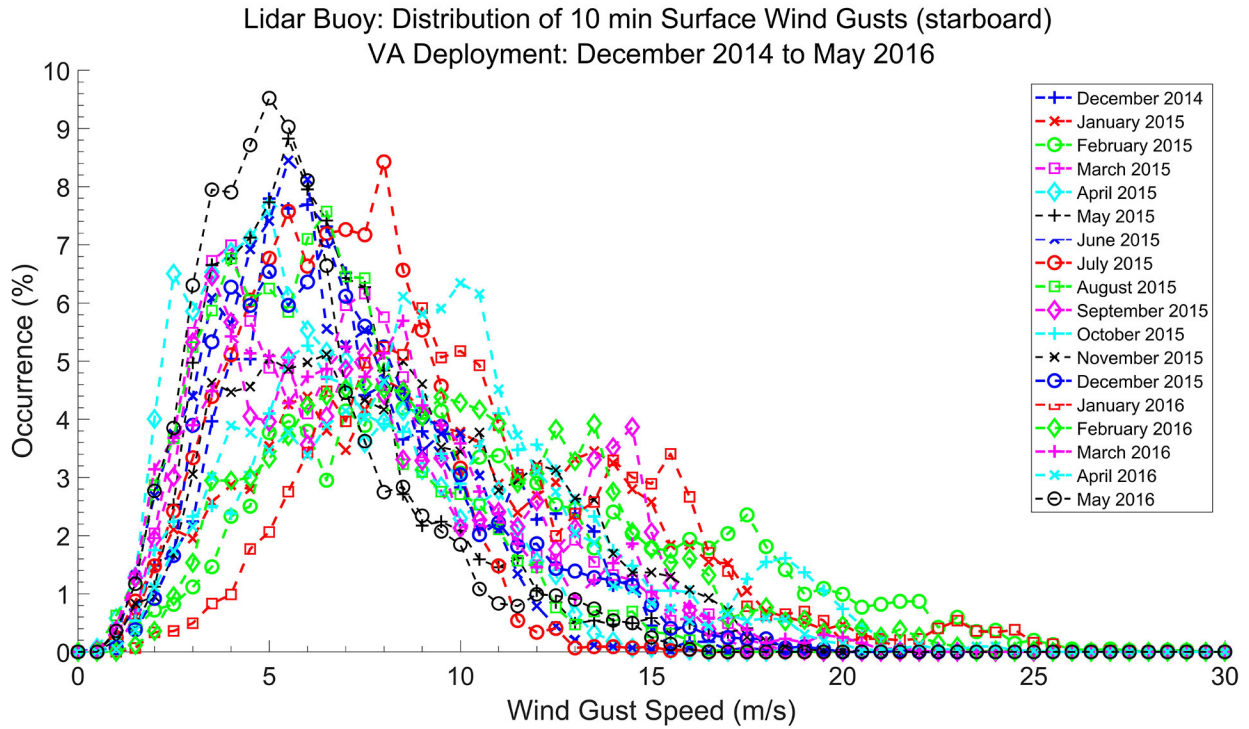


**Figure A.6. Distributions by month of surface wind gusts from the starboard cup anemometer.**

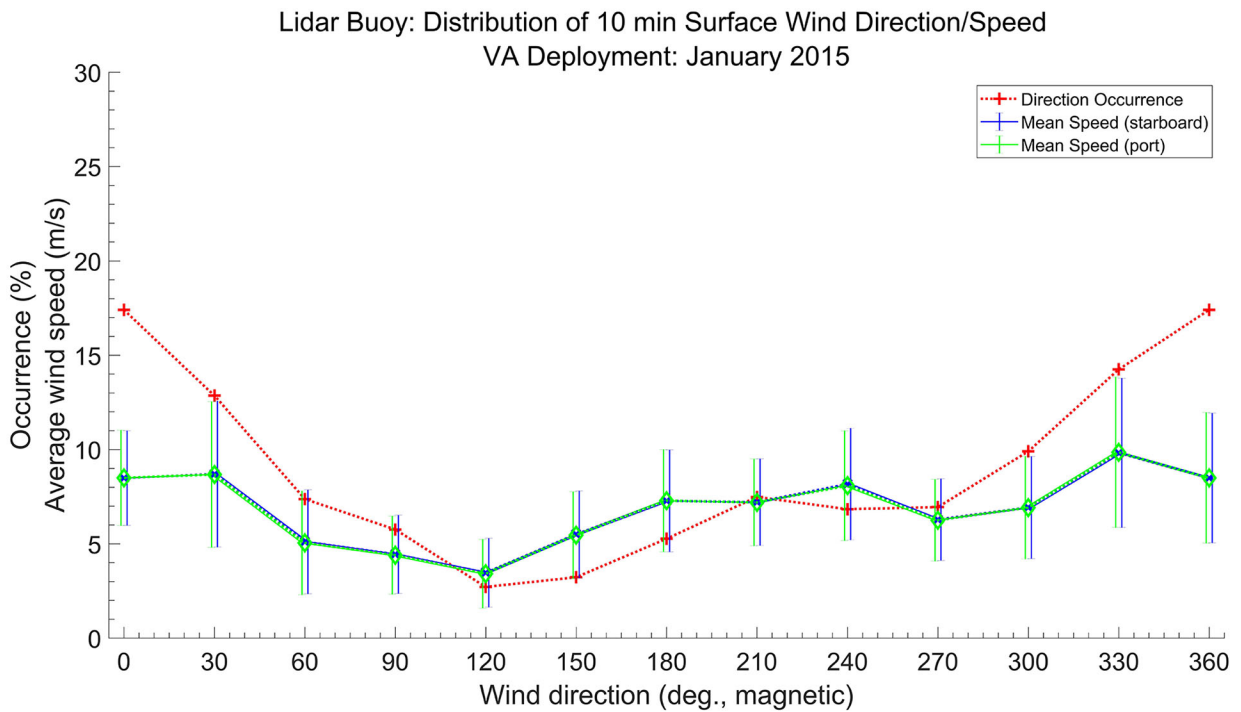


**Figure A.7. Surface wind speed as a function of direction for a typical winter month (January) together with the frequency distribution of directions.**

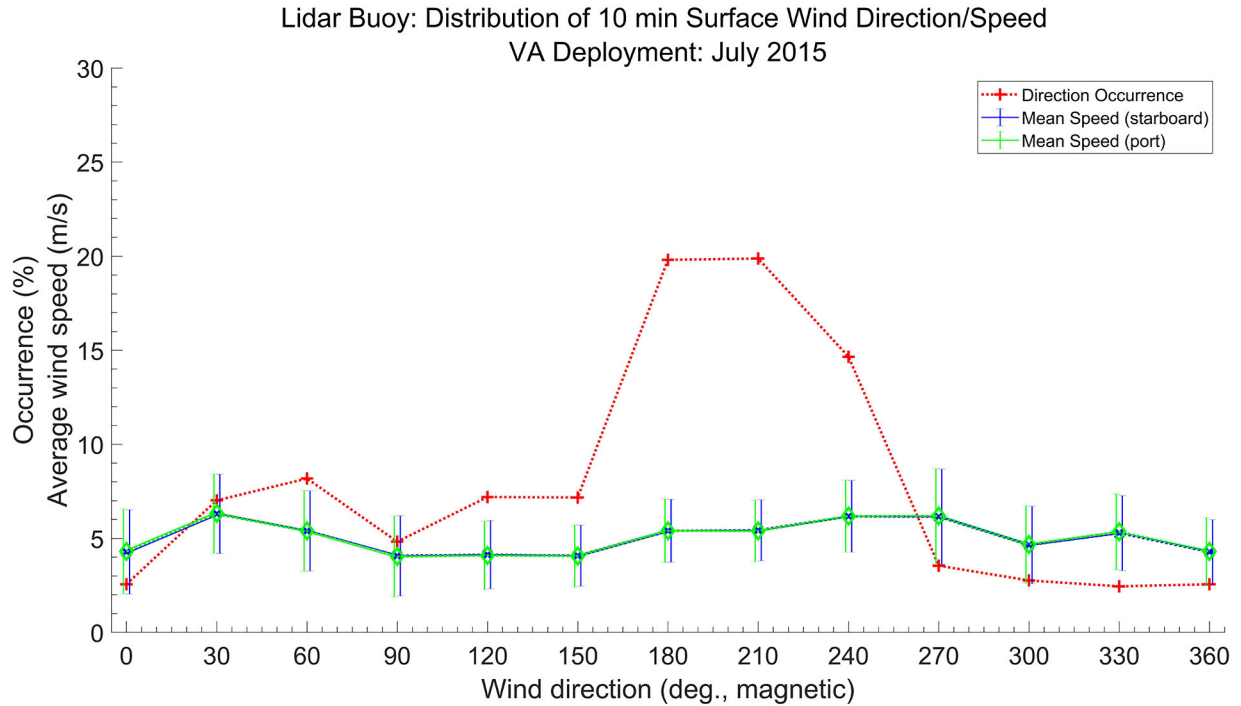


**Figure A.8. Surface wind speed as a function of direction for a typical summer month (July) together with the frequency distribution of directions.**

### A.1.2 Diurnal Wind Variations

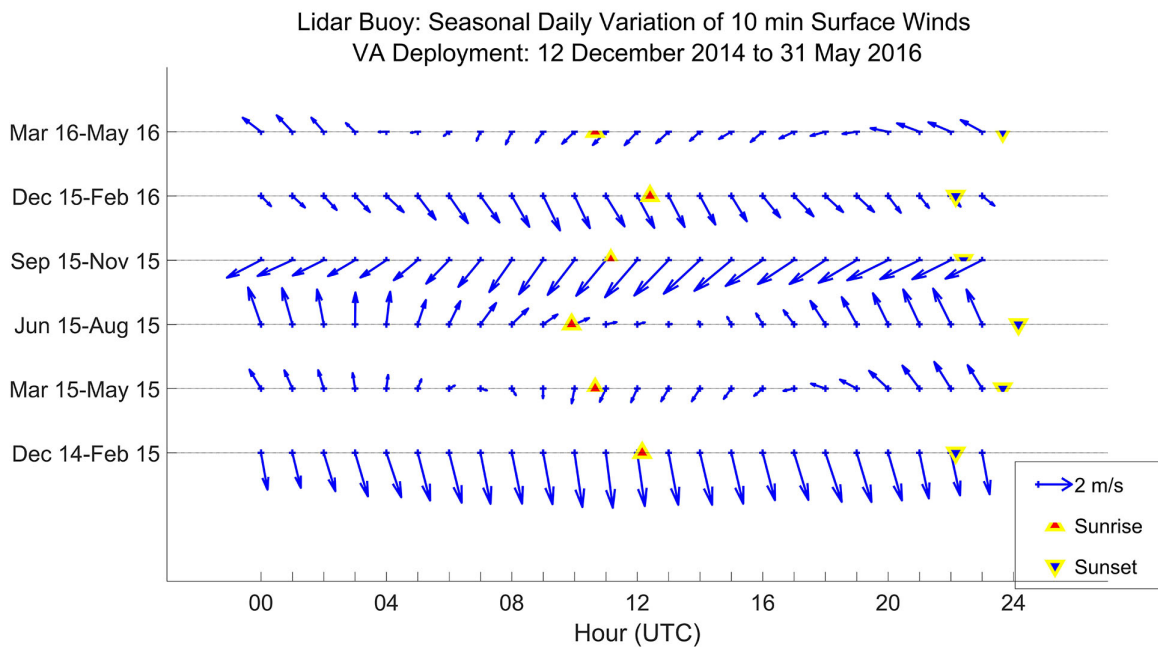


**Figure A.9. Hourly variation of the mean wind vector by season as measured by the Virginia buoy. Times are given in UTC with local sunrise and sunset indicated for each season. Note that the seasons in this figure are advanced by one month relative to figures discussed in the body of the report.**

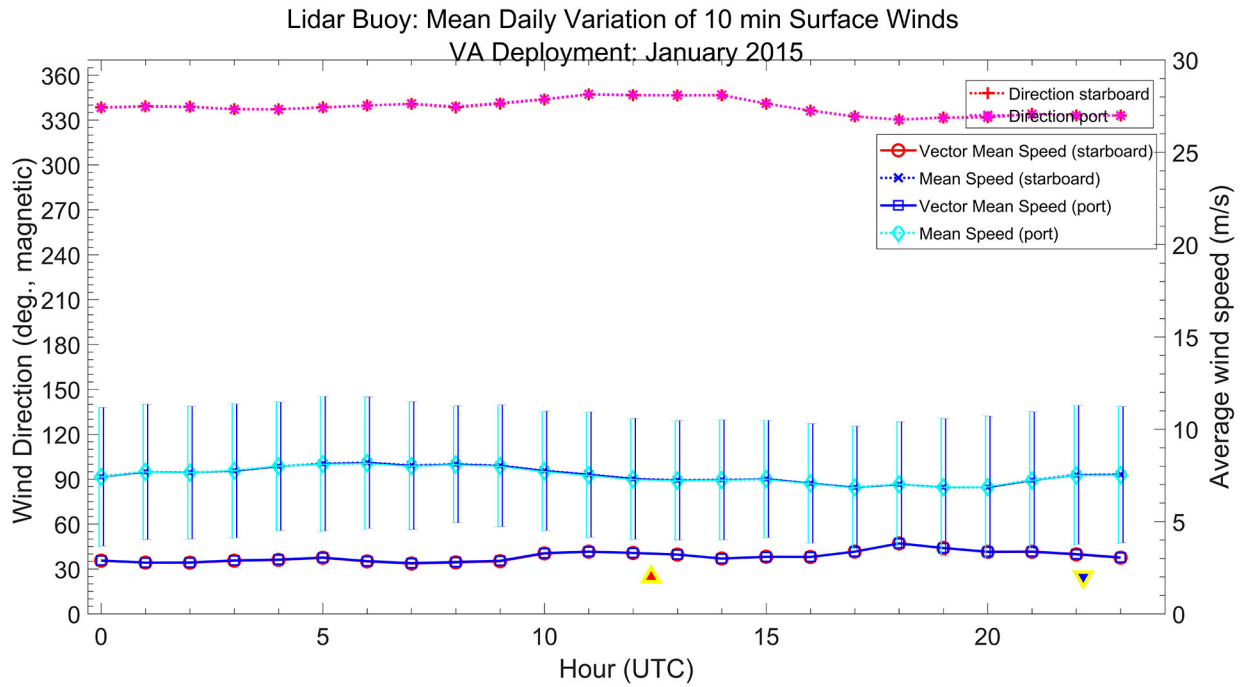


**Figure A.10. Vector and scalar mean wind speed and direction as a function of hour of day for January 2015.**

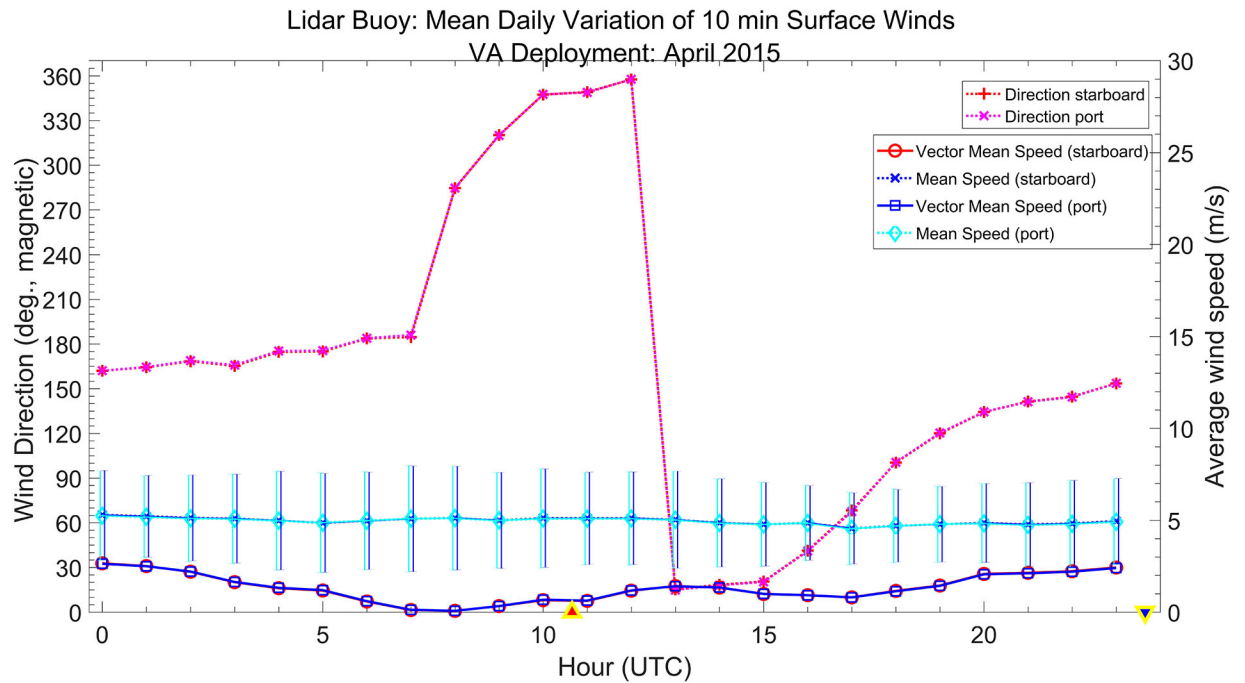


**Figure A.11. Vector and scalar mean wind speed and direction as a function of hour of day for April 2015.**

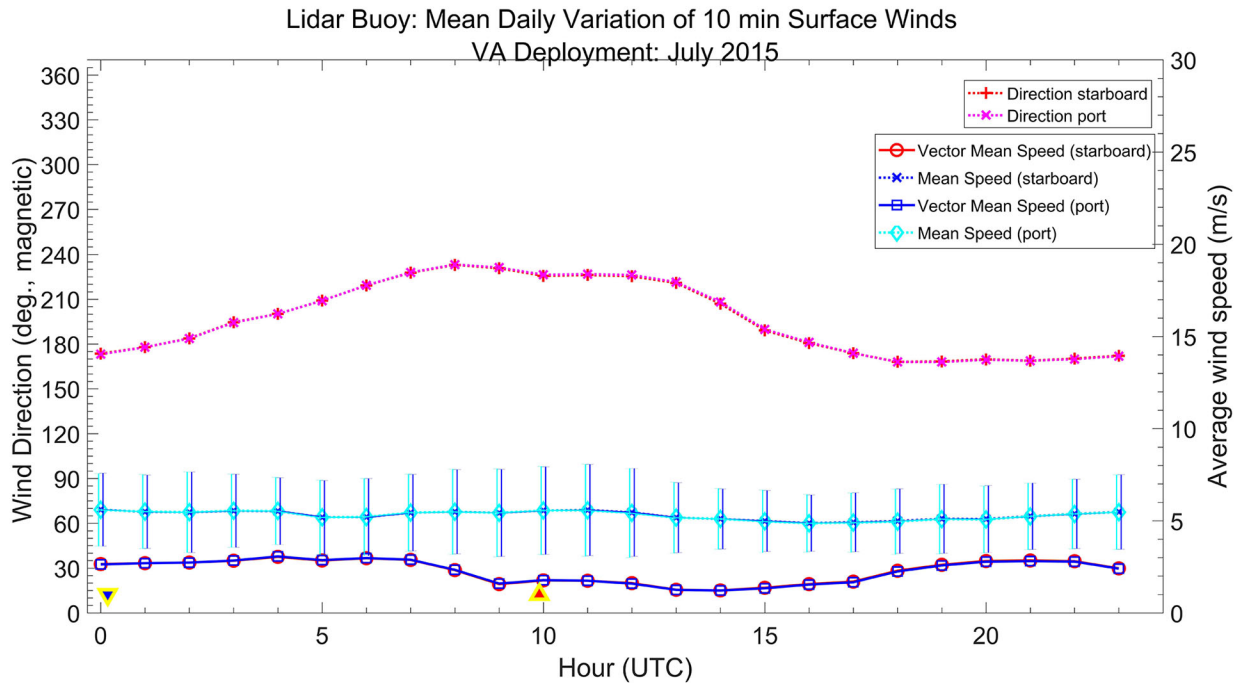


Figure A.12. Vector and scalar mean wind speed and direction as a function of hour of day for July 2015.

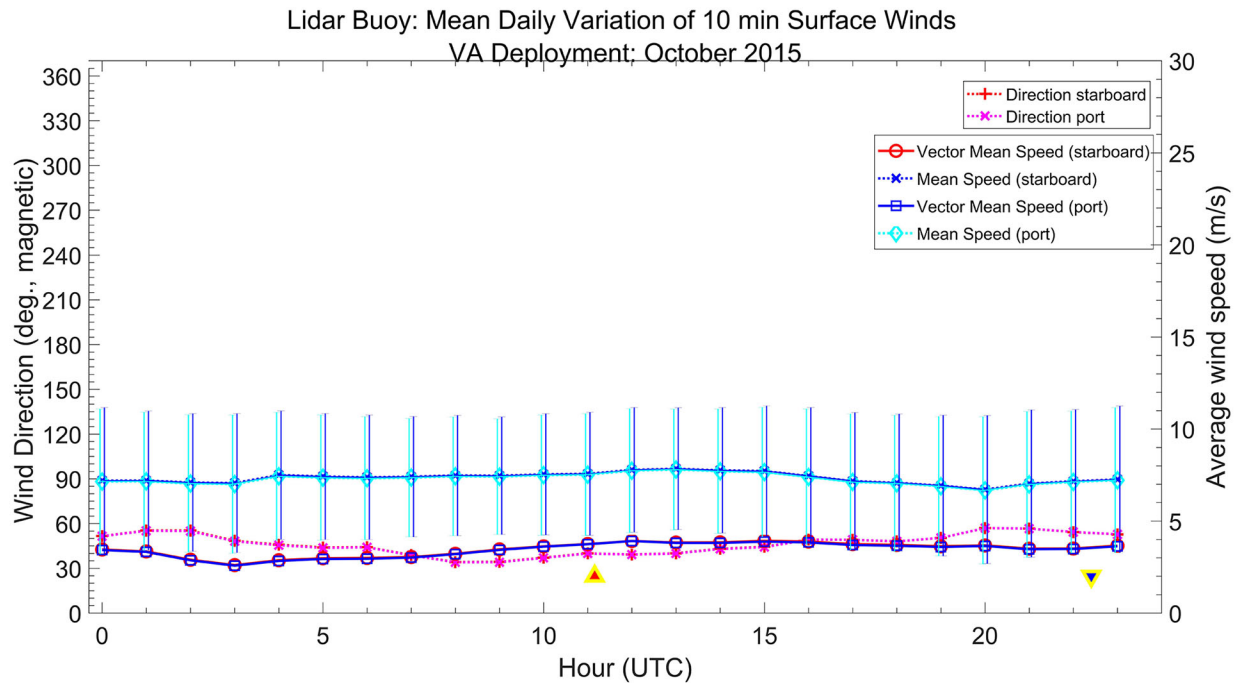
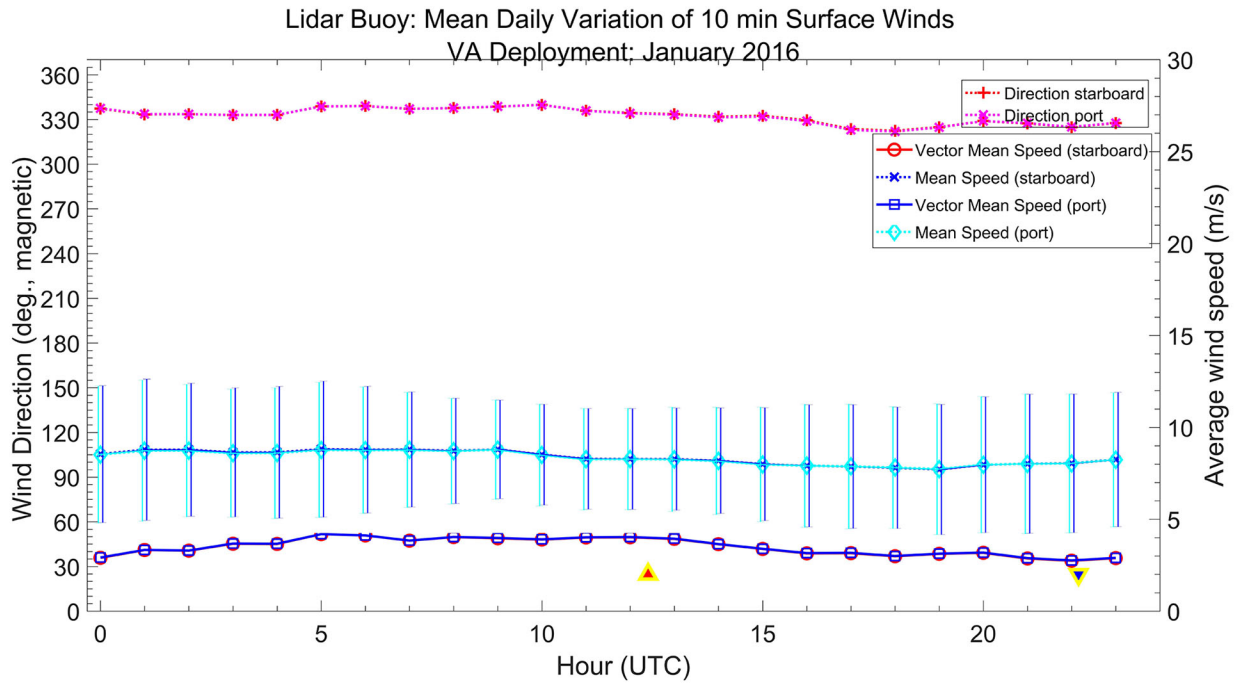
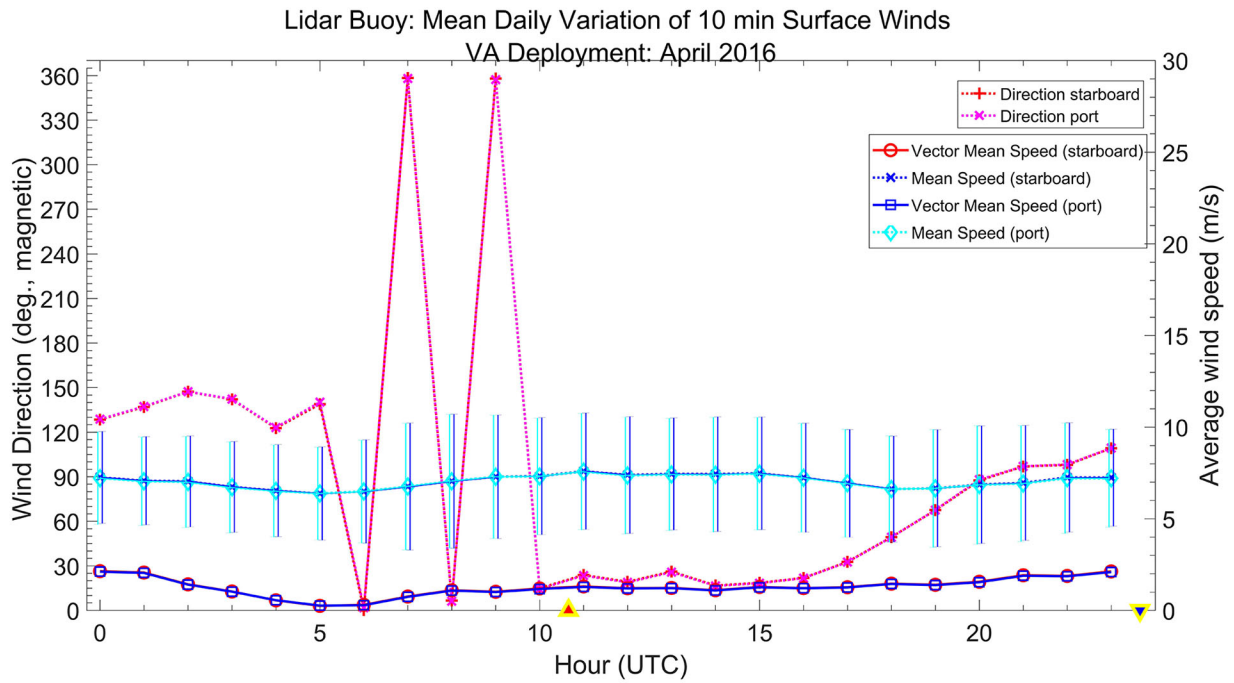


Figure A.13. Vector and scalar mean wind speed and direction as a function of hour of day for October 2015.



**Figure A.14. Vector and scalar mean wind speed and direction as a function of hour of day for January 2016.**



**Figure A.15. Vector and scalar mean wind speed and direction as a function of hour of day for April 2016.**

### A.1.3 Time Variation of Surface Temperatures

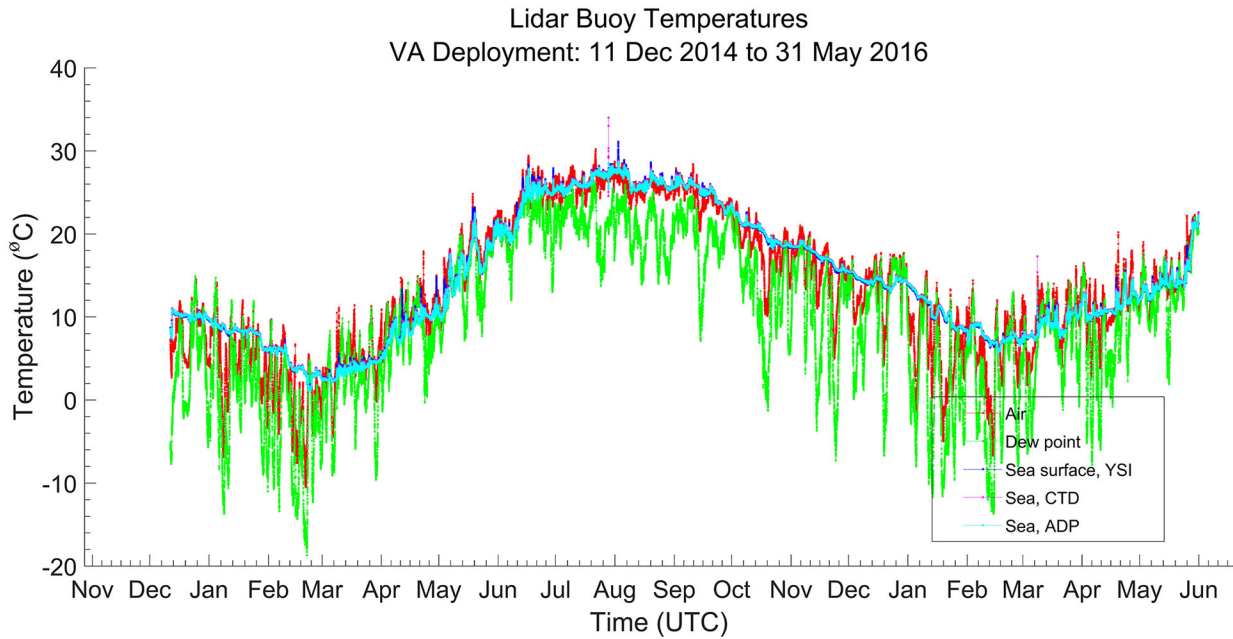


**Figure A.16.** Time series of air and water temperatures and dew point for the full duration of the Virginia buoy deployment.

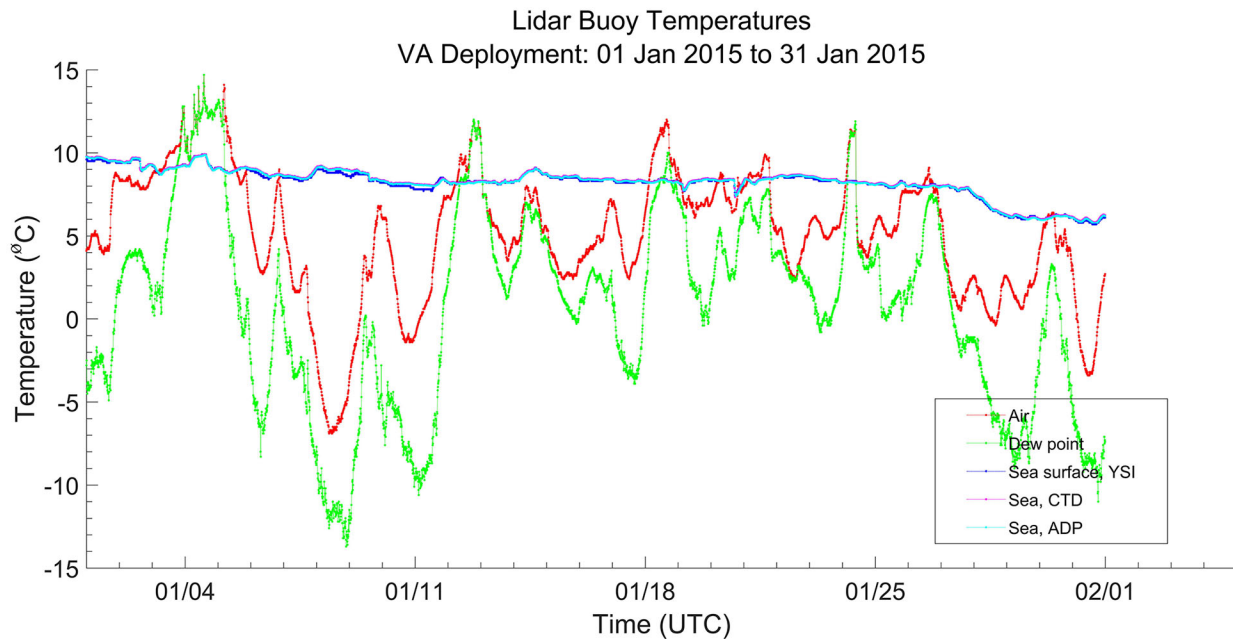


**Figure A.17.** Time series of air and water temperatures and dew point for January 2015.

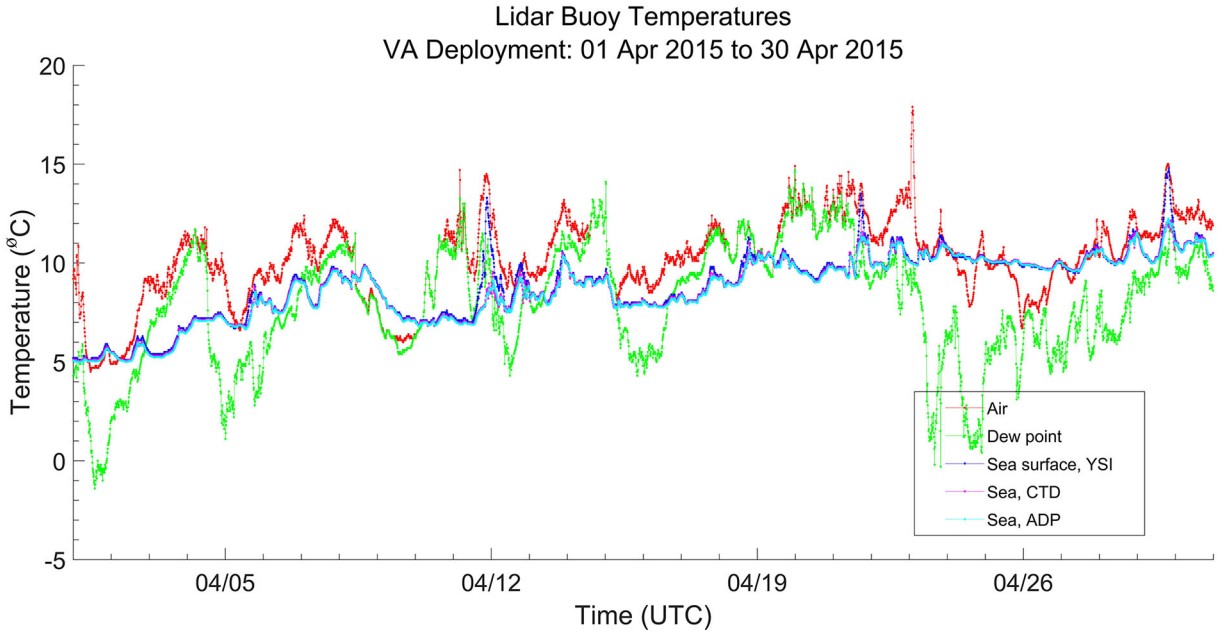


**Figure A.18. Time series of air and water temperatures and dew point for April 2015.**

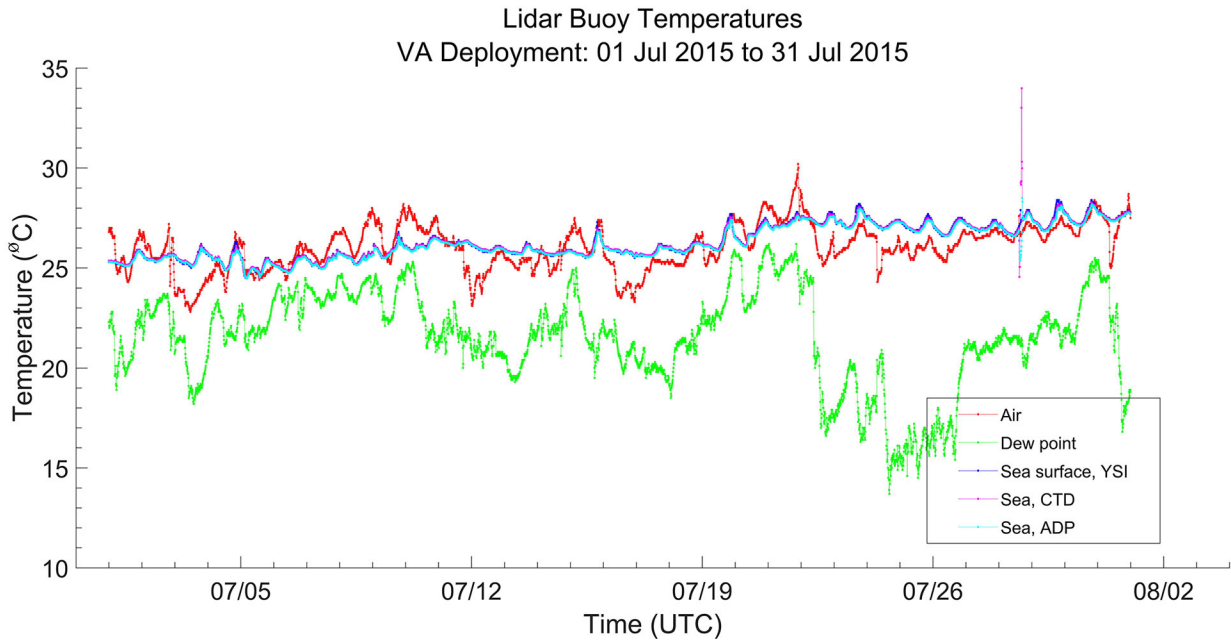


**Figure A.19. Time series of air and water temperatures and dew point for July 2015.**

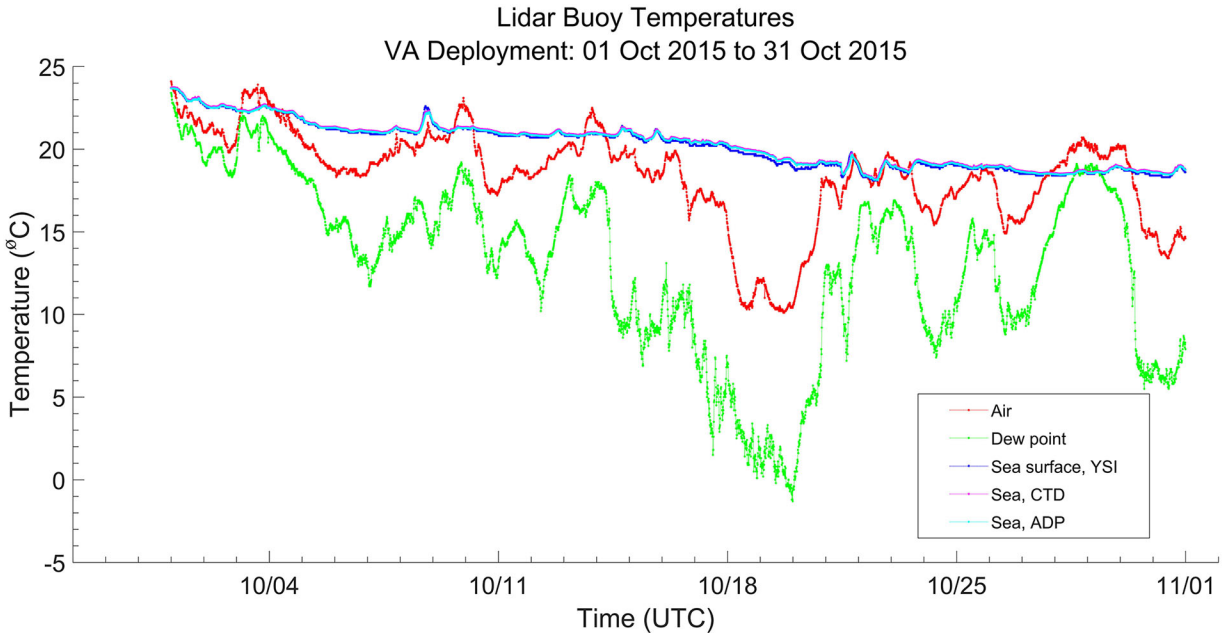


**Figure A.20. Time series of air and water temperatures and dew point for October 2015.**

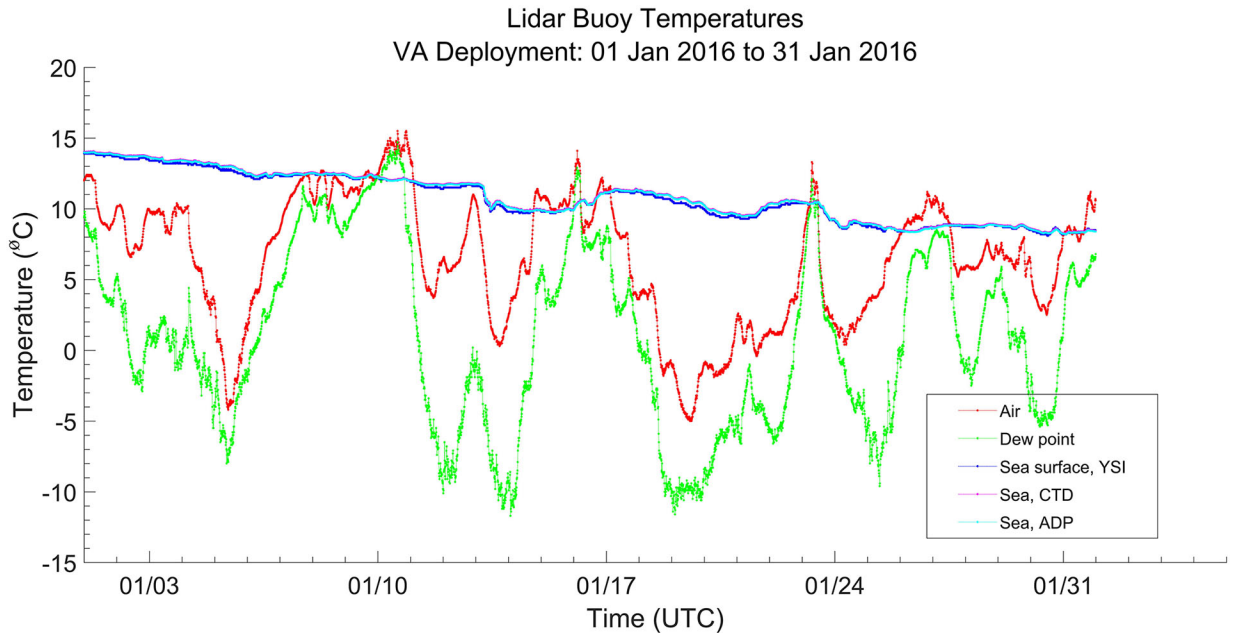


**Figure A.21. Time series of air and water temperatures and dew point for January 2016.**

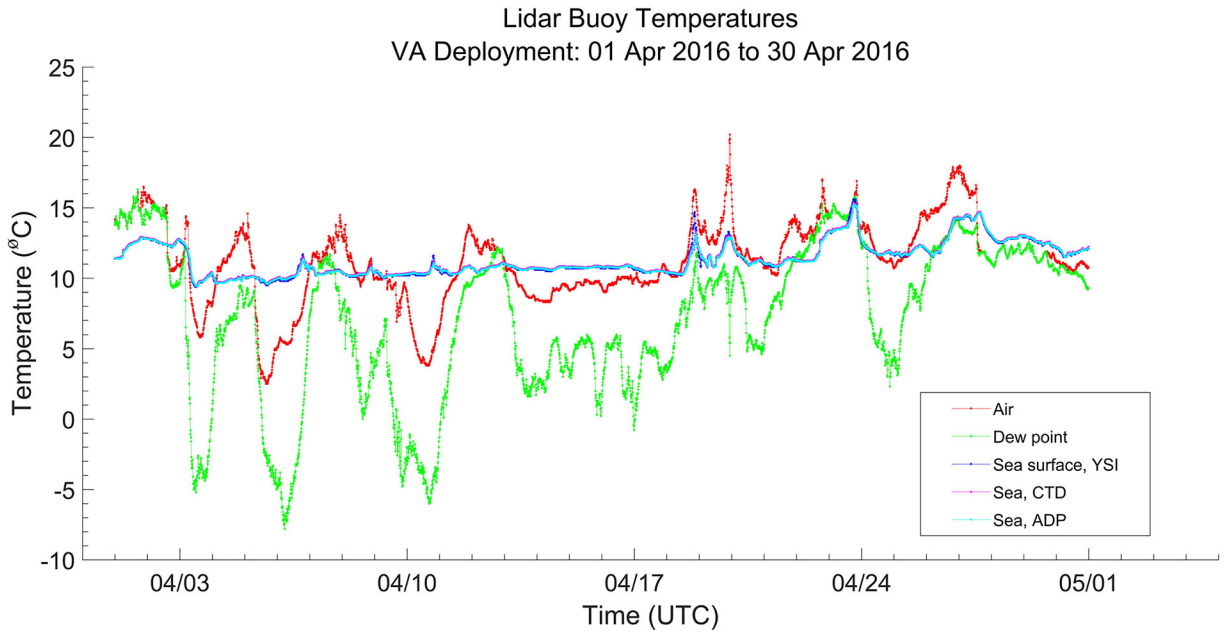


Figure A.22. Time series of air and water temperatures and dew point for April 2016.

#### A.1.4 Diurnal Variation of Temperatures

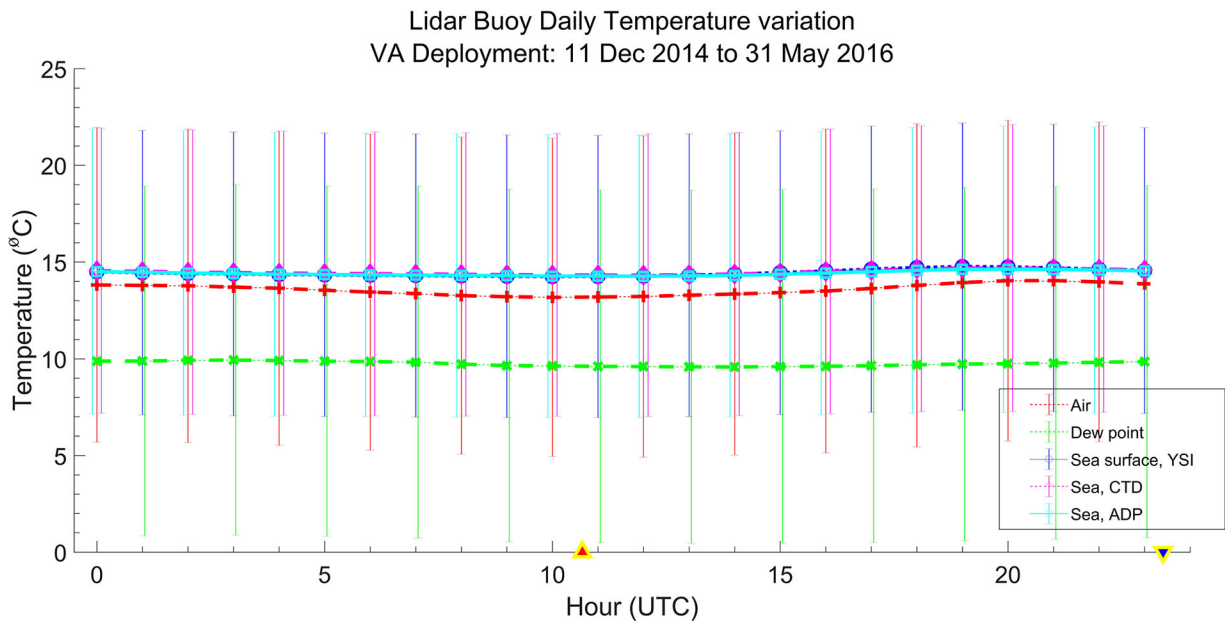
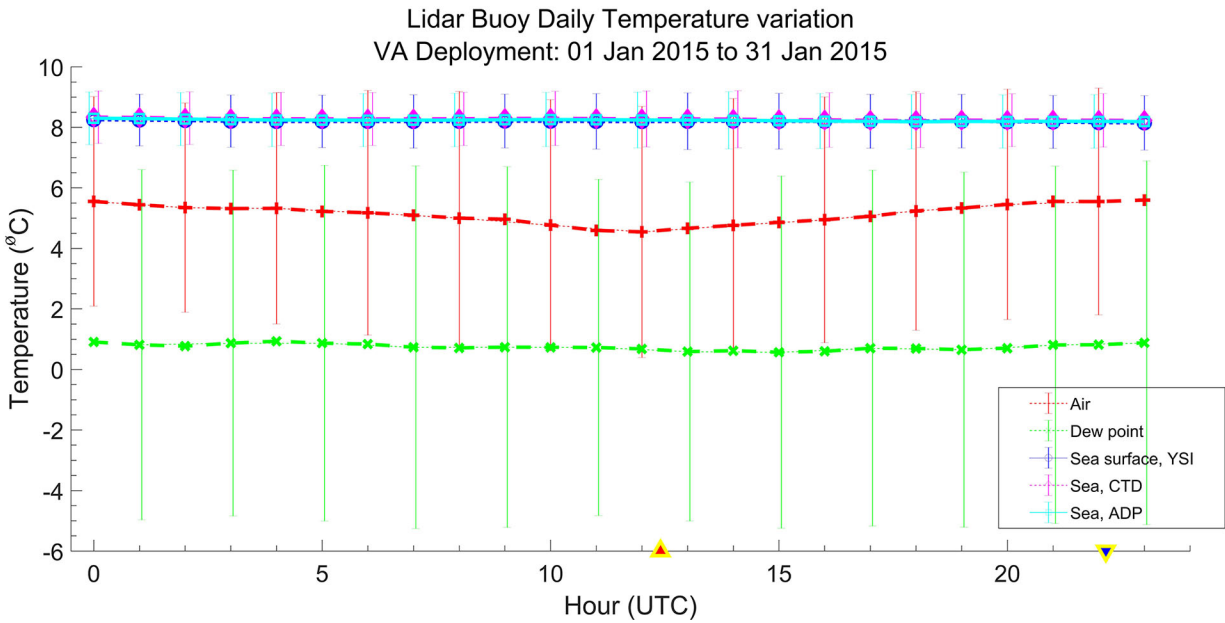
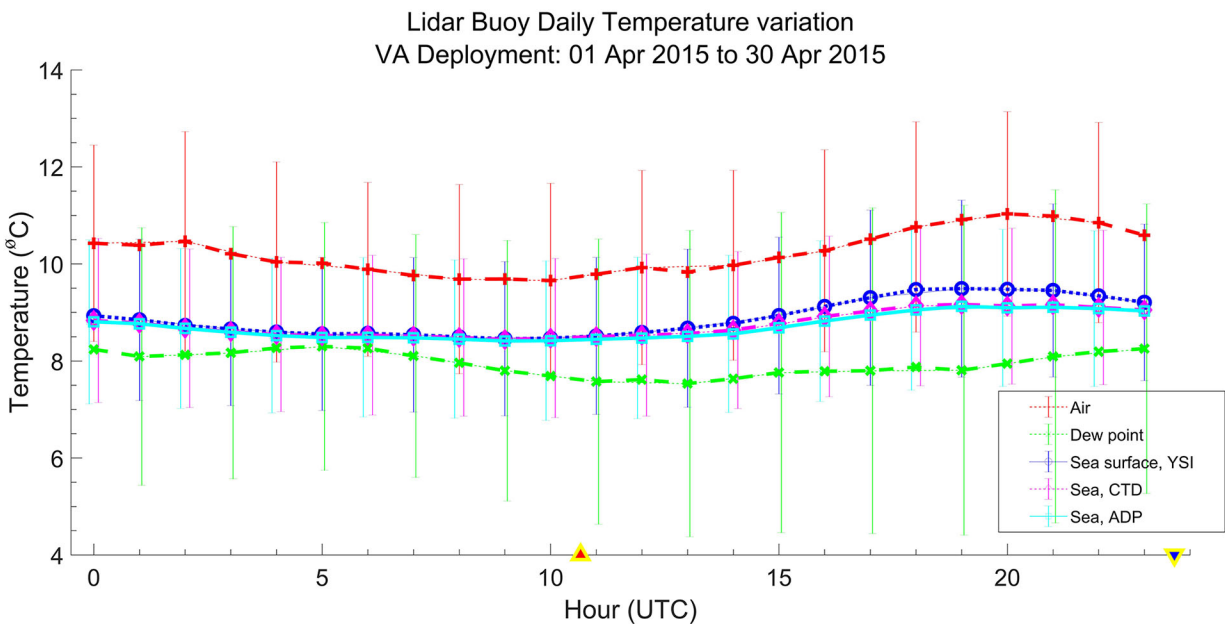


Figure A.23. Diurnal variation by hour of air and water temperatures and of dew point for the period of deployment of the Virginia buoy. Hour of day is in UTC, and mean times of sunrise and sunset are indicated by symbols on the abscissa.



**Figure A.24. Diurnal variation by hour of air and water temperatures and of dew point for January 2015. Mean times of sunrise and sunset are indicated by symbols on the abscissa.**



**Figure A.25. Diurnal variation by hour of air and water temperatures and of dew point for April 2015. Mean times of sunrise and sunset are indicated by symbols on the abscissa.**

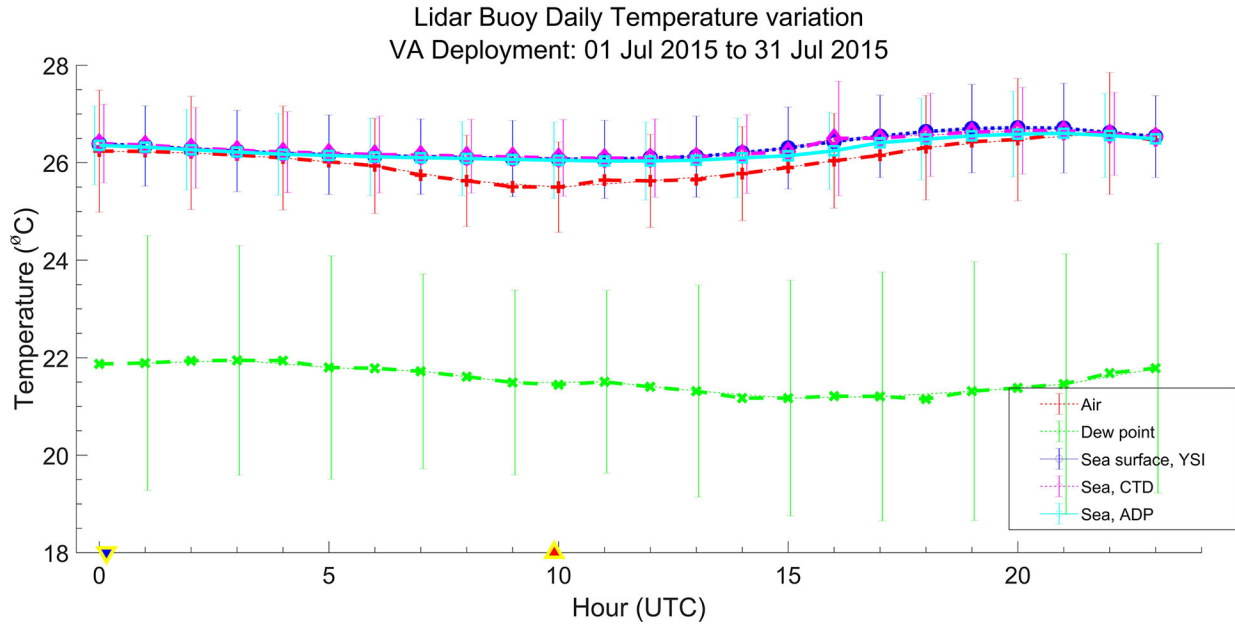


**Figure A.26. Diurnal variation by hour of air and water temperatures and of dew point for July 2015. Mean times of sunrise and sunset are indicated by symbols on the abscissa.**

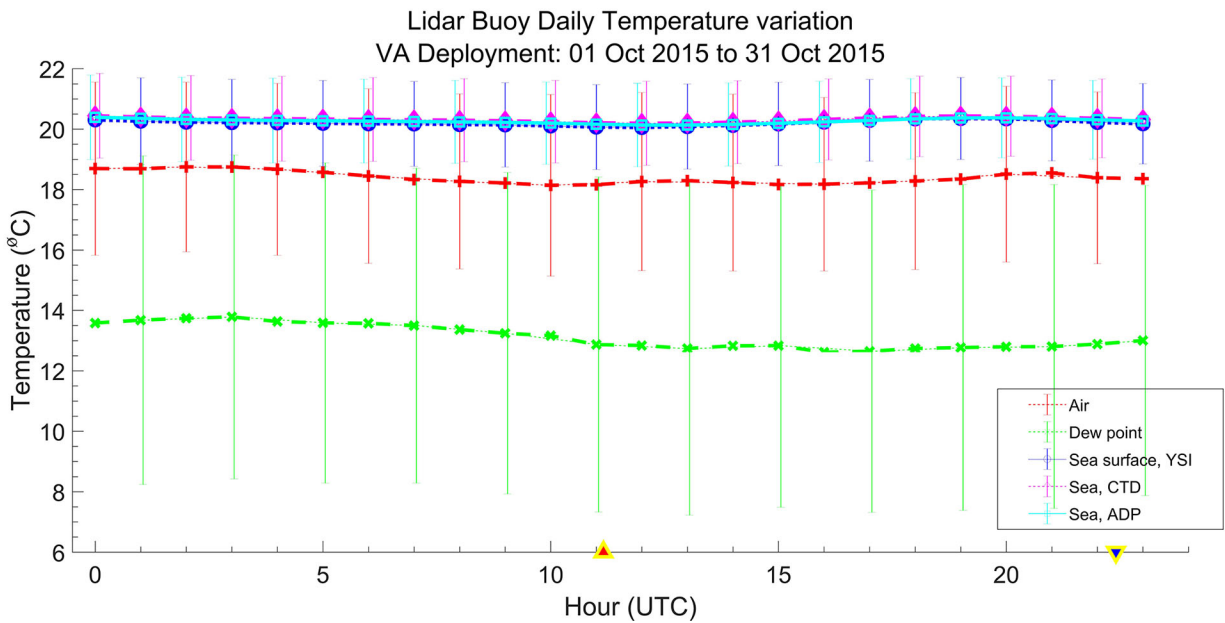


**Figure A.27. Diurnal variation by hour of air and water temperatures and of dew point for October 2015. Mean times of sunrise and sunset are indicated by symbols on the abscissa.**

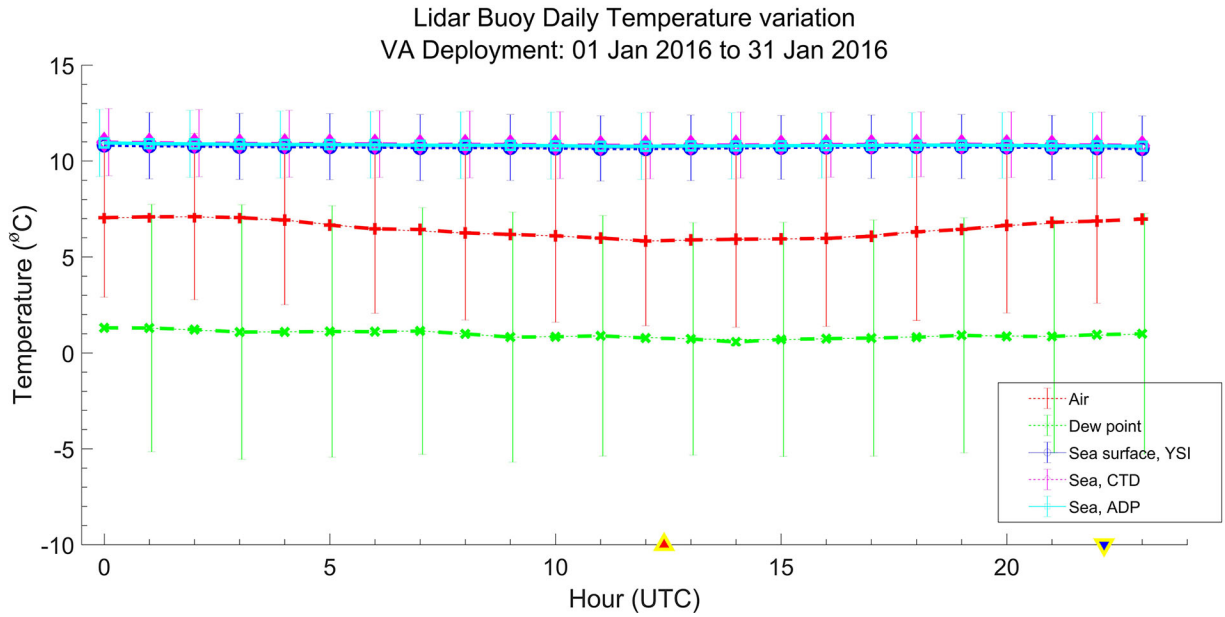


**Figure A.28. Diurnal variation by hour of air and water temperatures and of dew point for January 2016. Mean times of sunrise and sunset are indicated by symbols on the abscissa.**

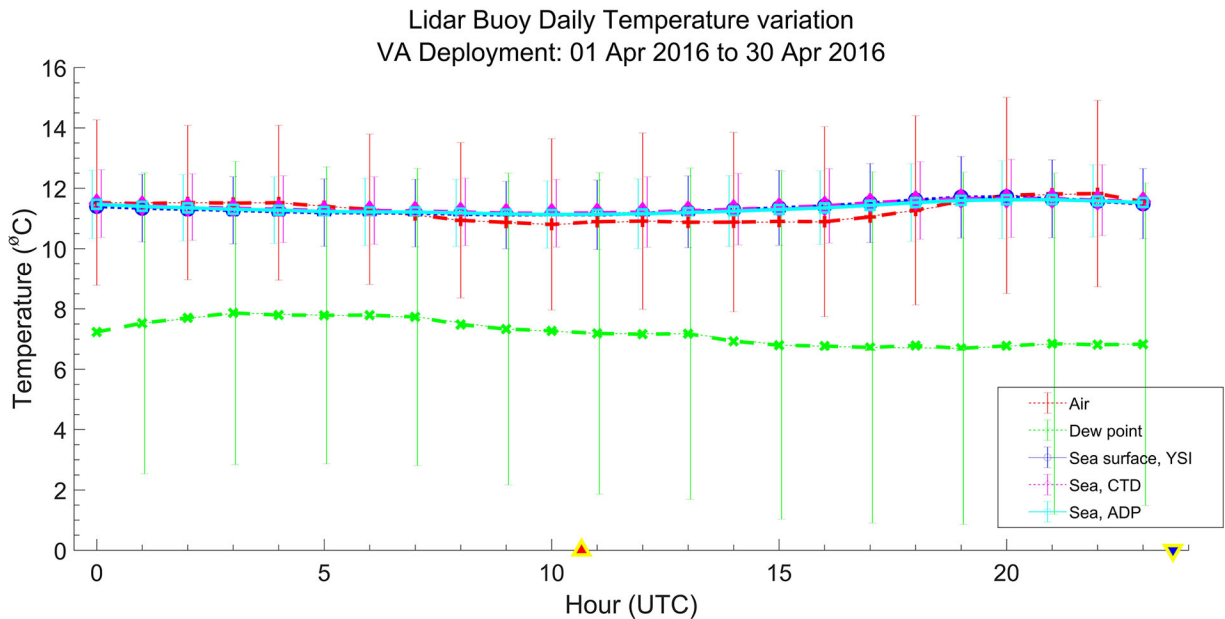


**Figure A.29. Diurnal variation by hour of air and water temperatures and of dew point for April 2016. Mean times of sunrise and sunset are indicated by symbols on the abscissa.**

### A.1.5 Seasonal Ocean Current Profiles

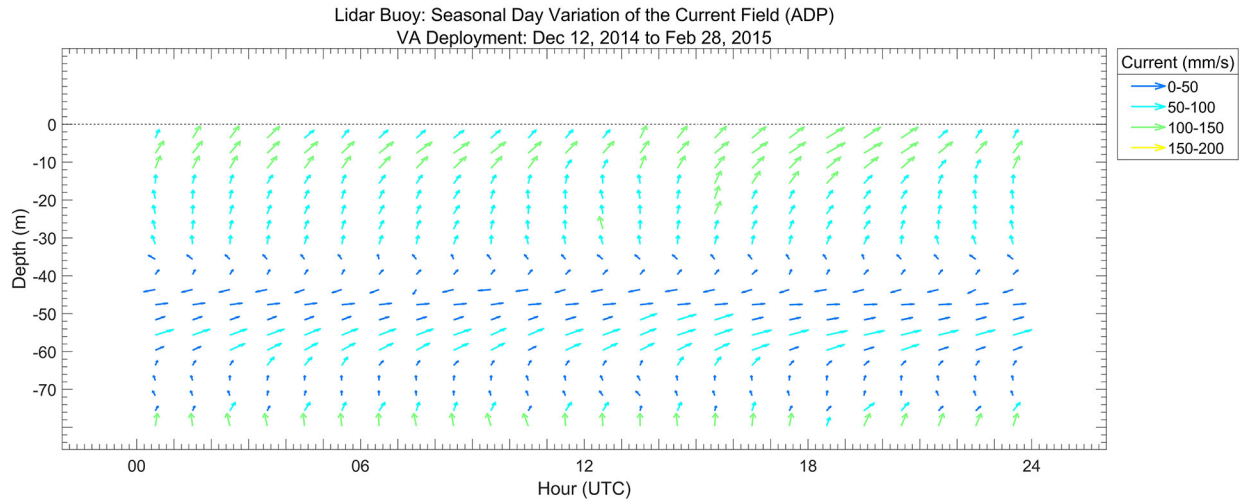


Figure A.30. Mean current profiles by hour of day from the Virginia buoy for winter 2015.

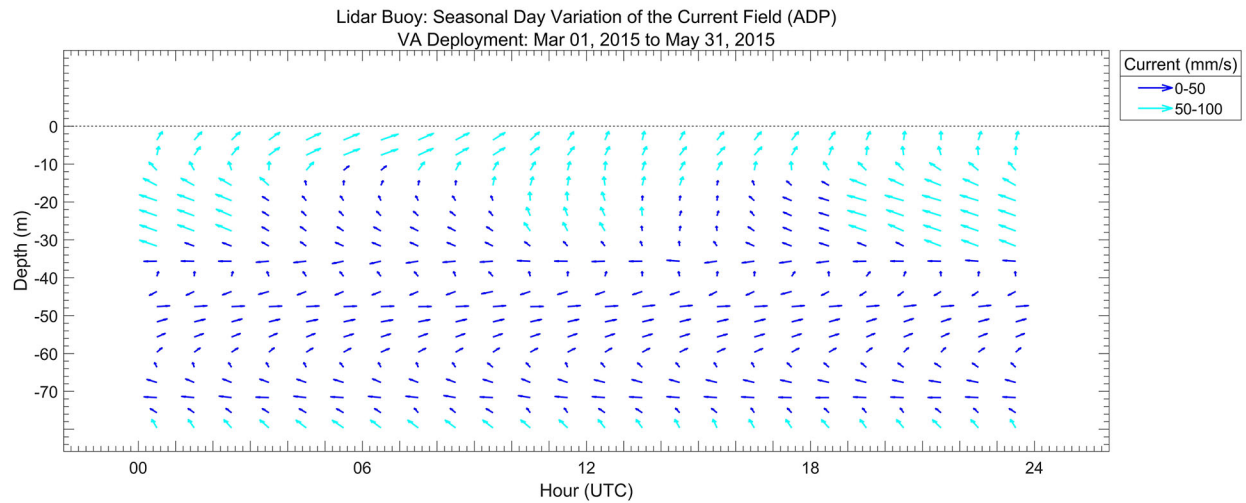
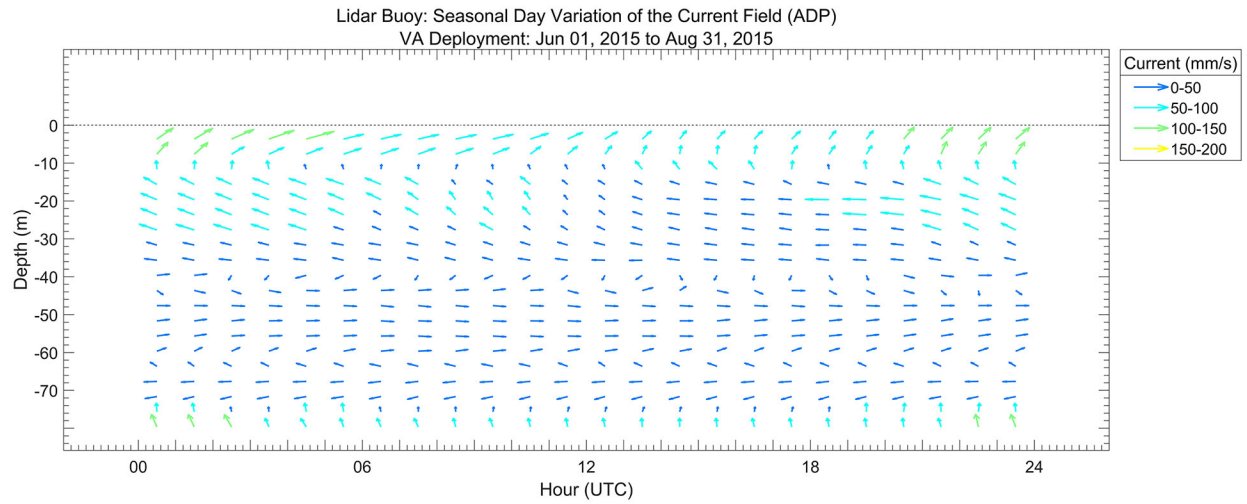
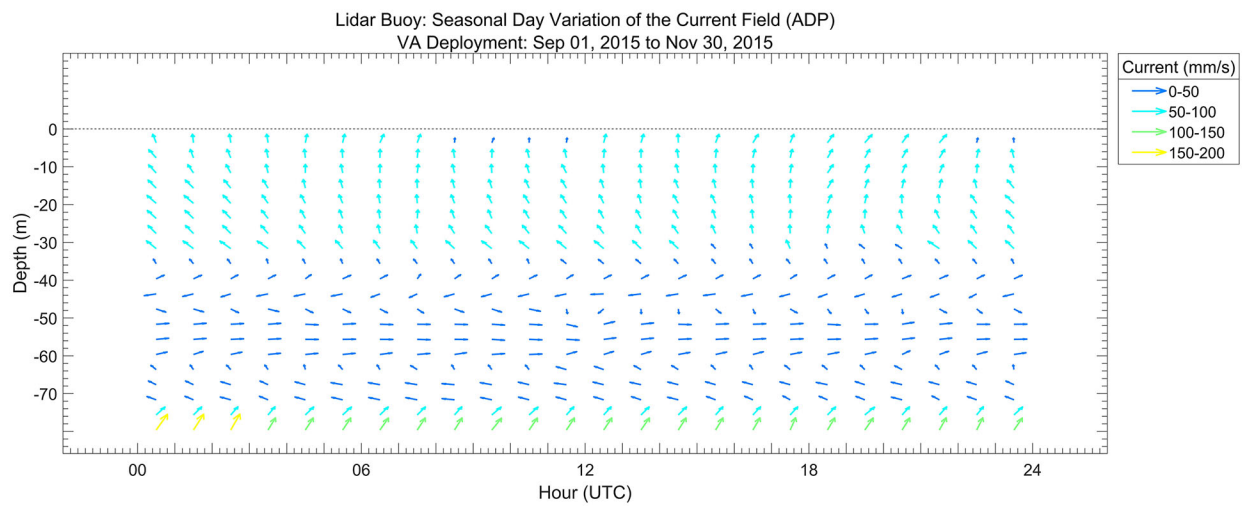


Figure A.31. Mean current profiles by hour of day from the Virginia buoy for spring 2015.



**Figure A.32. Mean current profiles by hour of day from the Virginia buoy for summer 2015.**



**Figure A.33. Mean current profiles by hour of day from the Virginia buoy for fall 2015.**

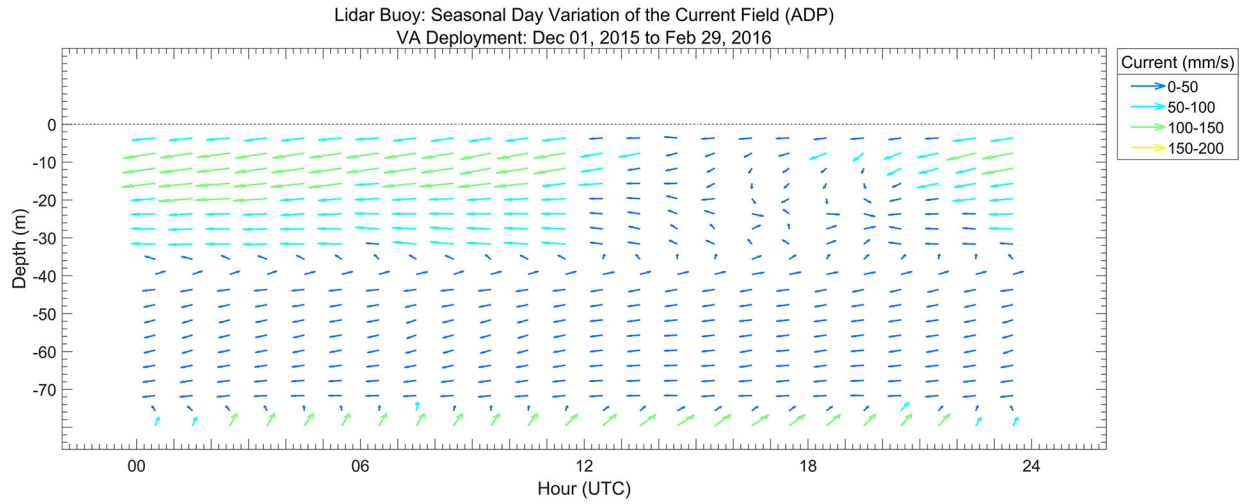


**Figure A.34. Mean current profiles by hour of day from the Virginia buoy for winter 2016.**

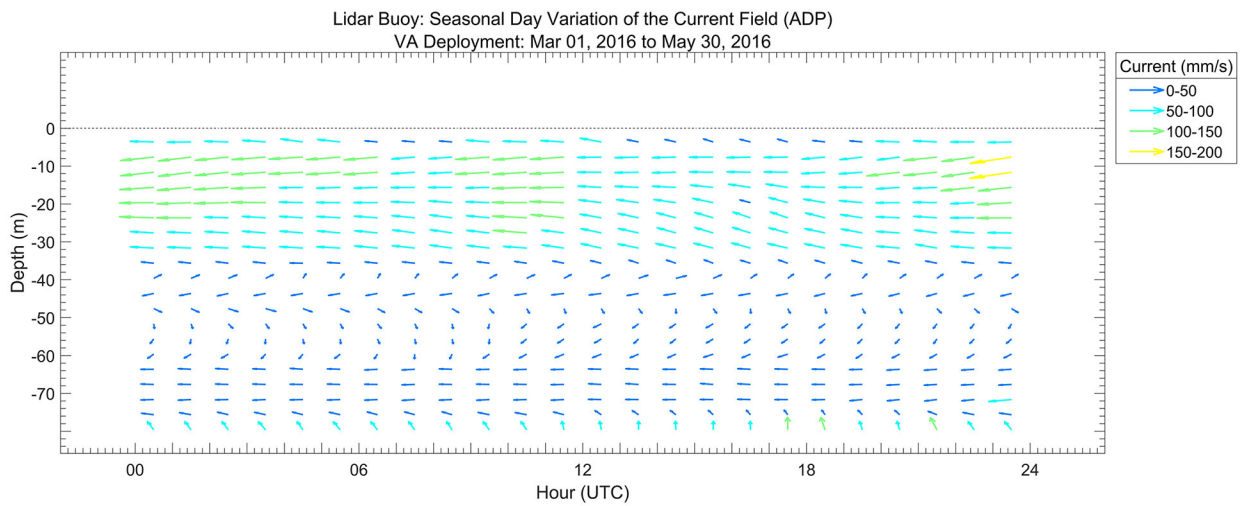


**Figure A.35. Mean current profiles by hour of day from the Virginia buoy for spring 2016.**

## A.2 New Jersey Buoy

### A.2.1 Distributions of Surface Wind Information

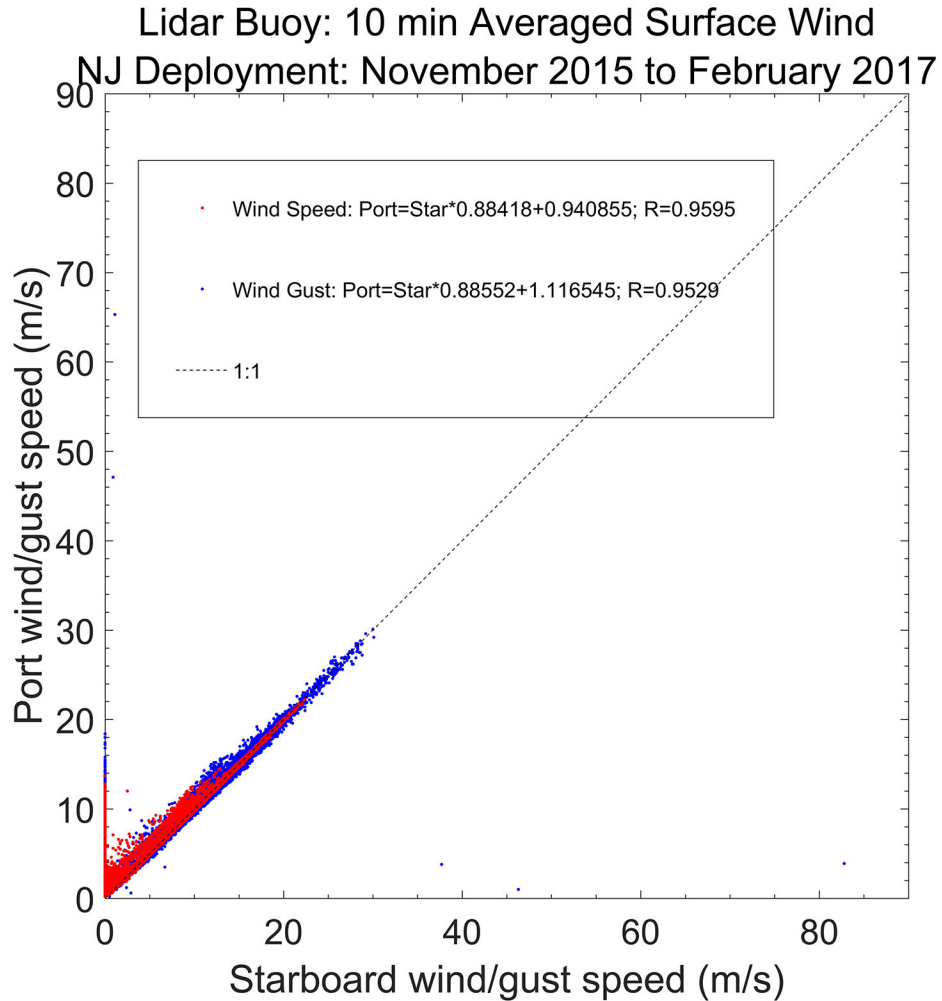


**Figure A.36. Correlation of 10 min. averaged wind speeds between the port and starboard anemometers on the New Jersey buoy. The poorer correlation than for the Virginia buoy reflects the decline in performance of the New Jersey buoy's starboard cup anemometer.**

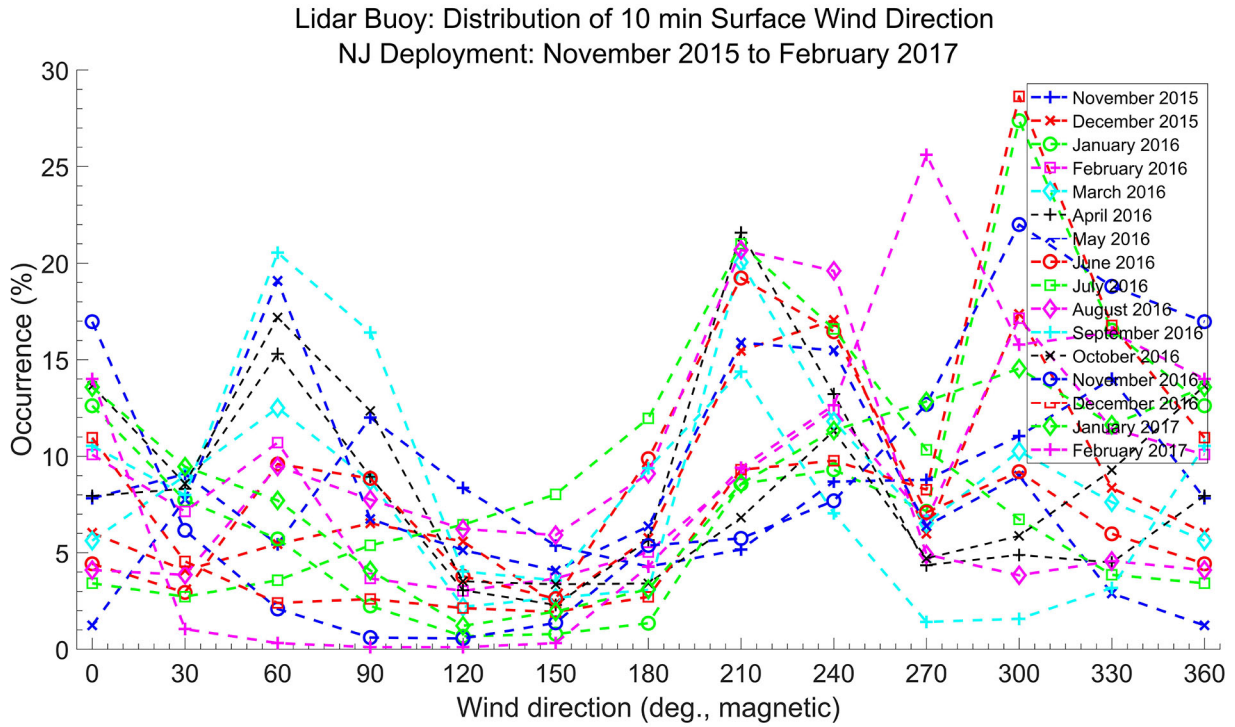


**Figure A.37. Distributions by month of wind direction from the wind vane on the New Jersey buoy.**

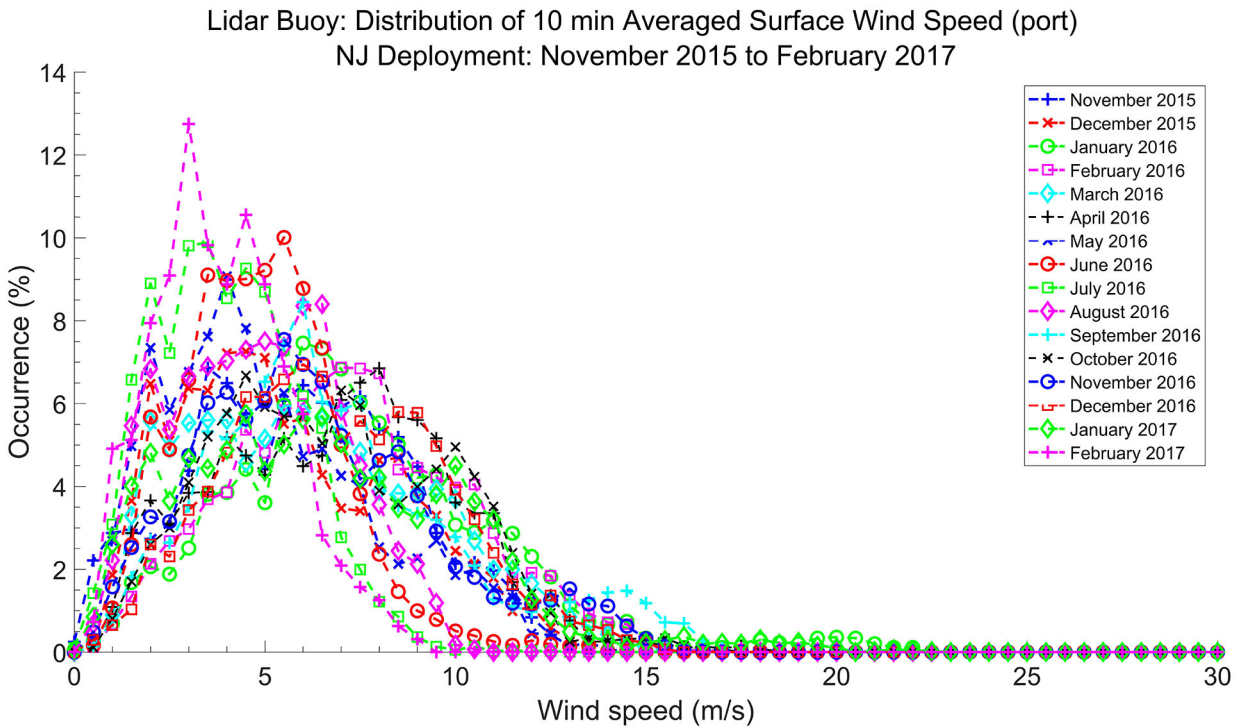


**Figure A.38. Distributions by month of surface wind speed from the port cup anemometer.**

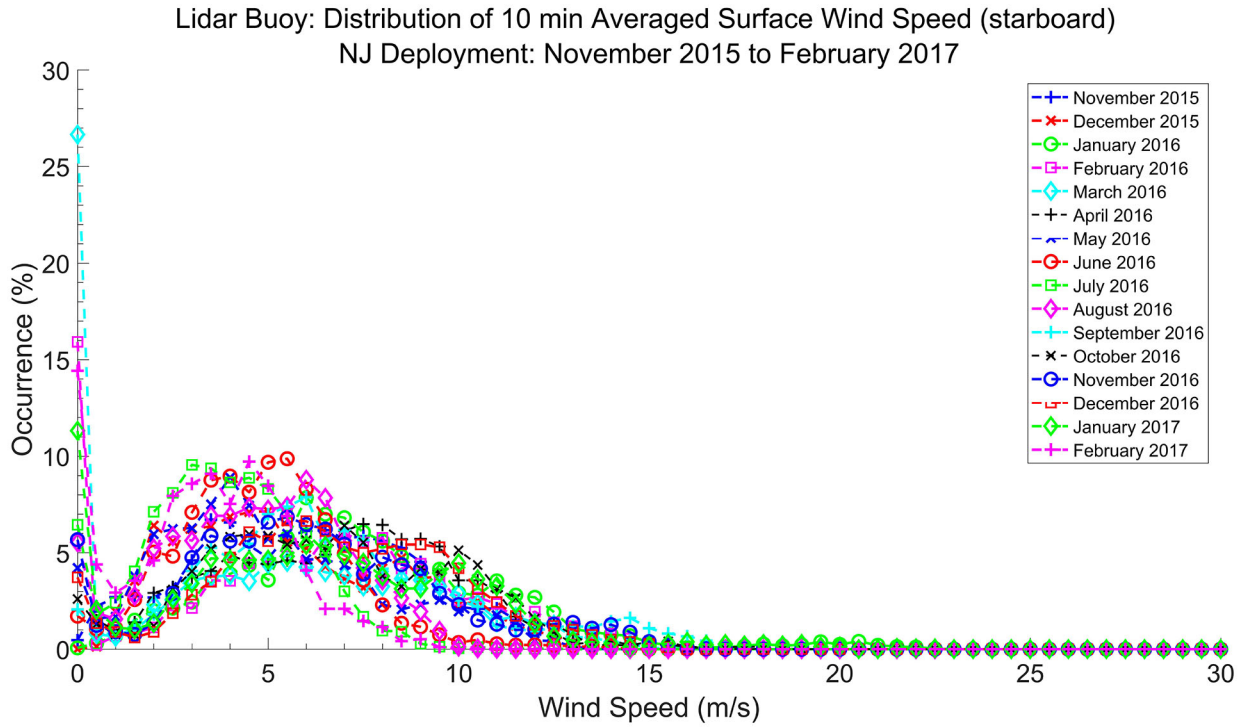


**Figure A.39. Distributions by month of surface wind speed from the starboard cup anemometer.**

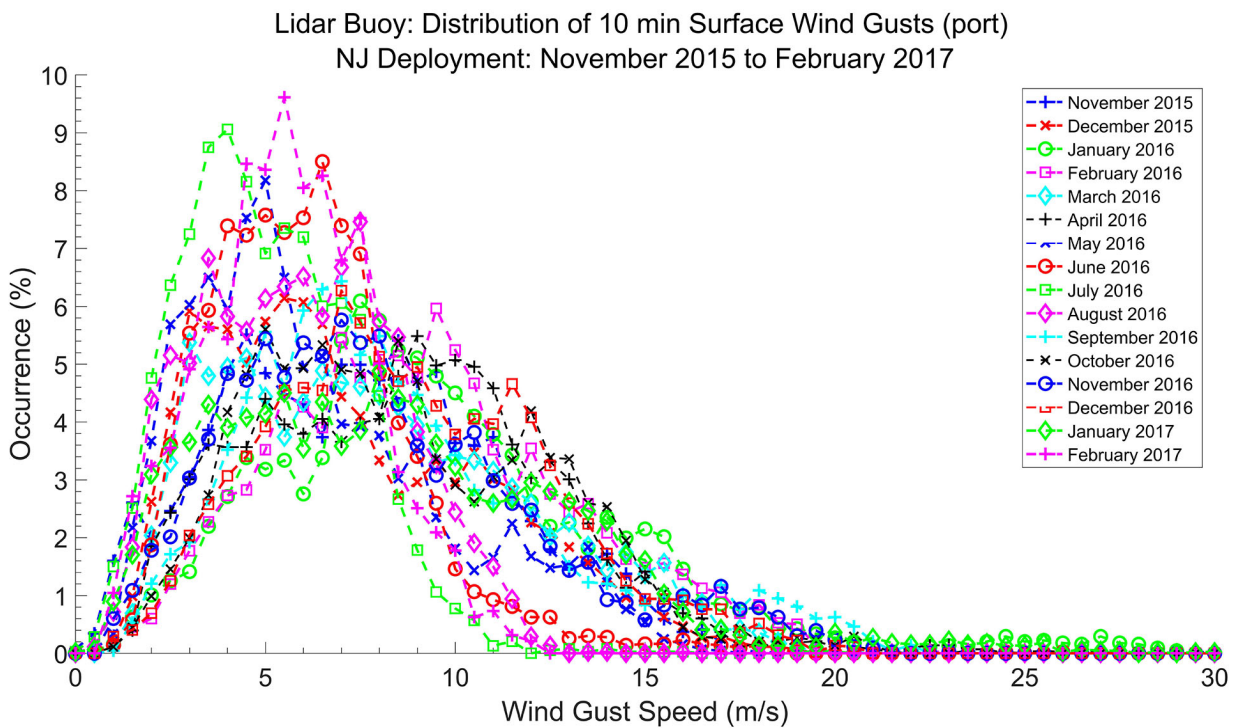


**Figure A.40. Distributions by month of surface wind gusts from the port cup anemometer.**

Lidar Buoy: Distribution of 10 min Surface Wind Gusts (starboard)  
 NJ Deployment: November 2015 to February 2017

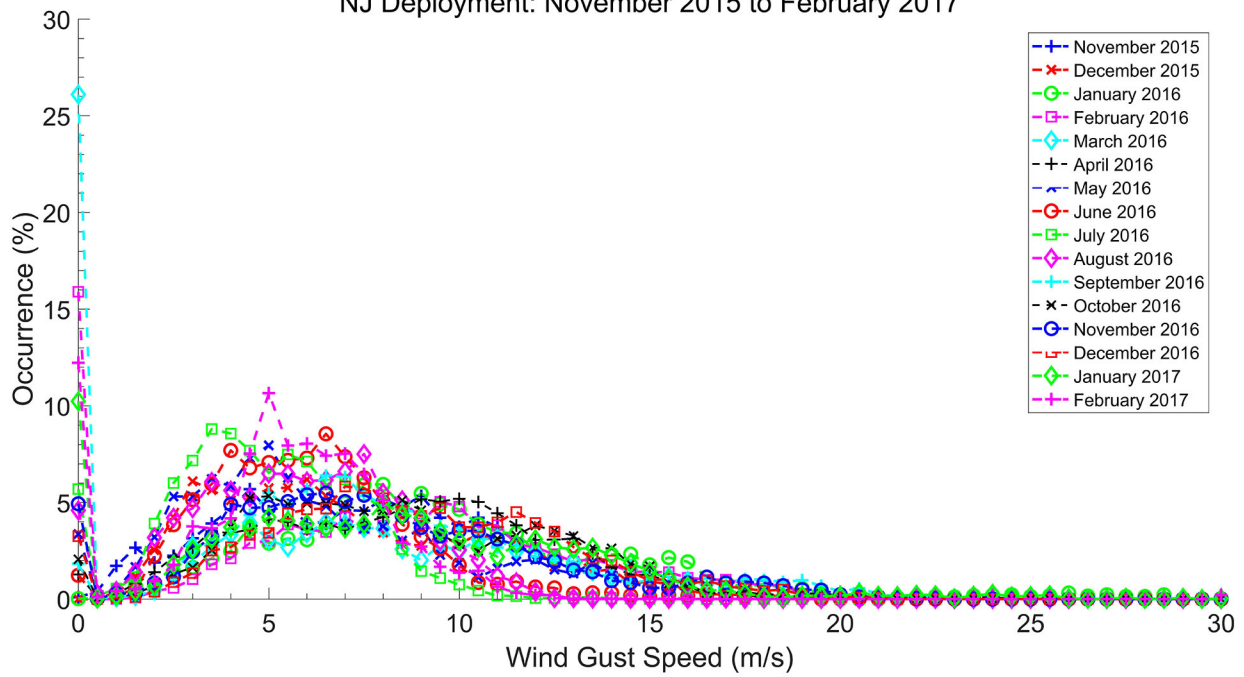


Figure A.41. Distributions by month of surface wind gusts from the starboard cup anemometer.

Lidar Buoy: Distribution of 10 min Surface Wind Direction/Speed  
 NJ Deployment: January 2016

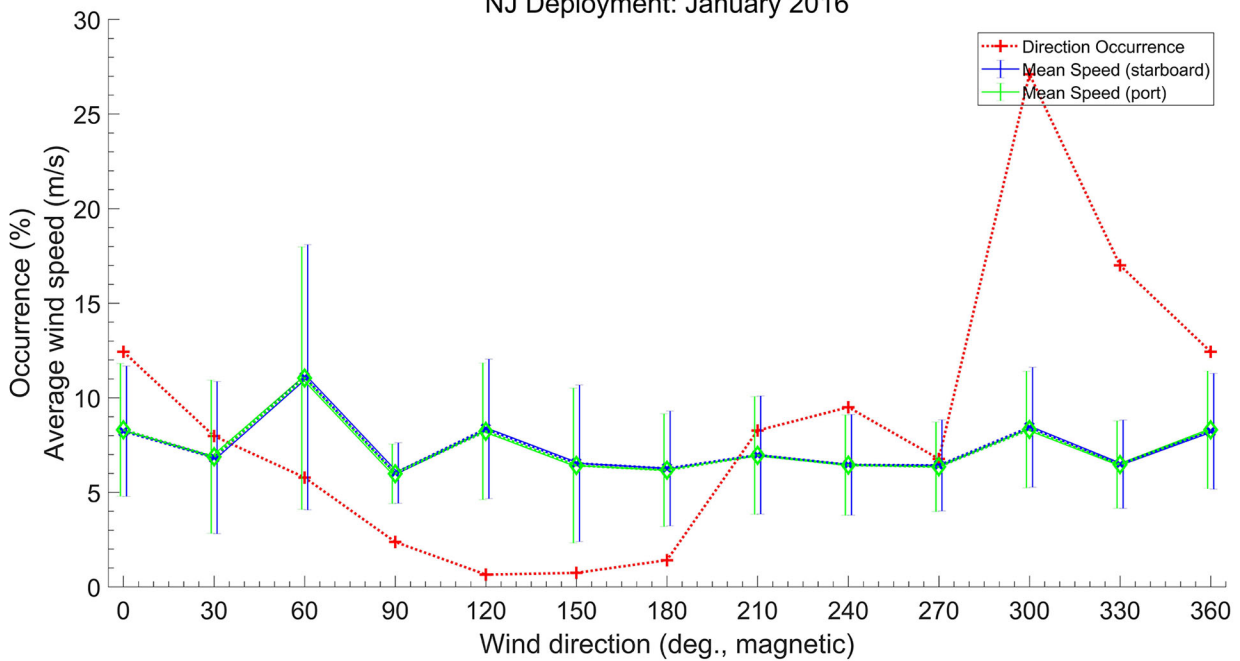
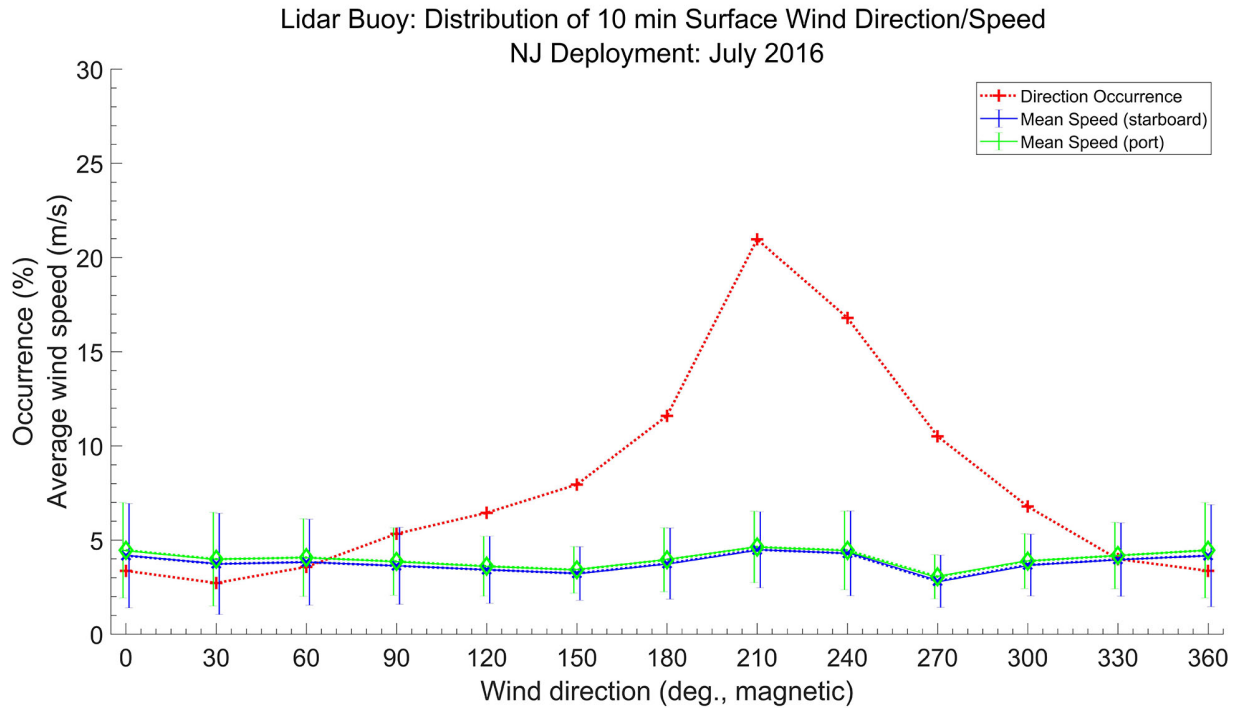
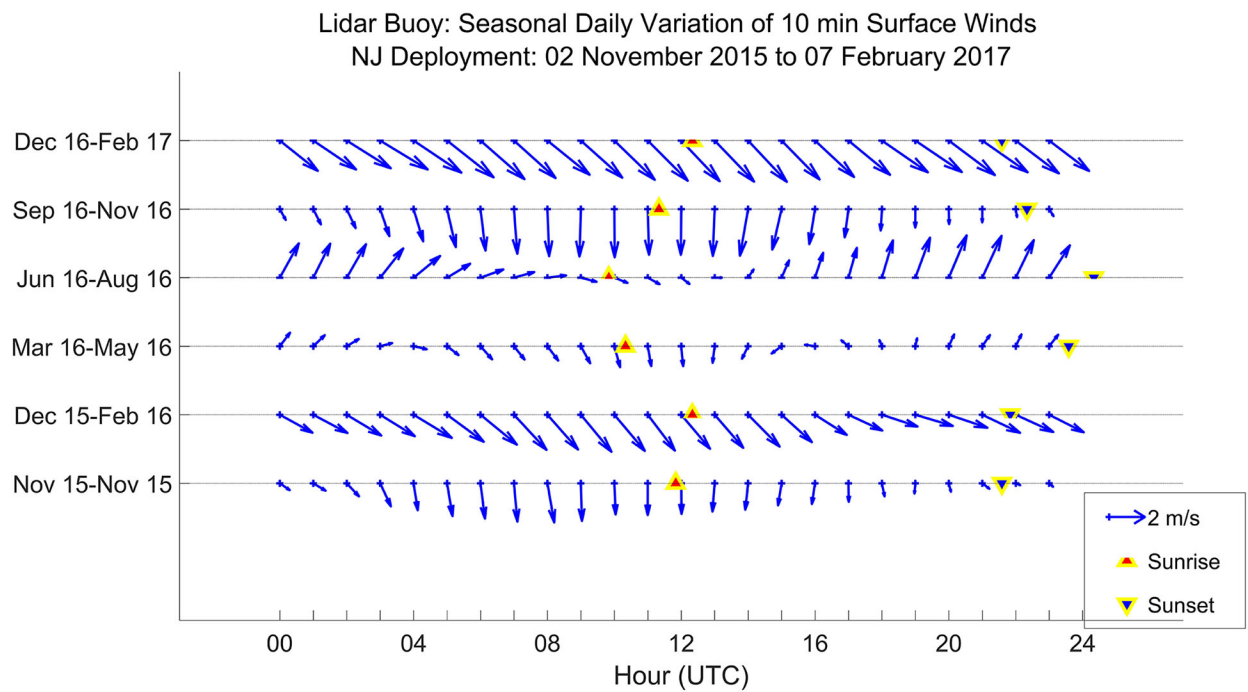


Figure A.42. Surface wind speed as a function of direction for a typical winter month (January) together with the frequency distribution of directions.



**Figure A.43. Surface wind speed as a function of direction for a typical summer month (July) together with the frequency distribution of directions.**

### A.2.2 Diurnal Wind Variations



**Figure A.44. Hourly variation of the mean wind vector by season as measured by the New Jersey buoy. Times are given in UTC with local sunrise and sunset indicated for each season.**

Note that the seasons in this figure are advanced by one month relative to figures discussed in the body of the report.

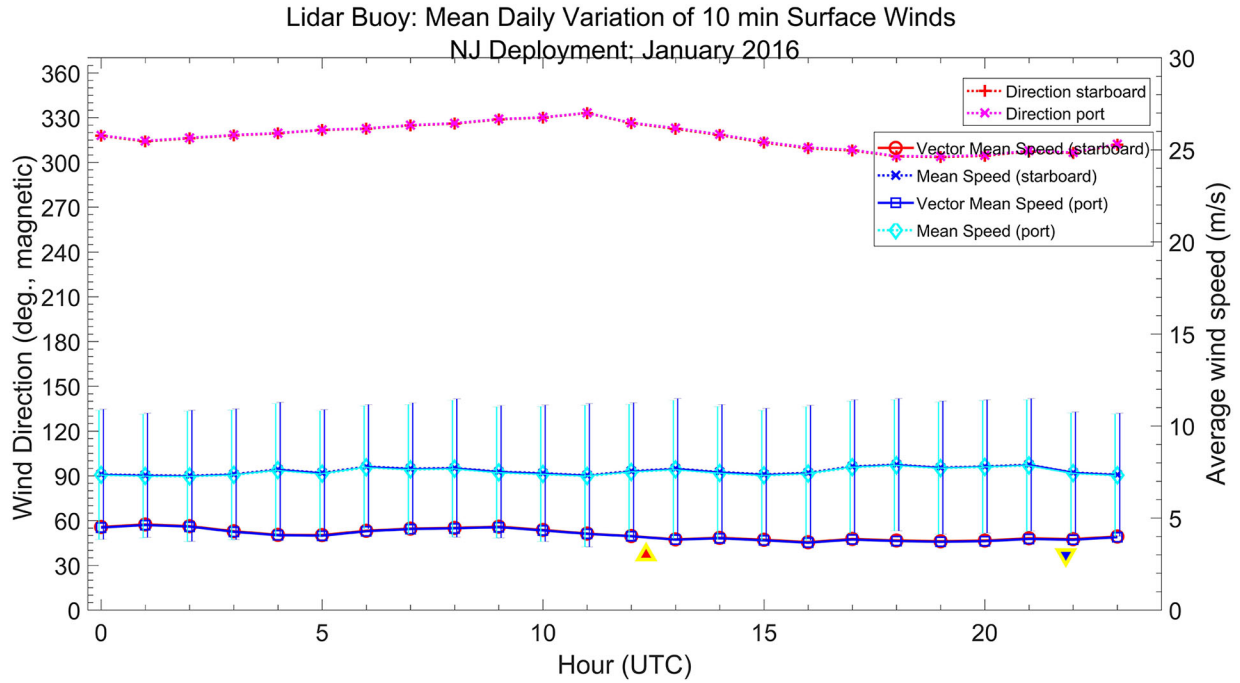


Figure A.45. Vector and scalar mean wind speed and direction as a function of hour of day for January 2016.

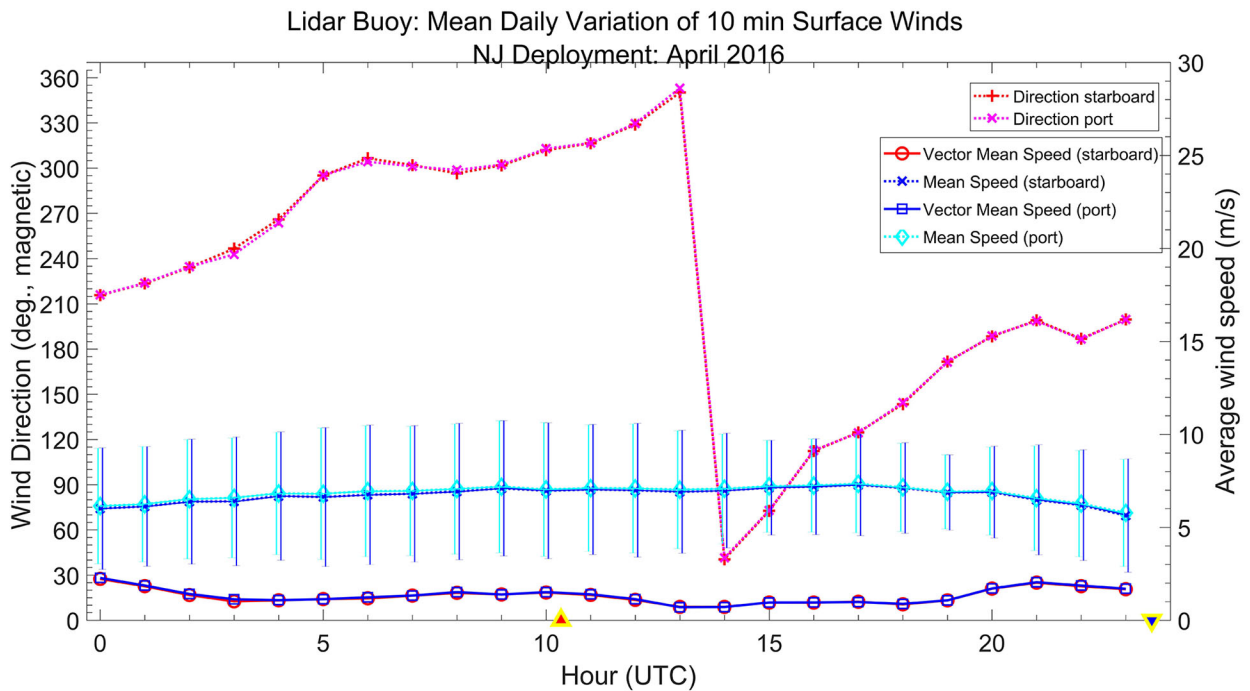


Figure A.46. Vector and scalar mean wind speed and direction as a function of hour of day for April 2016.

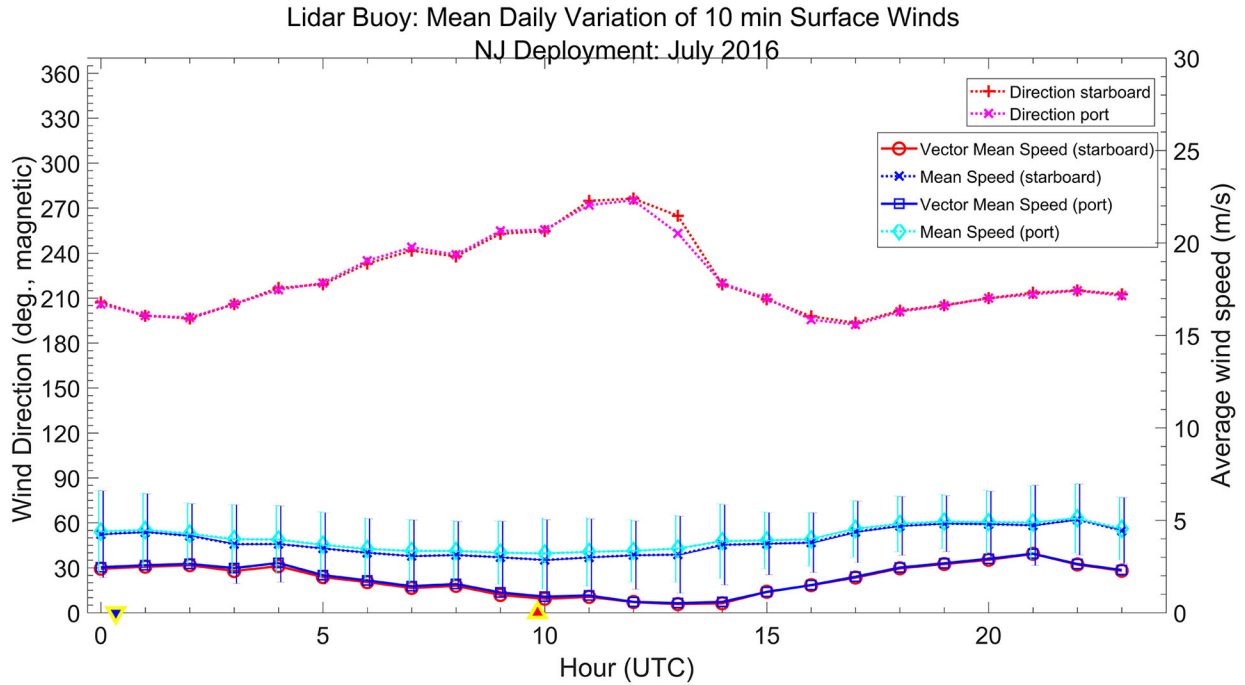


Figure A.47. Vector and scalar mean wind speed and direction as a function of hour of day for July 2016.

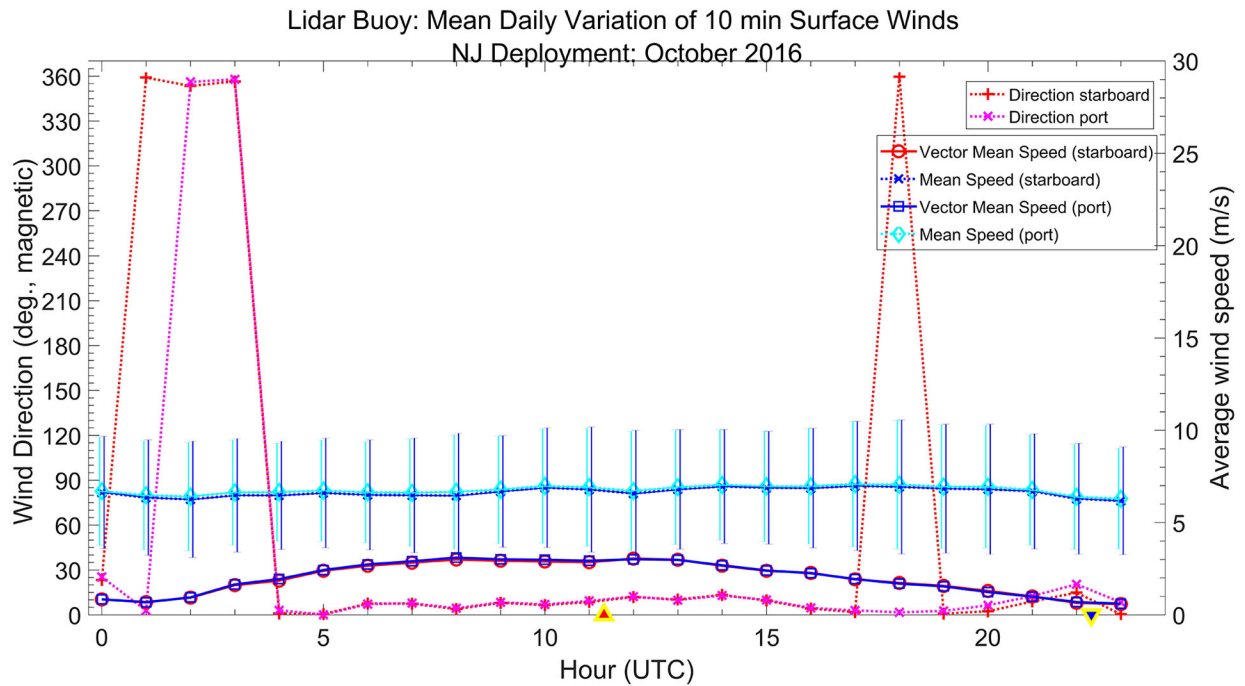


Figure A.48. Vector and scalar mean wind speed and direction as a function of hour of day for October 2016.

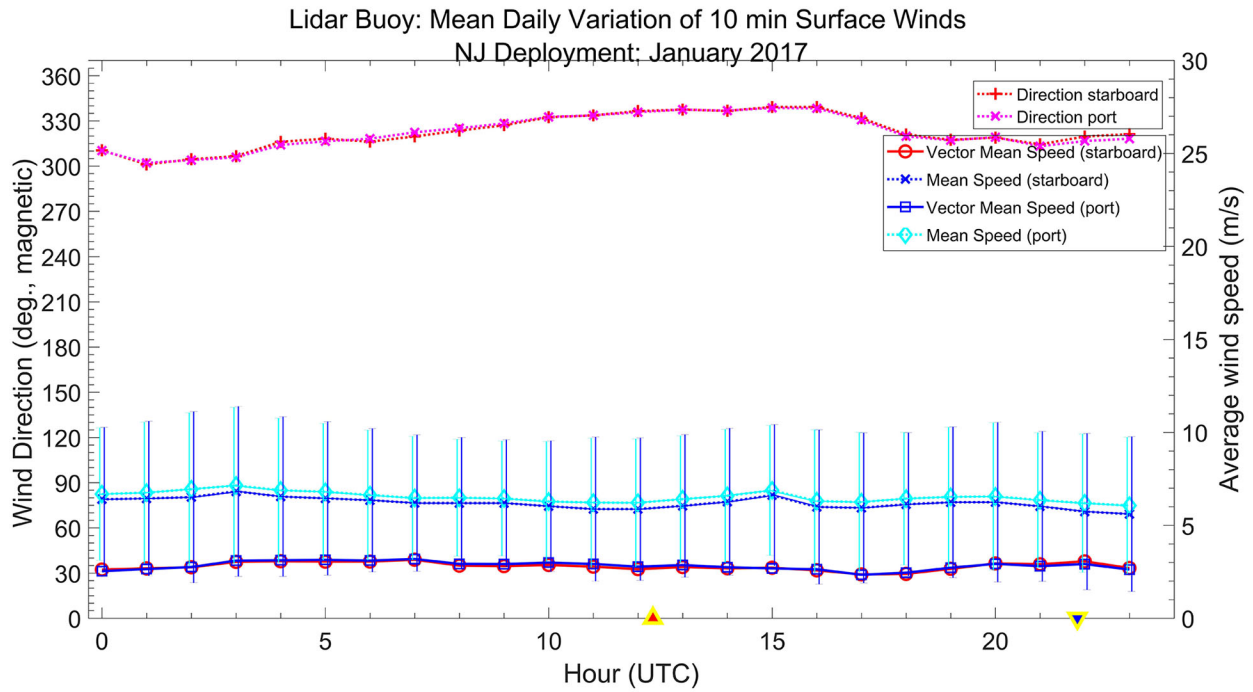


Figure A.49. Vector and scalar mean wind speed and direction as a function of hour of day for January 2017.

### A.2.3 Time Variation of Surface Temperatures

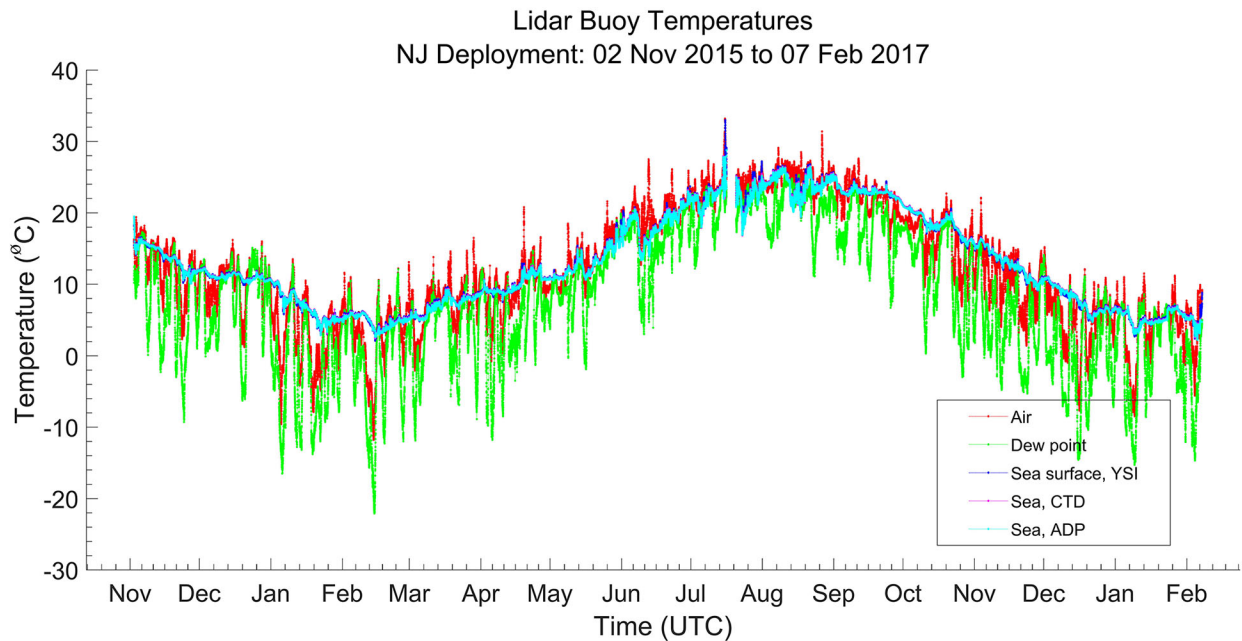
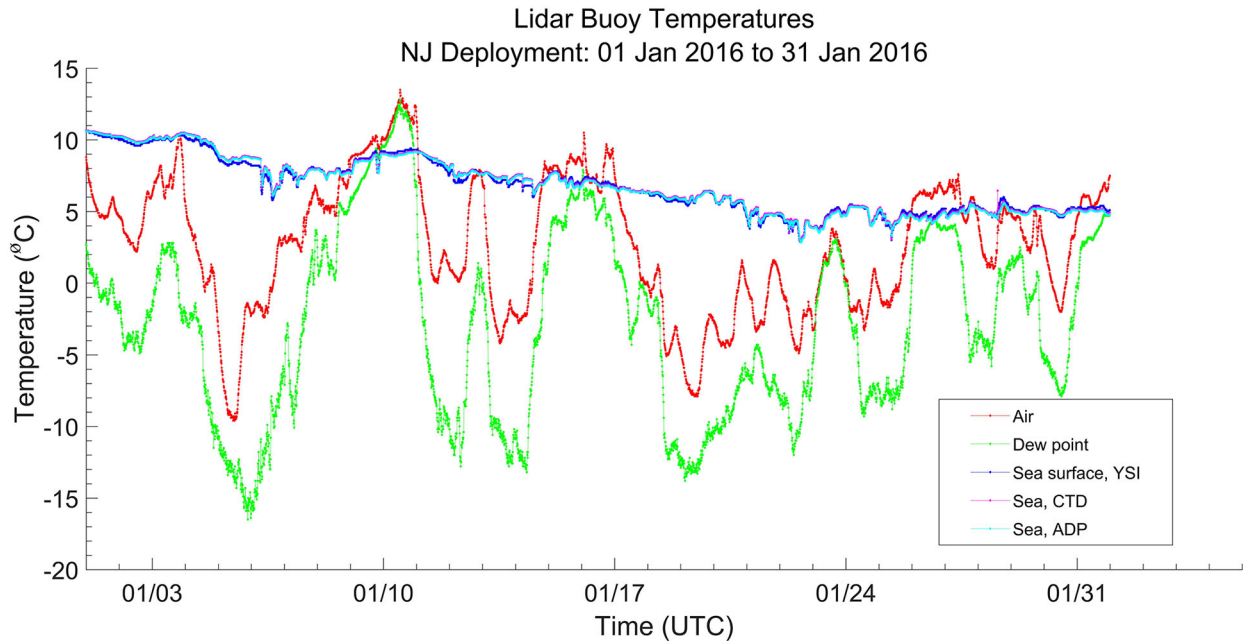
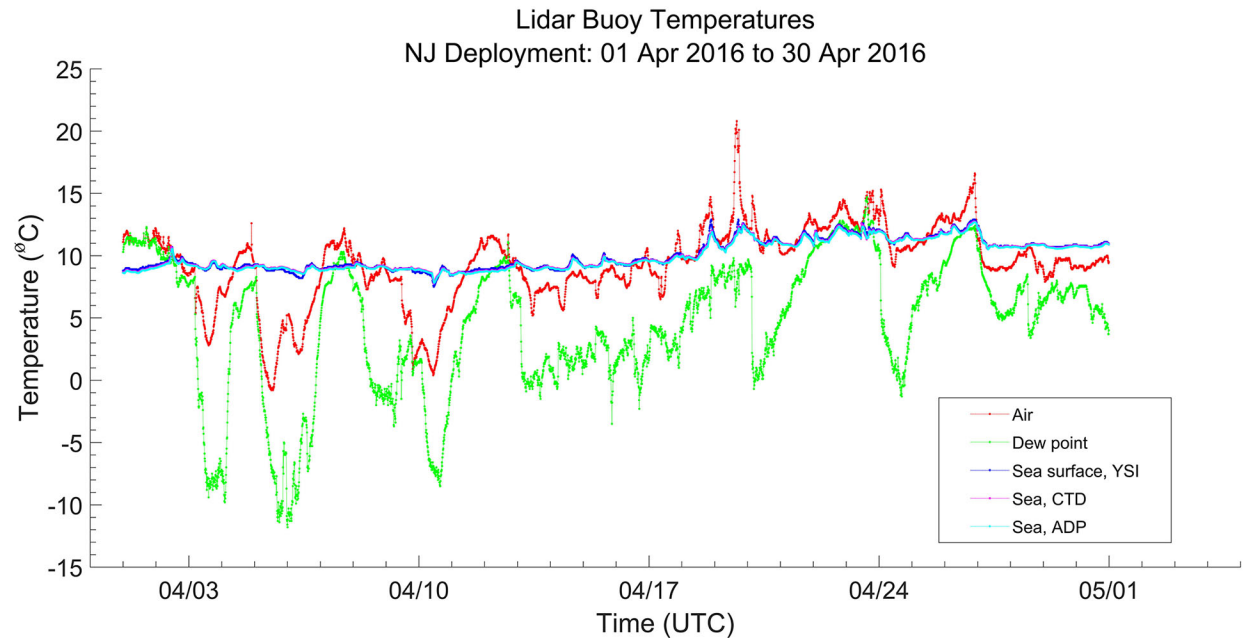


Figure A.50. Time series of air and water temperatures and dew point for the full duration of the New Jersey buoy deployment.



**Figure A.51. Time series of air and water temperatures and dew point for January 2016.**



**Figure A.52. Time series of air and water temperatures and dew point for April 2016.**

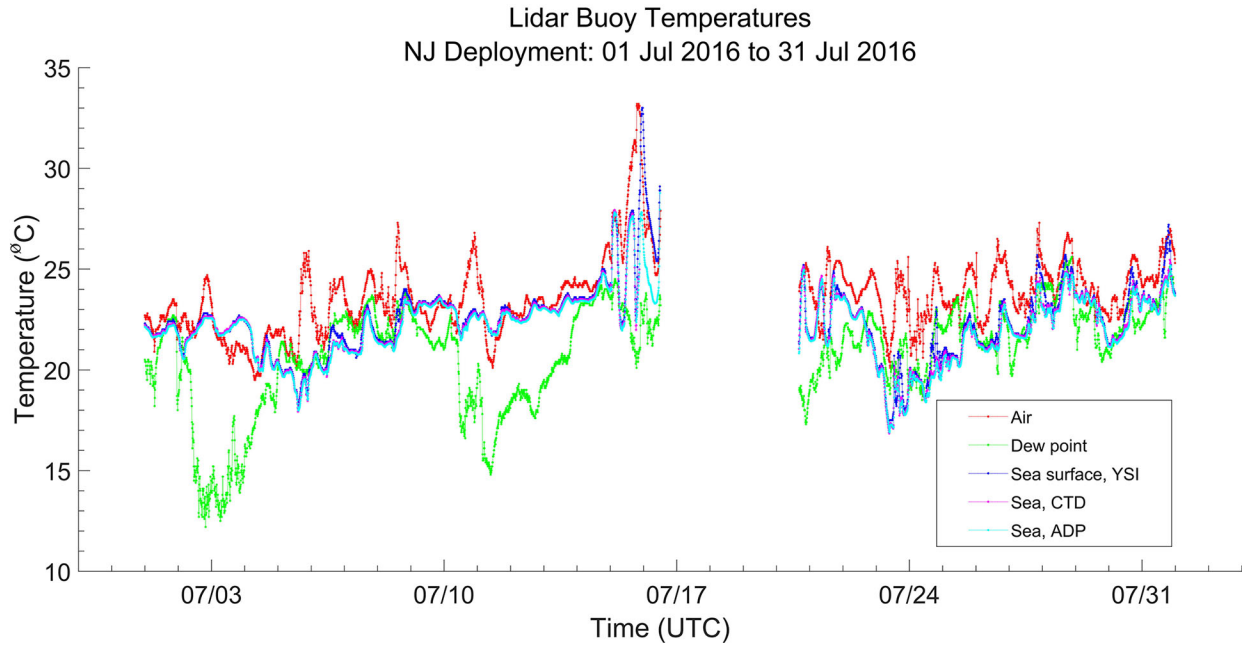


**Figure A.53. Time series of air and water temperatures and dew point for July 2016.**

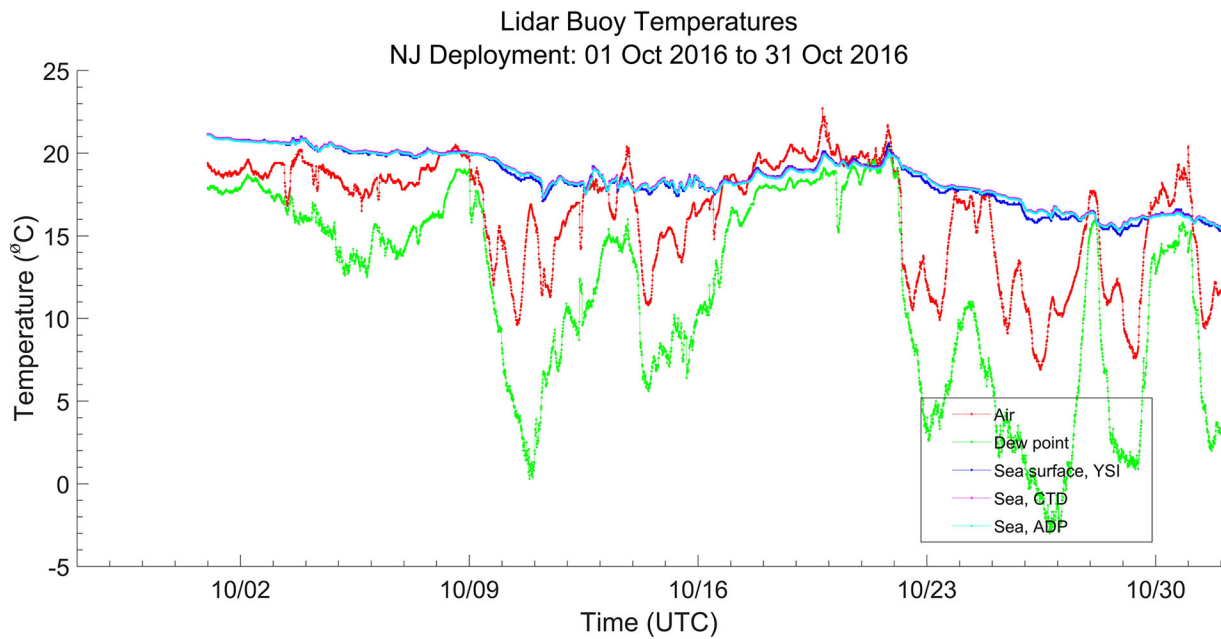


**Figure A.54. Time series of air and water temperatures and dew point for October 2016.**

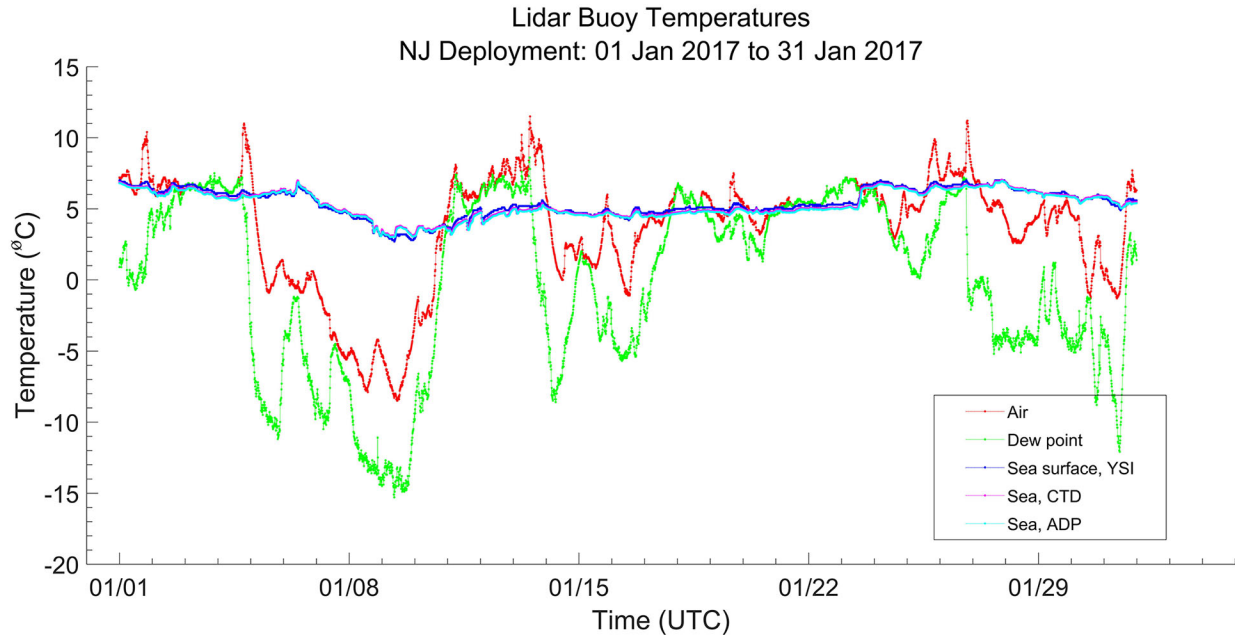


Figure A.55. Time series of air and water temperatures and dew point for January 2017.

### A.2.4 Diurnal Variation of Temperatures

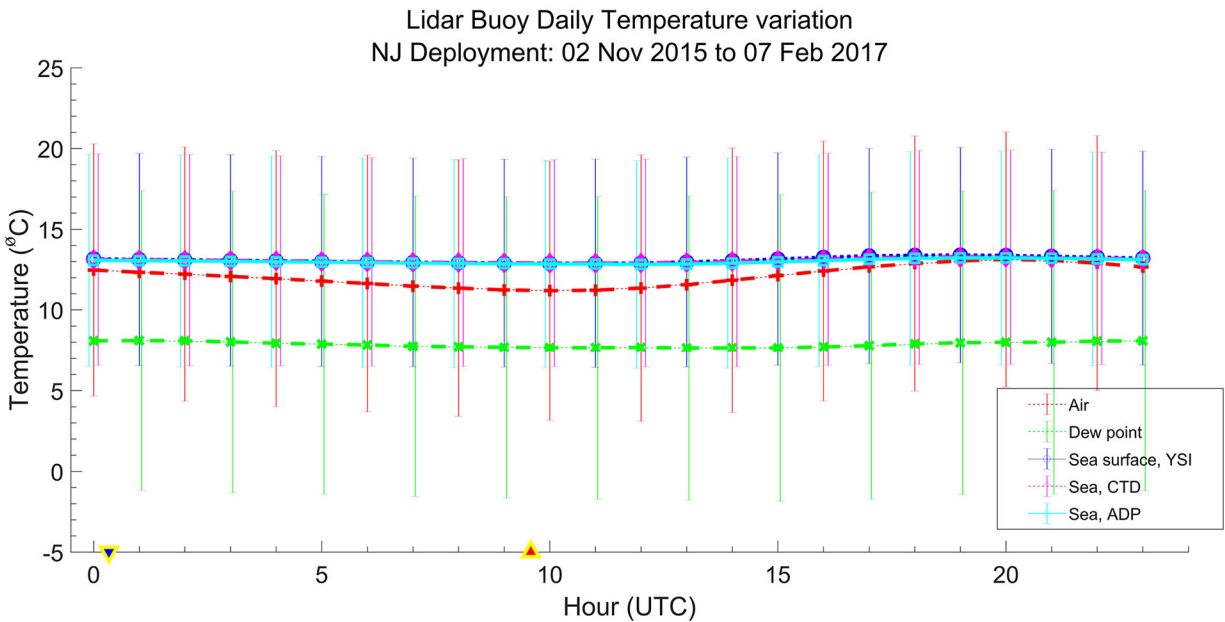
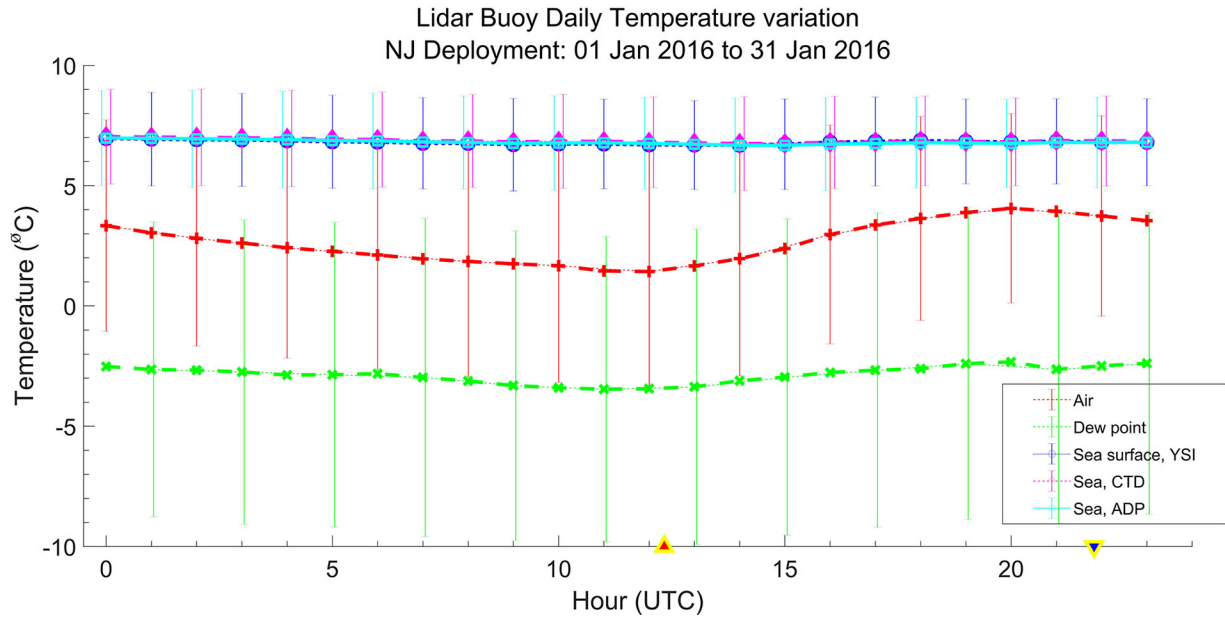
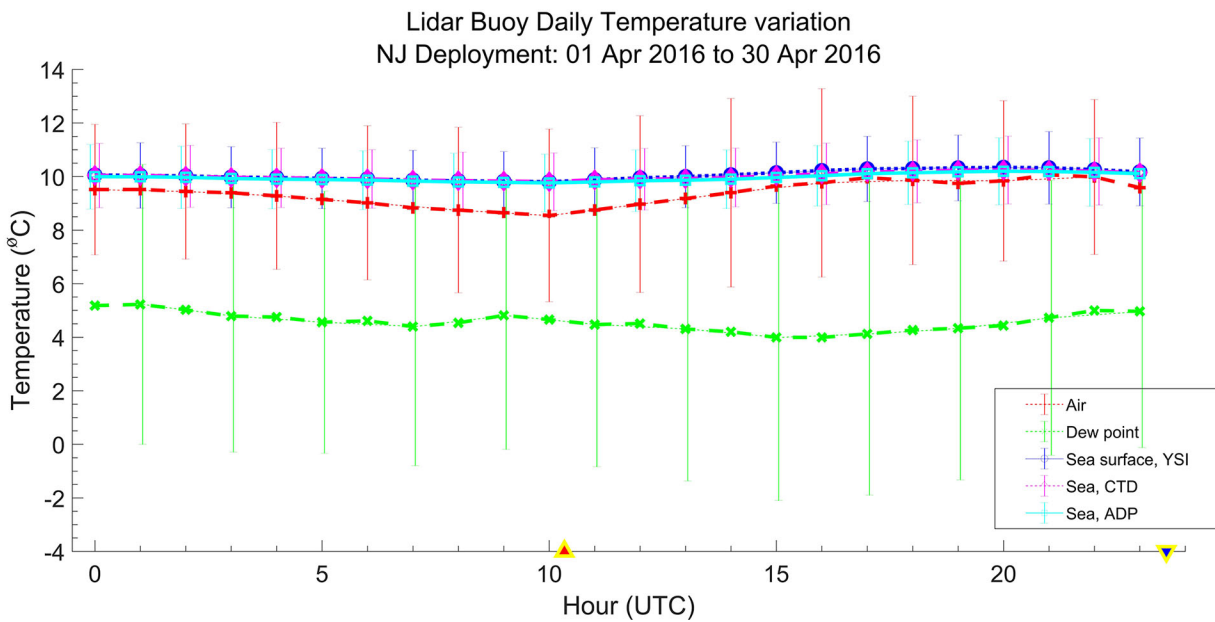


Figure A.56. Diurnal variation by hour of air and water temperatures and of dew point for the period of deployment of the New Jersey buoy. Hour of day is in UTC, and mean times of sunrise and sunset are indicated by symbols on the abscissa.



**Figure A.57. Diurnal variation by hour of air and water temperatures and of dew point for January 2016. Mean times of sunrise and sunset are indicated by symbols on the abscissa.**



**Figure A.58. Diurnal variation by hour of air and water temperatures and of dew point for April 2016. Mean times of sunrise and sunset are indicated by symbols on the abscissa.**

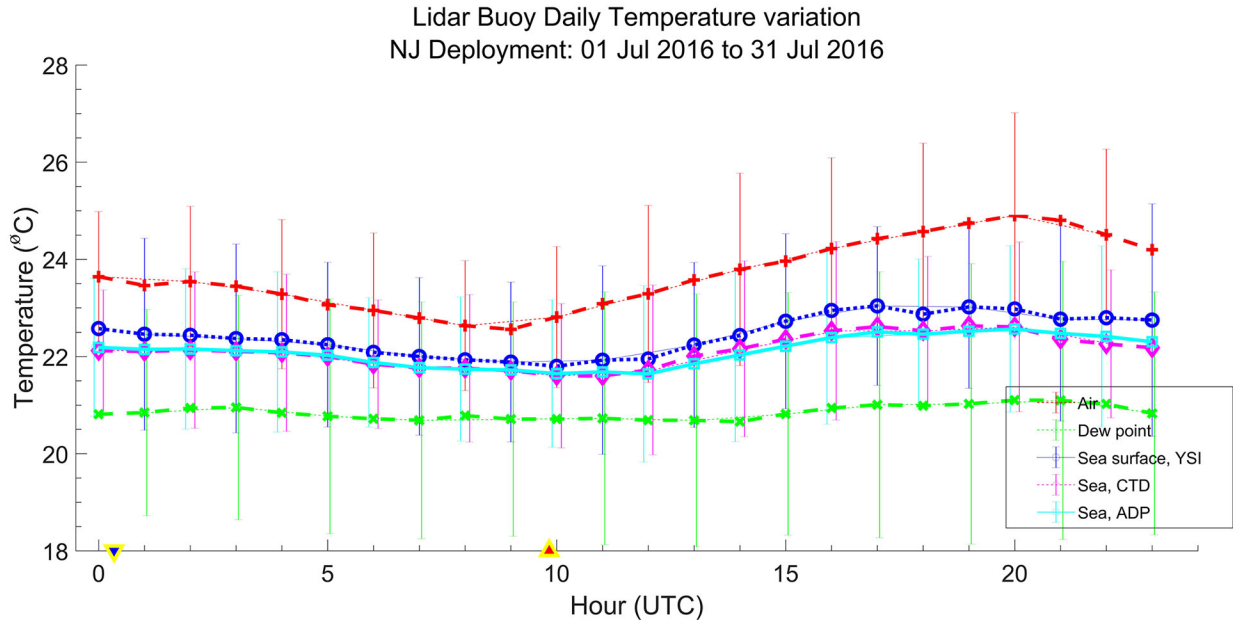


**Figure A.59. Diurnal variation by hour of air and water temperatures and of dew point for July 2016. Mean times of sunrise and sunset are indicated by symbols on the abscissa.**

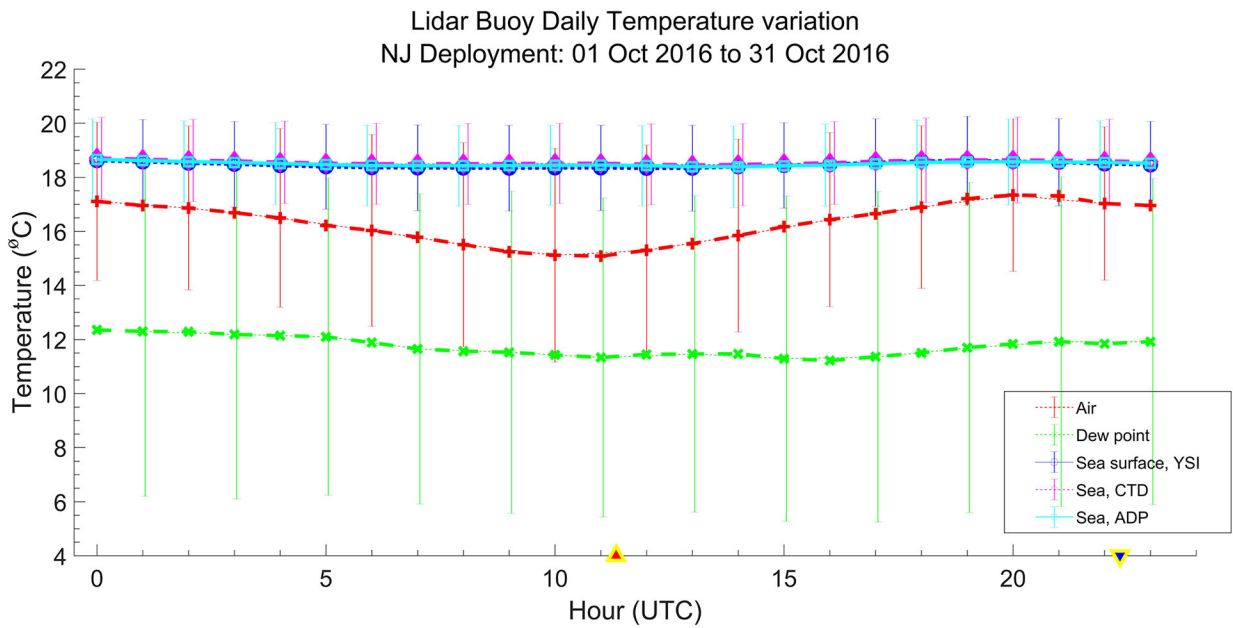


**Figure A.60. Diurnal variation by hour of air and water temperatures and of dew point for October 2016. Mean times of sunrise and sunset are indicated by symbols on the abscissa.**

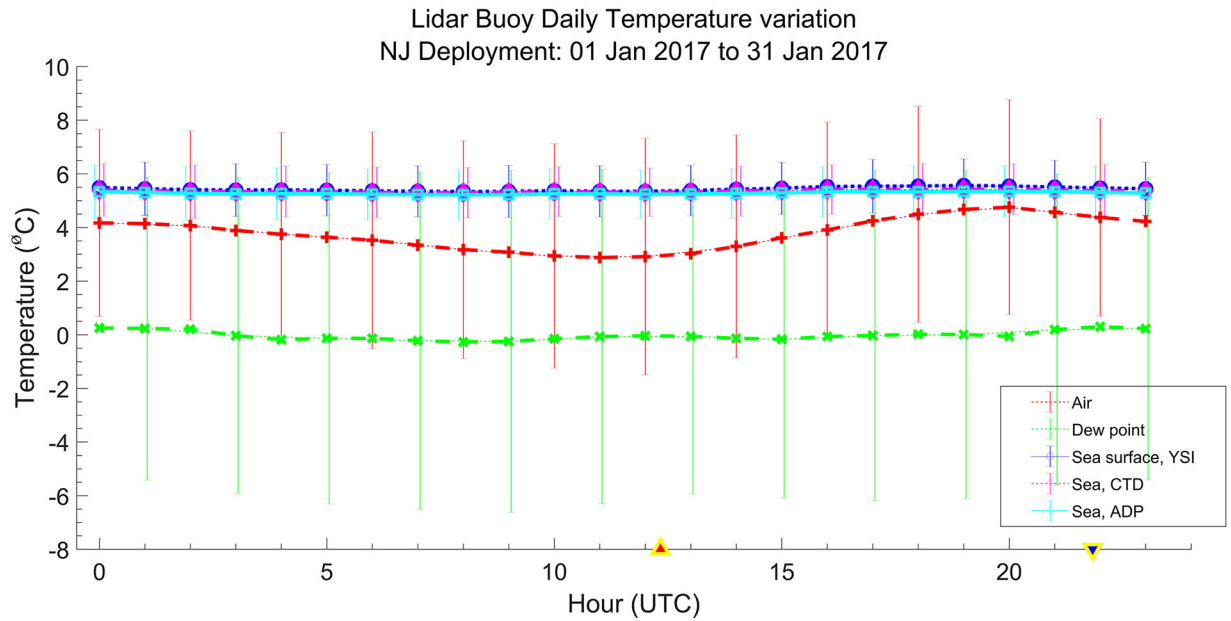


**Figure A.61. Diurnal variation by hour of air and water temperatures and of dew point for January 2016. Mean times of sunrise and sunset are indicated by symbols on the abscissa.**

### A.2.5 Seasonal Ocean Current Profiles

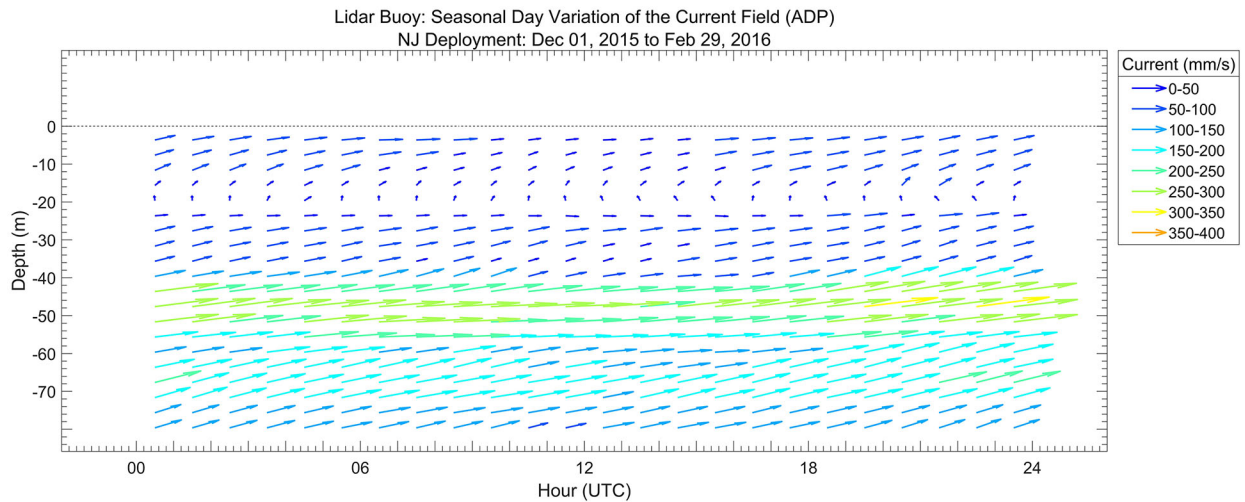


**Figure A.62. Mean current profiles by hour of day from the New Jersey buoy for winter 2016.**

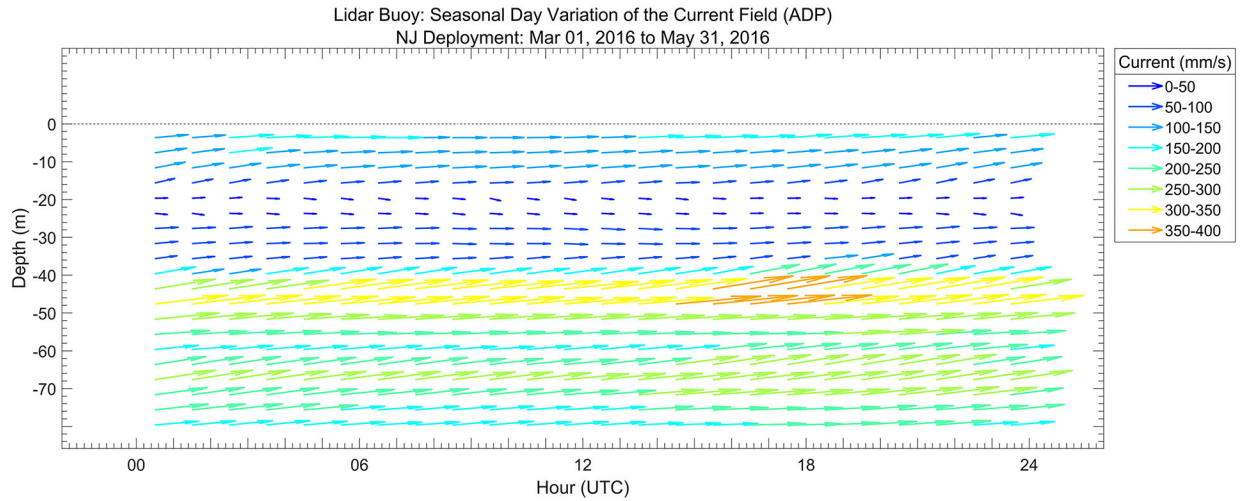


**Figure A.63. Mean current profiles by hour of day from the New Jersey buoy for spring 2016.**

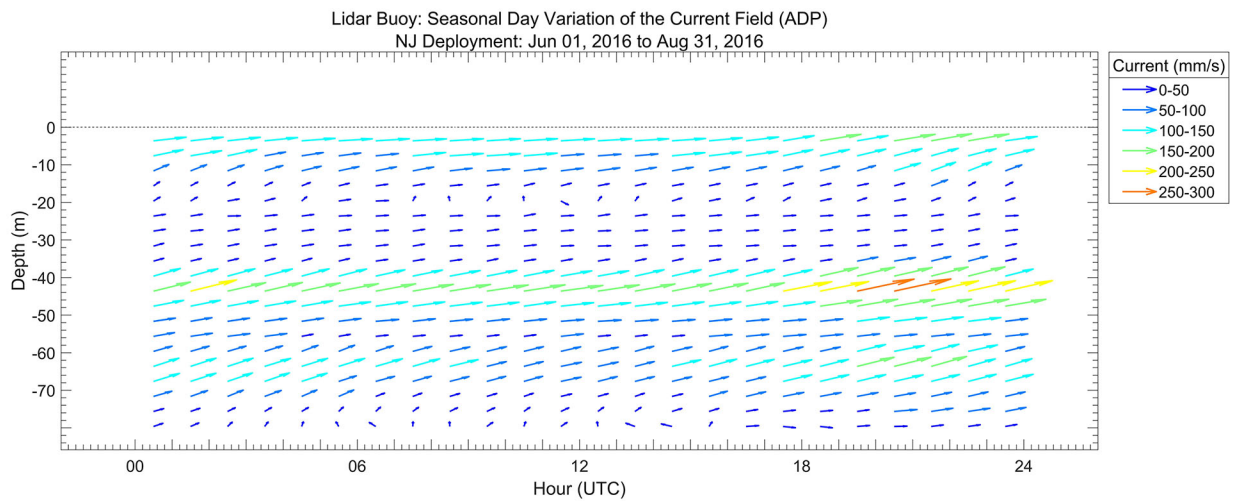


**Figure A.64. Mean current profiles by hour of day from the New Jersey buoy for summer 2016.**

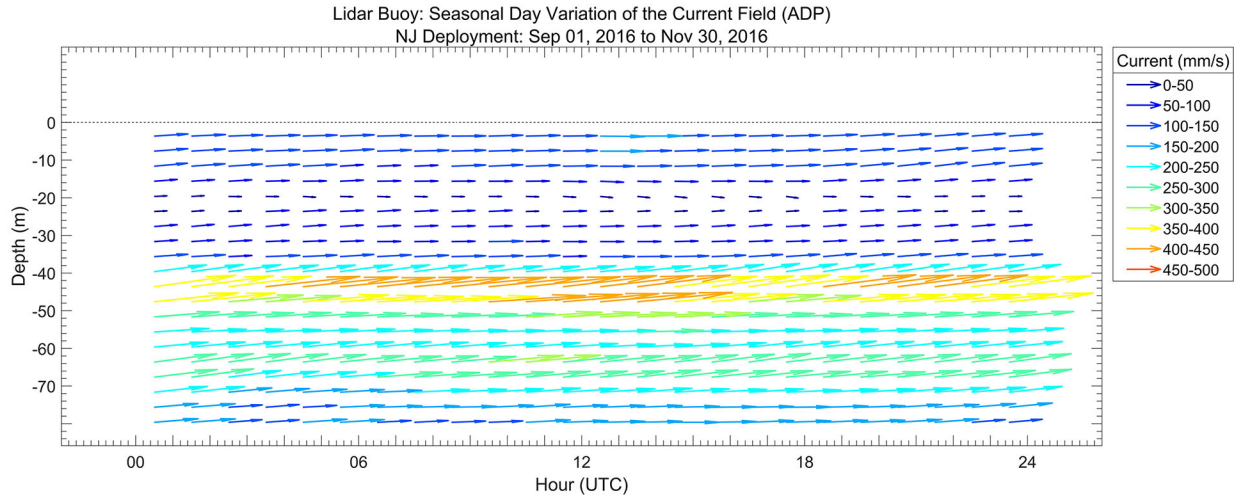


**Figure A.65. Mean current profiles by hour of day from the New Jersey buoy for fall 2016.**

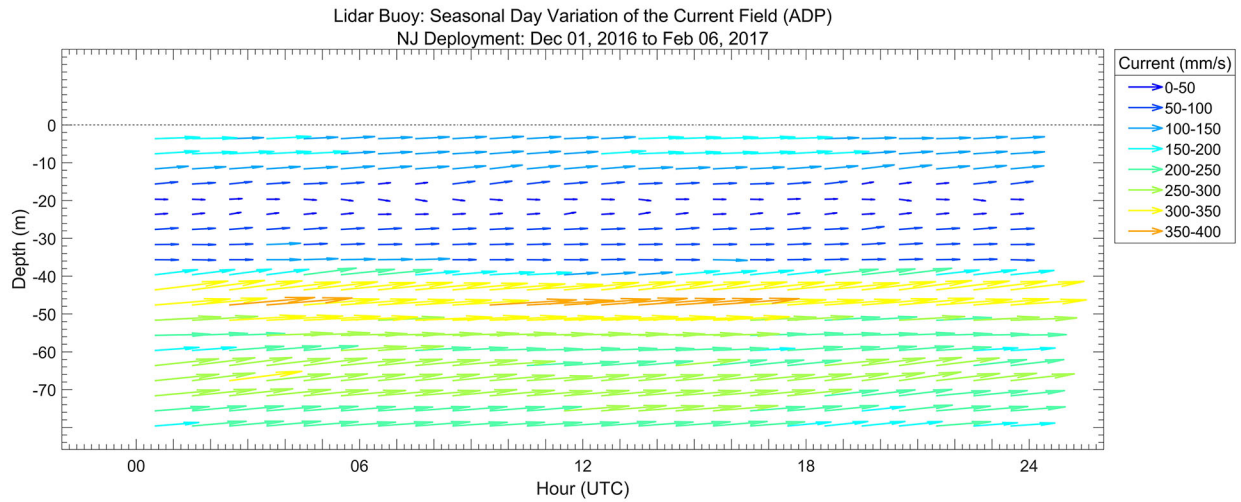


**Figure A.66. Mean current profiles by hour of day from the New Jersey buoy for winter 2017.**



**Pacific Northwest**  
NATIONAL LABORATORY

*Proudly Operated by **Battelle** Since 1965*

902 Battelle Boulevard  
P.O. Box 999  
Richland, WA 99352  
1-888-375-PNNL (7665)

U.S. DEPARTMENT OF  
**ENERGY**

---

[www.pnnl.gov](http://www.pnnl.gov)